# CALCULATION OF UNBALANCED MAGNETIC PULL IN CAGE INDUCTION MACHINES



Dissertation submitted to the
University of Cambridge for the
Degree of Doctor of Philosophy

by

David George Dorrell

of

Robinson College

May 1993

# Summary

If the rotor of an induction motor is not concentric with the stator then an electromagnetic force is generated in a direction that will increase the eccentricity. This is called unbalanced magnetic pull (UMP).

The first part of the work presented in this dissertation develops theoretical models which allow the calculation of the UMP in cage induction motors due to static rotor eccentricity. These account for any winding configuration including parallel stator winding connection.

The second part of the work verifies the models experimentally using two different cage induction motors. The agreement between predicted and measured values of UMP and line current is found to be good. The investigation leads to several new aspects of the damping effects of parallel stator windings and the cage rotor being highlighted.

# Indexing Terms

Electrical Machines

Induction Motors

Asynchronous Machines

Unbalanced Magnetic Pull

# Preface

The work described in this thesis was carried out by the author at Imperial College, London, between October 1989 and April 1990 and then at Cambridge University Engineering Department between April 1990 and April 1993 under the supervision of Dr. A.C. Smith. Except where stated, or otherwise indicated by citation, this dissertation describes the original work of the author. The contents of this dissertation have not been submitted in whole, or in part, for a degree or other qualification at any other academic institution.

I would like to acknowledge the help and guidance of my supervisor Sandy Smith during the course of this project and to the assistant staff of the Part I Electrical Lab. and the Engineering Workshops for construction of the experimental equipment.

Thanks must also be made to the Science and Engineering Research Council and GEC Alsthom Large Machine Ltd., Rugby for their financial support of this project.

# List of Symbols

| | |
|---|---|
| $\overline{B}^{n}_{b,a}$ | $n^{th}$ harmonic flux density coefficient of the $b^{th}$ phase band of the $a^{th}$ phase |
| $\overline{B}^{m,\nu,\mu}_{r}$ | $(\mu N_b + \nu)^{th}$ current harmonic and $m^{th}$ permeance harmonic rotor flux density coefficient |
| $\overline{B}^{m,\nu}_{rh}$ | $\nu^{th}$ winding harmonic and $m^{th}$ permeance harmonic rotor homopolar flux density coefficient |
| $\overline{B}^{m,n}_{s}$ | $n^{th}$ winding harmonic and $m^{th}$ permeance harmonic stator flux density coefficient |
| $\overline{B}^{m,n}_{sh}$ | $n^{th}$ winding harmonic and $m^{th}$ permeance harmonic stator homopolar flux density coefficient |
| $[C]$ | connection matrix |
| $[C']$ | connection matrix including the rotor harmonic currents |
| $C_{b,a}(w)$ | number of series turns in the $w^{th}$ slot of the $b^{th}$ phase band of the $a^{th}$ phase |
| $D$ | distance of rotor axis from stator axis |
| $\left[\overline{I}\right]$ | machine current matrix |
| $\left[\overline{I_L}\right]$ | machine current loop matrix |
| $\overline{I}_{b,a}$ | current coefficient of the $b^{th}$ phase band of the $a^{th}$ phase |
| $\overline{I}^{\nu}_{r}$ | rotor currentcoefficient of the $\nu^{th}$ current harmonic |
| $\overline{J}^{\nu,\mu}_{r}$ | rotor current density coefficient of the $\nu^{th}$ current harmonic and the $\mu^{th}$ permeance harmonic |
| $N_b$ | number of bars in rotor cage |
| $N_w$ | number of stator slots |
| $\overline{N}^{n}_{b,a}$ | $n^{th}$ harmonic winding coefficient of the $b^{th}$ phase band of the $a^{th}$ phase |
| $\overline{N}^{n}_{r}$ | $n^{th}$ harmonic winding coefficient of a rotor loop |
| $Q(m)$ | $m^{th}$ permeance harmonic coefficient |
| $R_1$ | stator radius in Z-plane |
| $R_2$ | rotor radius in Z-plane |
| $R_b$ | stator phase winding resistance |
| $R^{\nu}_{b}$ | effective rotor bar resistance |
| $R_{bar}$ | actual rotor bar resistance |

| | |
|---|---|
| $R_{er}$ | end-ring segment resistance |
| $R_g$ | airgap magnetic reluctance |
| $R_s$ | shaft and end-cap magnetic reluctance |
| $\left[\overline{V}\right]$ | machine voltage matrix |
| $\left[\overline{V_L}\right]$ | machine voltage loop matrix |
| $X_b$ | stator phase winding leakage reactance |
| $X_b^\nu$ | effective rotor bar leakage reactance |
| $X_{bar}$ | actual rotor bar leakage reactance |
| $X_{er}$ | end-ring segment leakage reactance |
| $X_{ba,dc}$ | coupling impedance between the $b^{th}$ band of phase $a$ and the $d^{th}$ band of phase $c$ |
| $X_{\nu,dc}$ | rotor-stator coupling impedance |
| $X_{ba,\nu}$ | stator-rotor coupling impedance |
| $X_{\nu',\nu}$ | rotor-rotor coupling impedance |
| $\left[\overline{Z}\right]$ | coupling impedance matrix |
| $\left[\overline{Z}_{r,r}\right]$ | rotor-rotor coupling impedance matrix |
| $\left[\overline{Z}_{r,s}\right]$ | rotor-stator coupling impedance matrix |
| $\left[\overline{Z}_{s,r}\right]$ | stator-rotor coupling impedance matrix |
| $\left[\overline{Z}_{s,s}\right]$ | stator-stator coupling impedance matrix |
| $\overline{Z}_{ba,dc}$ | self impedence of the $b^{th}$ band of phase $a$ |
| $b_n$ | flux density perpendicular to the stator surface |
| $b_t$ | flux density tangential to the rotor surface |
| $b(y,t)$ | airgap radial flux density |
| $b_r(x,y',t)$ | rotor airgap radial flux density |
| $c$ | distance of rotor and stator centres from origin in T-plane |
| $d$ | distance of rotor centre from origin in Z-plane |
| $e$ | denotes exponential function |
| $e(y,t)$ | airgap axial electric field |
| $g_{av}$ | effective airgap length when the rotor is concentric |
| $g$ | effective airgap length in T-plane |
| $g(y)$ | effective airgap length at point $y$ round the airgap |
| $i_{b,a}(t)$ | current flowing in the $b^{th}$ phase band of the $a^{th}$ phase |
| $i_r^\nu(t)$ | $\nu^{th}$ harmonic current flowing a rotor loop |

| | |
|---|---|
| $j$ | denoted imaginary part of complex number |
| $j_r(x, y', t)$ | $\nu^{th}$ harmonic current density distribution on the rotor surface |
| $j_{rl}(x, y', t)$ | $\nu^{th}$ harmonic current density distribution on the rotor surface due to the $l^{th}$ rotor loop |
| $j_s(y, t)$ | current density distribution on the stator surface |
| $k$ | machine radial number ($=\frac{1}{r}$) |
| $k'$ | machine radial number in Z-plane($=\frac{1}{r}$) |
| $k_r^n$ | $n^{th}$ harmonic rotor slot opening factor |
| $k_s^n$ | $n^{th}$ harmonic stator slot opening factor |
| $l$ | effective stack length of machine core |
| $m$ | permeance harmonic number |
| $n$ | winding harmonic number |
| $n_{b,a}(y)$ | winding distribution function of the $b^{th}$ phase band of the $a^{th}$ phase |
| $n_{rl}(x, y')$ | winding distribution function of the $l^{th}$ rotor loop |
| $p$ | pole-pair number of machine |
| $r$ | average airgap radius |
| $r_1$ | stator radius in T-plane |
| $r_2$ | rotor radius in T-plane |
| $s$ | degree of slip |
| $t$ | denotes time |
| $\overline{t}$ | phasor in T-plane |
| $\overline{t_1}$ | function describing stator in T-plane |
| $\overline{t_2}$ | function describing rotor in T-plane |
| $u$ | abscissa in T-plane |
| $u(t)$ | back e.m.f. induced in a winding |
| $u_{ba,dc}(t)$ | back e.m.f. induced in the $b^{th}$ band of phase $a$ by the $d^{th}$ band of phase $c$ |
| $v$ | ordinate in T-plane |
| $x$ | axial distance along machine or abscissa in Z-plane |
| $y$ | linear distance round airgap in stator reference frame or ordinate in Z-plane |
| $y'$ | linear distance round airgap in rotor reference frame (permeance harmonic method) or Z-plane (conformal transformation method) |

| | |
|---|---|
| $z$ | radial distance in radial direction across airgap |
| $\overline{z}$ | phasor in Z-plane |
| $\overline{z_1}$ | function describing stator in Z-plane |
| $\overline{z_2}$ | function describing rotor in Z-plane |
| $\Delta(y)$ | permeance harmonic series |
| $\Lambda$ | degree of rotor offset $(= \frac{D}{g_{av}})$ |
| $\Phi$ | homopolar flux coefficient |
| $\alpha$ | homopolar flux path coefficient |
| $\gamma$ | maxwell stress acting tangentially to the stator surface |
| $\delta$ | angle of skew of rotor bar |
| $\lambda$ | pitch between two adjacent rotor bars (in radians) |
| $\theta_w$ | angular position of the $w^{th}$ stator slot |
| $\mu$ | rotor differential leakage harmonic number |
| $\mu_o$ | permeability of free space |
| $\nu$ | rotor current and field harmonic number |
| $\omega$ | denotes angular speed, usually supply frequency in rad/sec |
| $\omega_r$ | rotational speed of rotor in rad/sec |
| $\omega_s$ | supply frequency of machine in rad/sec |
| $\omega^\nu$ | frequency of $\nu^{th}$ rotor harmonic current in rad/sec |
| $\sigma$ | maxwell stress acting normal to the stator force |

# Contents

# Chapter 1

# Introduction

## 1.1 Background

The squirrel cage induction motor is the workhorse of modern industry. Its high efficiency and robustness making it ideal for many applications from fractional-watt to megawatt ratings. Even the drawback of limited operating speed range has now been overcome with the introduction of variable frequency supplies.

Analysis of the machine has been improved continually for many decades and is normally based on the per-phase equivalent circuit. This has led to machine design becoming more systematic and operation more predictable, especially with the incorporation of fast computing into the design office. There are still problems however that cannot easily be predicted with any degree of accuracy and still rely on design compromises to prevent them becoming a problem. Unbalanced magnetic pull ( UMP ) falls into this category.

There are two principal reasons for this. First, the computational facilities were not available to model UMP without resorting to a number of simplifying assumptions. Secondly, the actual experimental measurement of UMP was very difficult. The advent of modern, fast computers and accurate piezo-electric transducers has now made the calculation and measurement of UMP a realistic proposition.

## 1.2 Description of the Problem

If the rotor of an induction machine is mechanically centred within the stator and slotting effects are ignored then the net electromagnetic force will create a rotating moment about its axis. However, this is an unstable point and any mechanical deviation from this position will create a net radial force pulling the rotor even further out of alignment. This is called unbalanced magnetic pull. The consequences of this are numerous: excessive bearing wear; vibration; noise and, under extreme conditions, contact between the rotor and stator. Assuming that the inner stator surface and outer rotor surface are perfectly circular then there are two types UMP caused by rotor misalignment: static UMP and dynamic UMP.

Static UMP is caused by the axis of the rotor not being aligned with that of the stator although it still rotates about it own axis. This is normally due to manufacturing tolerances. Excessive static UMP normally occurs when the bearings are incorrectly positioned or worn. For simplicity, this is generally modelled with the rotor and stator axes parallel to each other, hence obtaining constant airgap down the axial length of the machine. Whilst the tolerances and wear in similar types of bearings with the weight of the rotor acting upon them may lead to this situation, it is unlikely that bearings at both ends would have the same offset. However, predicting the UMP in a machine with a non-uniform axial airgap is still a problem that has, as yet, remained intractable.

Dynamic UMP is caused by the rotor not turning about its own axis though it is still rotating about the stator axis. Obviously, static and dynamic UMP can exist simultaneously. The usual causes of dynamic UMP are also manufacturing tolerances, wear and incorrect manufacture. Rotor "whirl" near a critical speed is another source of dynamic eccentricity and is an important consideration in larger, flexible shaft machines. Like static eccentricity, dynamic eccentricity is generally modelled with uniform axial airgap. If the source is tolerance, wear or "whirl" then this is likely to give a reasonable representation of the situation. Incorrect manufacture is less likely to produce this situation since it is improbable that two bearings would be incorrectly mounted in the same way.

## 1.3 Survey of Literature

The causes of unbalanced magnetic pull have been studied for many years. As early as 1918 a review of work already carried out was published [1]. Early papers, such as that of Rosenburg [2] used $B-H$ curves in order to try and calculate the imbalance of flux in the airgap and hence quantify the UMP. His extensive paper also notes the effect of UMP on the critical speed, an important criterion in machine design. Robinson in 1943 [3], Crawford in 1951 [5] and Covo in 1954 [6] were still using this method, making little distinction between different non-salient machines.

Summers in 1955 [7] began to develop the theory of UMP by using rotating field components in a two-pole machine, concluding that static UMP due to motor deformations produce twice-line-frequency vibrations, dynamic UMP due to rotor irregularities and imbalances produce twice-running-frequency vibrations and that these react to produce beat vibrations of twice-slip-frequency. Robinson [12] extended this by showing that, with mechanical resonance, line-frequency vibrations can also exist. This was shown experimentally by Jordan in 1967 [17] and Rai in 1974 [39]. These vibrations being superimposed on any steady pull that may be generated. In addition to these low frequency vibration components, rotor eccentricity is also known to cause noise. The causes of machine noise were extensively reviewed by Ellison and Moore [26] and further work on noise due to eccentricity was carried out by Ellison and Yang [31][45]. Cameron et al continued this theme using high frequency noise to detect rotor eccentricity [60][64][69].

Swann in 1963 [13] gave an interesting solution of a series connected machine with a blank, eccentric rotor. He used a conformal transformation of two eccentric circles to two concentric circles, hence transforming a machine with eccentric rotor and symmetrical windings to one with a concentric rotor but asymmetrical windings. Once the field is solved in the latter it can be mapped back to the former.

It is well known that parallel paths in the stator windings can lead to a large reduction in UMP but can have a detrimental effect by increasing vibration under certain conditions. Krondl in 1956 [9] and Harlin in 1965 [14] attempted to assess this phenomenon but these seem to be isolated cases. Only recently have techniques

existed to analyse parallel stator windings with an offset rotor successfully [72] [73] using a finite element analysis. However, this method is still extraordinarily time consuming requiring the whole machine to be modelled.

The rotating field method of modelling the machine is the most common way of predicting UMP. Jordan [10][17][35][47][49][50] published many papers with various authors which detail this. Jordon also attempted a model of a cage rotor, one of the few authors to do so, its damping effect on the UMP being very difficult to calculate. These papers covered many different aspects of UMP. The airgap permeance was represented by a constant plus a sinusoidal component, leading to modulation of the fundamental rotating field and hence UMP. The airgap permeance is, in fact, an infinite series (which is well illustrated by Enslin [46]) although most authors reduce this to the first harmonic term. This can be shown to be a poor approximation when the eccentricity is large. Jordan's papers show the two-pole machine to be a special case where a "homopolar flux" can exist. This flux crosses the airgap only once and returns via the shaft and casing. However, using a permeance approach leads to the conclusion that homopolar flux could exist in any machine but is most likely to be significant in two-pole motors. The phenomenon was reported by Crawford [28] and investigated by Kovacs in 1977 [41]. Belmans et al studied the effects of homopolar flux on 2-pole machines in great detail in the 1980's [49][50][52][55][58][61][62][63][68]. These papers, together with that of Fruchtenicht [47] also brought out the idea of dynamic UMP in flexible shaft machines being treated as a negative spring constant.

Frohne [16][19][20] carried out an extensive study, highlighting how different field harmonics are generated by the rotor being eccentric. He goes on to show that UMP is produced by the interaction of two fields having a pole-pair number differing by one. Schuisky [32] produced an interesting report stating that the field harmonics are damped by the rotor to differing degrees depending on their pole number. He follows this by investigating the effect of slip on the harmonic field damping.

Kucera [29] and Abdel-Kader [54] took a different approach and considered the effect of an eccentric rotor on the output torque and power. Stringer [23] introduced the problem of shaft voltages caused by homopolar flux and the damage that can occur in bearings due to the resultant circulating current. Akiyama [40] investigated the

non-uniform nature of machine heating when the rotor is eccentric. Wright et al [51] concentrated on the effect of UMP on critical speeds of flexible shaft machines, showing a large reduction in critical speed when the rotor is eccentric. This was also investigated by Belmans et al [56][61].

A technique for representing rotating fields as space vectors was put forward by Stepina in 1970 [30]. Another space vector method developed more thoroughly by Eastham and Williamson [37] and furthered by Williamson and Smith [48] allowed the calculation of an impedance matrix defining all stator and rotor currents and fields. This method was successfully implemented for the prediction of UMP caused by broken rotor bars [57][66][67]. This problem was also modelled using finite element analysis by Ito et al [43].

The number of different analyses available lead to contradicting results. Many of the early methods of calculating UMP were tested by von Kaehne in 1962 [11] and reviewed by Binns and Dye in 1972 [36]. The validation of any method is experimental verification, especially with techniques that make many assumptions and approximations. The main difficulty however remains the inability to measure UMP to any reasonable degree of accuracy. Some researchers measure the airgap flux using search coils and assume the magnitude of the UMP will be that calculated using Maxwell stresses [34][36]. However, it is usually only the forces normal to the surface which are considered, the tangential component being assumed negligible. There is also the case of unbalanced magnetic push [24][25], where conductors are pushed towards the bottom of a slot. Again, this is assumed to be negligible.

The most intensive experimental studies of UMP were carried out by the Electrical Research Association [15][21][22][33][38][39]. They put a lot of effort into building equipment to measure the eccentricity of the motor accurately and fabricated bearing housings with strain gauges to measure the UMP. Static and dynamic UMP of a series connected six-pole motor which could have either a blank, wound or cage rotor were investigated with this test rig. Whilst they attempted to predict UMP for the blank and wound rotor, no cage rotor predictions were made. One of the main conclusions from this work was the effect of saturation on the UMP. If the stator voltage is increased the UMP increases as voltage squared until the machine is

run overvoltage at which point the UMP begins to level out and eventually begins to reduce as the machine saturates. It was also found that the cage rotor damped the UMP significantly. This study offers the best available experimental data into UMP caused by rotor eccentricity and is often quoted, the results even used directly for comparison [69]. Other experimental investigations [18][27] use static machines with DC currents flowing in the windings to represent a snap-shot in time. The forces acting on the rotor are then measured using load cells supporting the rotor. The relevance of stationary tests where there are no moving fields is somewhat limited. Belmans et al [61][62][68] measured the offset of the rotor due to dynamic eccentricity, using the assumption of dynamic UMP acting as a negative spring constant to relate the degree of rotor offset to the UMP. Some successful experimental investigations, where UMP is measured directly, use piezo-electric transducers in the form of a mounting table where forces in three directions can be measured. By mounting the stator on the table and supporting the rotor seperately then the forces between the stator and rotor can be measured with ease. This method has been used to observe the UMP due to broken rotor bars [57][66][67] and due to pole changing [70][71].

## 1.4 Project Development

The survey of literature indicated several aspects of UMP due to rotor eccentricity which still remain unclear. Generally these amount to the development of a clear analytical solution of a cage induction motor in which stator winding connections and the influence of the rotor currents can be taken into account. This would necessitate the calculation of all machine currents from which the various field components and hence UMP can be calculated.

The winding analysis developed by Eastham and Williamson [37] and Williamson and Smith [48] gives a flexible method to analyse any machine winding. This can be used in conjunction with either the conformal transformation method [13] or the permeance harmonic technique [46] in order to model the eccentric airgap. The modelling of both static and dynamic eccentricity together would produce an excessively complicated model. It was therefore decided to concentrate on static eccentricity.

This would ensure that the experimental equipment was reasonably straightforward to construct since the rotor could use bearings already fitted and it would not need heavy rebalancing to counteract rotation off its own axis.

The initial stages of the project were directed towards the development of models of the machine with stator windings only. This was done using both conformal transformation and permeance harmonic methods. These were compared and verified experimentally.

The permeance harmonic technique was further developed to include the cage rotor. The main advantage of this approach was its ability to produce analytical expressions for the field harmonics and UMP. From this the influence of higher harmonics could be assessed, a point neglected in literature. Rotor skew could also be taken into account with this method. This model was again verified experimentally.

# Chapter 2

# Machine Analysis

## 2.1 Introduction

The usual definition of static eccentricity describes the rotor as turning about its own axis with the stator and rotor axes parallel rather than coincident (fig. 2.1). The harmonic conductor density method of analysing machine windings [48] was implemented to allow the calculation of currents in individual coil groupings and rotor bars and is described in this chapter. The analysis can be used in two ways when dealing with a rotor which is not concentric with the stator. The machine can be transformed from a machine with an eccentric rotor to one with a concentric rotor by means of a conformal transformation. This transforms the machine from one which has electric symmetry but magnetic asymmetry to one which has magnetic symmetry but electric asymmetry when considering the geometry of the electric and magnetic circuits. The ability of the harmonic conductor density method to analyse asymmetrical windings makes this a suitable approach to the problem. The alternative is to assume the airgap can be represented as a harmonic series, from which a set of permeance waves are produced. These modulate the flux density harmonics (produced when the rotor is centred) to produce harmonics both above and below the fundamental. The harmonic conductor density method expresses the current density as a spatial series, allowing permeance modulation when obtaining the airgap flux density distribution.

Initially, the project developed models using both the conformal transformation

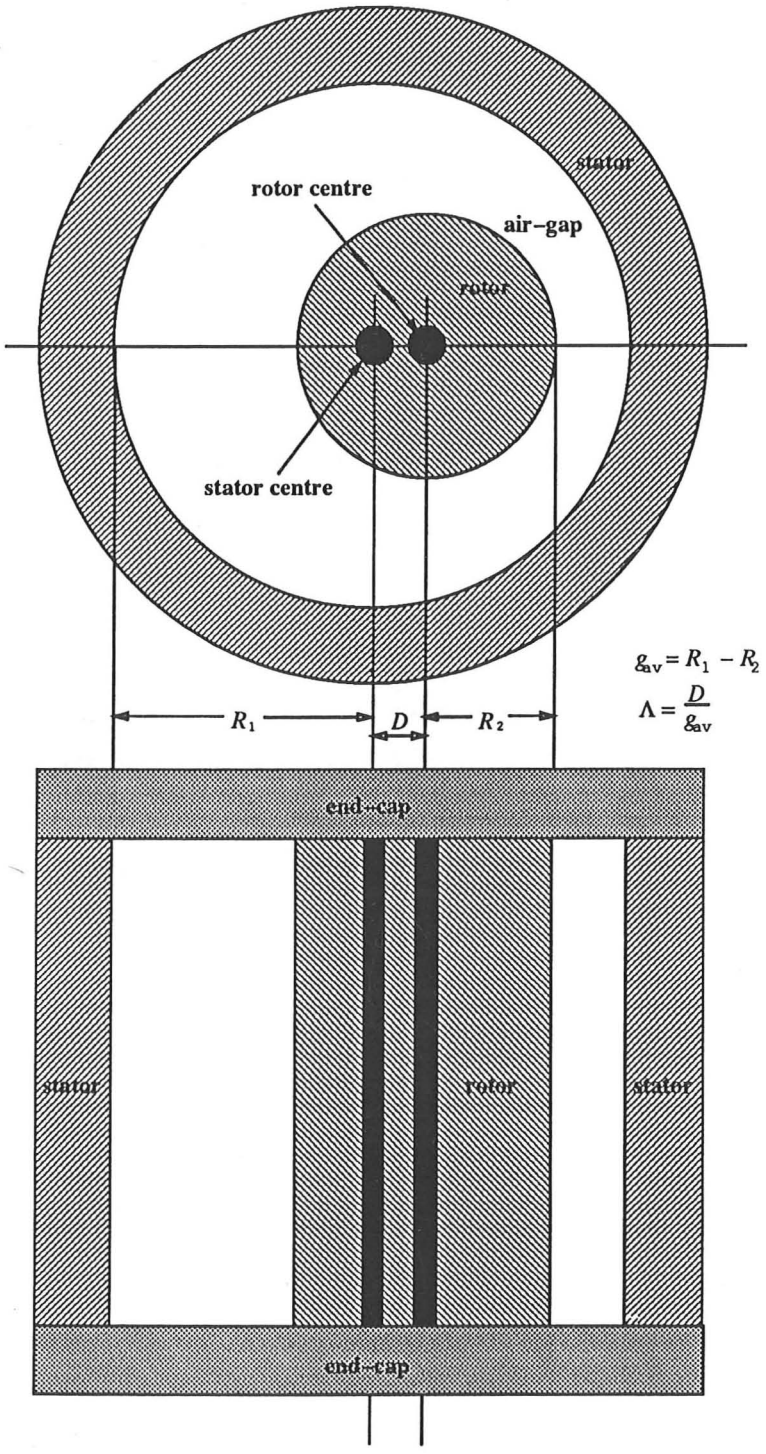


Figure 2.1: Rotor Positioning in Stator

technique and the permeance harmonic technique for the stator windings (the rotor being considered as being a laminated blank). The conformal transformation algorithm was more straightforward to implement. However it was necessary to use numerical methods to obtain the flux density distribution and hence there was no analytic solution for UMP. The permeance method, on the other hand, gave direct expressions for the flux density distribution but the algorithm was more cumbersome.

The permeance method was also considered easier to develop to include a rotor model since, when using the conformal transformation, the positioning of the slots on the rotor as it rotates will be continually changing. Coupling this with the advantage of analytical expressions for the flux density distribution and UMP, then it was decided to concentrate on the permeance method for the full machine model with a cage rotor.

## 2.2 Coupling Impedence Method Using Harmonic Conductor Density Distribution

### 2.2.1 Introduction

In order to determine the UMP it is first necessary to calculate the currents flowing in the various stator windings and rotor bars. This can be done using the coupling impedence method.

Machine analysis breaks down the airgap flux density into a harmonic series of travelling waves with different pole numbers rotating in either direction. These are derived from the currents and the spatial positioning of the stator and rotor conductors, which can finally be expressed in the form of a harmonic Fourier series of surface current density distributions. These series will have both time and space components. The currents flowing in the machine conductors provide the time varying components, the space components can be obtained by taking the analysis one step further and considering the density of the winding conductors as a Fourier series. This leads to an expression for the conductor density distribution in terms

of a harmonic series and can be obtained using complex Fourier analysis to account for the magnitude and positioning of conductors on the stator and rotor surfaces. Whilst this is far too involved for hand calculations it is a reasonable computational proposition. This method has several advantages, the main one being that any asymmetrical winding can be considered. In addition to this, the electric field in the airgap can be derived and the e.m.f. induced into any winding calculated, leading to expressions for the coupling impedances between the various machine windings. These can be expressed in the form of an impedence matrix. The machine currents can be obtained from a knowledge of the applied voltages when the matrix is solved.

### 2.2.2 Harmonic Conductor Density Distribution

The first stage of the analysis is to develop expressions which can take into account any stator winding and the rotor bars. In a machine with asymmetrical windings, fields will be produced which may have sub-fundamental machine pole-numbers. It is therefore important to work from a fundamental pole-number of two, even though the actual pole-number of the machine may be higher. All fields produced will then be integral harmonics of the fundamental. To accommodate parallel connection of the stator phase bands, each series group of coils has to be accounted for individually. Connecting phase bands in parallel is often done by manufacturers and allows operation at a reduced voltage and it is also known to reduce UMP. Appendix A contains the derivation of an expression for the complex conductor density distribution of a winding on either the stator or rotor surface. The winding distribution of the $b^{th}$ phase band of the $a^{th}$ phase is

$$n_{b,a}(y) = \sum_{n=-\infty}^{\infty} \overline{N}^n_{b,a} e^{-jnky} \tag{2.1}$$

where the co-ordinate system used gives $y$ in the tangential direction around the airgap circumference, $z$ radially across the airgap and $x$ in the axial direction of the machine and

$$\overline{N}^n_{b,a} = \frac{1}{2\pi r} \sum_{w=1}^{N_w} k^n_s C_{b,a}(w) e^{jn\theta_w} \tag{2.2}$$

If the conductors are being considered as point filaments on the stator surface then the slot opening factor $k^n_s$ is taken as unity. The average air-gap radius is $r$, $\theta_w$ is

the angular position of the $w$th slot and $C_{b,a}$ is the number of series turns of the winding in the slot. The winding distribution for the rest of the phase bands are found in a similar manner.

The current flowing in the $b^{th}$ band of phase $a$ can be defined as

$$i_{b,a}(t) = \mathrm{Re}\left[\overline{I}_{b,a}e^{j\omega t}\right] \tag{2.3}$$

where $\omega$ is the supply frequency.

The current density distribution on the stator surface is then

$$j_s(y,t) = \mathrm{Re}\left[\sum_{n=-\infty}^{\infty}\sum_{b}\sum_{a}\overline{N}^{n}_{b,a}\overline{I}_{b,a}e^{j(\omega t - nky)}\right]. \tag{2.4}$$

The rotor cage can be analysed in a similar manner by considering two adjacent bars and the connecting end-ring segments to be one coil. This is also shown in appendix A.

In many machines the stator or rotor slots can be skewed. However in the analysis put forward in this chapter it is assumed that only the rotor slots are skewed. This leads to a further complication, the harmonic conductor density distribution in equation 2.1 has only tangential positioning of the conductors. Since a rotor slot will vary its position down the length of the machine if it is skewed then the axial variation the conductor positioning has to be accounted for. This is explained in more detail in appendix D.

The equation 2.1 uses a stator reference frame. Unless the machine is stalled, however, the rotor and stator will be rotating with respect to each other and a rotor reference frame has to be used when considering the cage model. The distance $y'$ indicates a tangential distance round the circumference of the rotor surface from a zero reference on the rotor. Refering to figure 2.2, the stator and rotor reference frames can be related as follows

$$y = y' + \left(\frac{\omega_r r}{p}\right)t \tag{2.5}$$

where $\omega_r$ is the rotor rotational speed, $p$ is the number of pole pairs and $r$ is the average air-gap radius. This gives

$$y = y' + \left(\frac{\omega_s\,(1-s)\,r}{p}\right)t \tag{2.6}$$

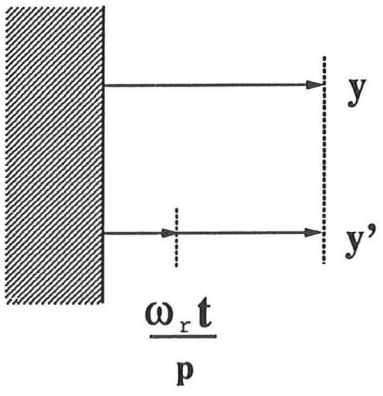


Figure 2.2: Rotor Co-ordinate Reference

where $\omega_s$ is the mains frequency and $s$ is the slip.

The expression for the $l^{th}$ rotor loop conductor distribution (including rotor skew - see appendix D) then becomes

$$n_{rl}(x, y') = \sum_{n=-\infty}^{\infty} \overline{N}_r^n e^{jn(l\lambda - ky')} e^{-jnx \tan\delta} \tag{2.7}$$

where $\lambda$ is the pitch between two adjacent bars and

$$\overline{N}_r^n = \frac{-jk_r^n sin\left(n\frac{\lambda}{2}\right)}{\pi r}, \tag{2.8}$$

where $k_r^n$ is rotor slot opening factor.

The rotor current density is then obtained by multiplying the loop density by the loop current. If the stator flux varies sinusoidally with $\nu$ pole-pairs, the e.m.f.'s induced into the loops will have a phase difference of $\nu\lambda$ radians between adjacent loops. Therefore, the $\nu^{th}$ current harmonic in the $l^{th}$ loop will be

$$i_l^\nu(t) = \mathrm{Re}\left[\overline{I}_r^\nu e^{j(\omega^\nu t - \nu l\lambda)}\right] \tag{2.9}$$

where the rotor current frequency is

$$\omega^\nu = \left(1 - \frac{\nu}{p}(1-s)\right)\omega_s. \tag{2.10}$$

Therefore, the $\nu^{th}$ harmonic current density of the $l^{th}$ rotor loop is

$$j_{rl}^\nu(x, y', t) = \mathrm{Re} \sum_{n=-\infty}^{\infty} \frac{-jk_r^n sin\left(n\frac{\lambda}{2}\right)}{\pi r} \overline{I}_r^\nu e^{j(\omega_\nu t + (n-\nu)l\lambda - nky')} e^{-jnkx \tan\delta}. \tag{2.11}$$

The total rotor current density for the $\nu^{th}$ harmonic can be obtained by summing the $\nu^{th}$ current in all the rotor loops

$$j_r^{\nu}(x,y',t) = \sum_{l=0}^{N_b-1} j_{rl}^{\nu}(x,y',t) \tag{2.12}$$

where $N_b$ is the number of bars.

This can be simplified using the summation in appendix B which produces

$$j_r^{\nu}(x,y',t) = \mathrm{Re} \sum_{\mu=-\infty}^{\infty} \overline{J}_r^{\nu,\mu} e^{j(\omega_\nu t-(\mu N_b+\nu)ky'-(\mu N_b+\nu)kx\tan\delta)} \tag{2.13}$$

where

$$\overline{J}_r^{\nu,\mu} = N_b \overline{N}_r^{\nu,\mu} \overline{I}_r^{\nu}. \tag{2.14}$$

Hence the complete $\nu^{th}$ harmonic rotor current density can be defined by the $\nu^{th}$ harmonic current flowing in just one loop.

The flux density produced by an unskewed current distribution can be calculated from Amperes law

$$b(y,t) = \int \mu_o \frac{j(y,t)}{g(y)}.\mathrm{d}y \tag{2.15}$$

and the electric field in the airgap

$$e(y,t) = \int \frac{\mathrm{d}b(y,t)}{\mathrm{d}t}.\mathrm{d}y \tag{2.16}$$

where $g(y)$ is the airgap length. The detailed expressions for the flux density and the electric field will be quite different between the conformal and permeance harmonic method and are described in their respective sections. Using the expressions for the electric field the coupling impedences can be calculated. The back e.m.f. induced in the $b^{th}$ band of phase $a$ is given by

$$u(t) = \mathrm{Re} \int_0^{2\pi r} -e(y,t) n_{b,a}(y) l.\mathrm{d}y \tag{2.17}$$

where $l$ is the effective stack length. If $e(y,t)$ is split into winding components then the e.m.f. induced into the $b^{th}$ band of phase $a$ by the $d^{th}$ band of phase $c$ is

$$u_{ba,dc}(t) = \mathrm{Re}\left[jX_{ba,dc}\overline{I}_{d,c}e^{j\omega t}\right]. \tag{2.18}$$

This expression is used to illustrate the approach in defining the coupling impedence, in this case between two phase bands . The coupling impedences between the rotor loops and the stator windings can be derived in a similar fashion.

### 2.2.3 Impedance Matrix Analysis

The previous section showed how the harmonic conductor density method can be used to obtain a set of coupling impedances. The first stage of the project assumed that the rotor was a laminated blank. Considering only the stator windings, the impedence matrix is defined as follows

$$\begin{bmatrix} \overline{v}_{1,1} \\ \cdots \\ \overline{v}_{b,a} \\ \cdots \\ \overline{v}_{B,A} \end{bmatrix} = \left[ \overline{\mathbb{Z}} \right] \begin{bmatrix} \overline{i}_{1,1} \\ \cdots \\ \overline{i}_{b,a} \\ \cdots \\ \overline{i}_{B,A} \end{bmatrix} \tag{2.19}$$

where

$$\left[ \overline{\mathbb{Z}} \right] = \begin{bmatrix} \overline{Z}_{11,11} & .. & jX_{11,ba} & .. & jX_{11,BA} \\ .. & .. & .. & .. & .. \\ jX_{ba,11} & .. & \overline{Z}_{ba,ba} & .. & jX_{ba,BA} \\ .. & .. & .. & .. & .. \\ jX_{BA,11} & .. & jX_{BA,ba} & .. & \overline{Z}_{BA,BA} \end{bmatrix} \tag{2.20}$$

The size of the impedence matrix will depend on the number of parallel windings used. If all the phase bands are connected in series then the matrix will be $3 \times 3$. The self impedence $\overline{Z}_{ba,ba}$ includes the leakage and winding resistance

$$\overline{Z}_{ba,ba} = R_b + jX_b + jX_{ba,ba} \tag{2.21}$$

The phase band currents can be related to the terminal line currents by a connection matrix and consideration of the mesh loop currents. The simplest case is shown in fig. 2.3

$$\left[\overline{I}\right] = [C] \left[\overline{I}_L\right] \tag{2.22}$$

where

$$\left[\overline{I}\right] = \begin{bmatrix} \overline{I}_1 \\ \overline{I}_2 \\ \overline{I}_3 \end{bmatrix}, \tag{2.23}$$

$$\left[\overline{I}_L\right] = \begin{bmatrix} \overline{I}'_1 \\ \overline{I}'_2 \end{bmatrix} \tag{2.24}$$

and

$$[C] = \begin{bmatrix} 1 & 0 \\ 0 & -1 \\ -1 & 1 \end{bmatrix}. \tag{2.25}$$

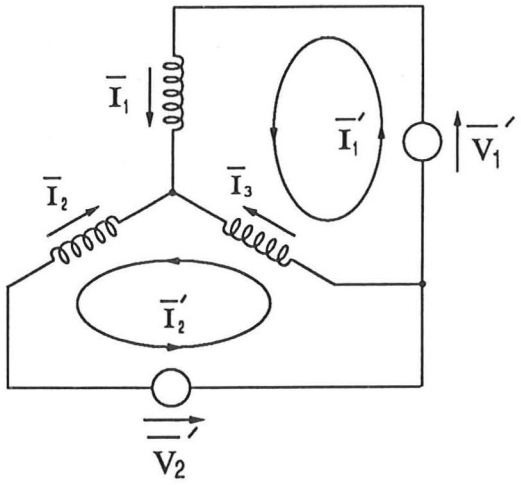


Figure 2.3: Series Connected Windings

This can be extended to cover any series/parallel winding combination by use of more loop currents. Similarly, the phase band voltages are

$$\left[\overline{V}_L\right] = [C]^T \left[\overline{V}\right]. \tag{2.26}$$

The only non-zero loop voltages will be the voltage sources of the balanced supply. This gives an effective impedance matrix

$$\left[\overline{Z}'\right] = [C]^T \left[\overline{Z}\right] [C] \tag{2.27}$$

such that

$$\left[\overline{V}_L\right] = \left[\overline{Z}'\right] \left[\overline{I}_L\right]. \tag{2.28}$$

The solution sequence to determine the stator currents is then as follows

**1** Calculate the impedance matrix $\left[\overline{Z}\right]$.

**2** Formulate the connection matrix and hence calculate the effective impedance matrix $\left[\overline{Z}'\right]$.

**3** Solve for the loop currents

$$\left[\overline{I}_L\right] = \left[\overline{Z}'\right]^{-1} \left[\overline{V}_L\right]. \tag{2.29}$$

**4** Solve for the phase band currents

$$\left[\overline{I}\right] = [C] \left[\overline{I}_L\right]. \tag{2.30}$$

The permeance harmonic method was extended to include the rotor loop currents. A matrix similar to that of 2.19 can be formed which includes the rotor harmonic currents

$$\begin{bmatrix} \overline{v}_{1,1} \\ \cdots \\ \overline{v}_{d,c} \\ \cdots \\ \overline{v}_{D,C} \\ 0 \\ \cdots \\ 0 \\ \cdots \\ 0 \end{bmatrix} = \left[ \overline{\mathrm{Z}} \right] \begin{bmatrix} \overline{i}_{1,1} \\ \cdots \\ \overline{i}_{d,c} \\ \cdots \\ \overline{i}_{D,C} \\ \overline{i}_{r}^{-\nu} \\ \cdots \\ \overline{i}_{r}^{0} \\ \cdots \\ \overline{i}_{r}^{\nu} \end{bmatrix} \tag{2.31}$$

where the impedance matrix can be partitioned into the various stator and rotor impedances

$$\left[ \overline{\mathrm{Z}} \right] = \begin{bmatrix} \mathrm{Z}_{s,s} & \mathrm{Z}_{s,r} \\ \mathrm{Z}_{r,s} & \mathrm{Z}_{r,r} \end{bmatrix}. \tag{2.32}$$

A connection matrix similar to that used previously can also be defined in order to link the terminal voltages to the stator windings. The most simple case of series stator connections is

$$\begin{aligned} \left[ \overline{\mathrm{I}} \right] &= \begin{bmatrix} & & 0 & .. & 0 & .. & 0 \\ & [C] & .. & .. & .. & .. & .. \\ & & 0 & .. & 0 & .. & 0 \\ 0 & 0 & 1 & .. & 0 & .. & 0 \\ .. & .. & .. & .. & .. & .. & .. \\ 0 & 0 & .. & .. & 1 & .. & .. \\ .. & .. & .. & .. & .. & .. & .. \\ 0 & 0 & 0 & .. & 0 & .. & 1 \end{bmatrix} \left[ \overline{\mathrm{I}}_L \right] \\ &= \left[ \mathrm{C}' \right] \left[ \overline{\mathrm{I}}_L \right] \end{aligned} \tag{2.33}$$

where the submatrix $[C]$ is defined by equation 2.25. The other non-zero terms are the diagonals. A similar equation for the loop voltages exists

$$\left[\overline{V}_L\right] = [C']^T \left[\overline{V}\right] \tag{2.34}$$

An impedance matrix can then be formed

$$\left[\overline{Z}'\right] = [C']^T \left[\overline{Z}\right] [C'] \tag{2.35}$$

The loop currents $\left[\overline{I}_L\right]$ and hence the phase band currents $\left[\overline{I}\right]$ can then be calculated in the same way as previously. All the stator phase-band currents and the

rotor harmonic currents have now been calculated. The particular derivations for obtaining the coupling impedances from the conformal transformation method and the permeance harmonic method will be described in the following sections.

## 2.3 Conformal Transformation Technique

### 2.3.1 Introduction

The conformal transformation method uses an inversion to transpose two circles which are eccentric to each other to a plane with two circles which are concentric. The position of the windings can also be plotted in the new plane to give a representation of a machine which has a constant airgap but asymmetrical windings. The windings themselves are considered as filament conductors on the stator surface. The nature of the mapping is such that the flux linkages between the two windings is the same whatever plane is considered. Hence the coupling impedances can be calculated in the T-plane (containing the concentric circles) in order to obtain the machine currents. However, the flux density in the T-plane plane has to be mapped back into the Z-plane (eccentric circles) in order to calculate the UMP since the flux density distributions between the two planes are different

### 2.3.2 The Conformal Transformation

The conformal transformation of two eccentric circles to two concentric circles utilises a simple inversion

$$\overline{z} = \frac{1}{\overline{t}}. \tag{2.36}$$

By finding a suitable values for $d$ in fig. 2.4 and $c$ in fig. 2.5 the eccentric rotor machine as represented by circles 1 and 2 in the Z-plane, can be mapped on the T-plane as two concentric circles ( 1 and 2 ). The Z-plane circles can be written as

$$\overline{z}_1 = d - D + R_1 e^{j\theta_z} \tag{2.37}$$

and

$$\overline{z}_2 = d + R_2 e^{j\theta_z}. \tag{2.38}$$

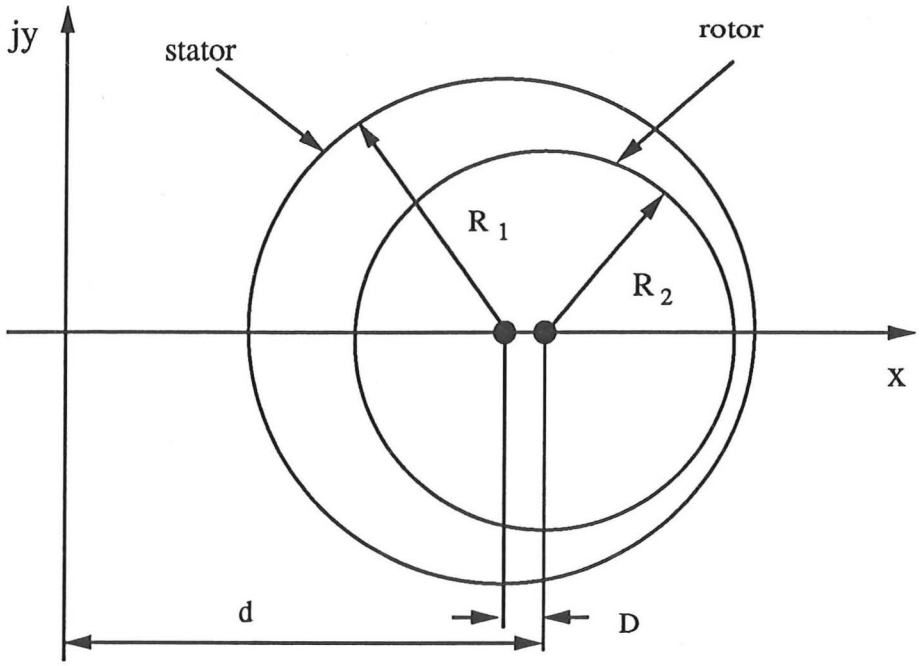


Figure 2.4: Z-Plane

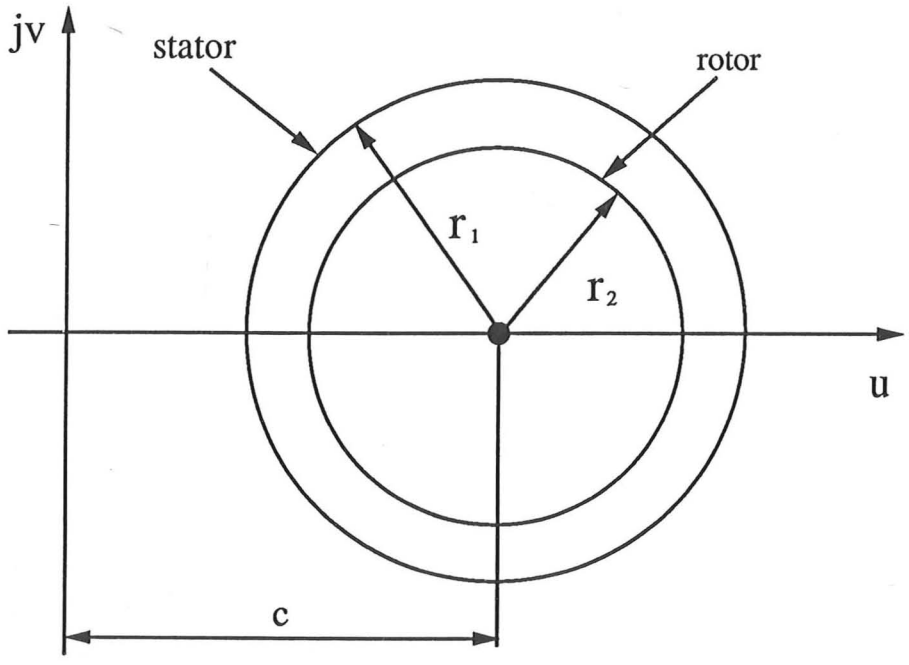


Figure 2.5: T-Plane

Similarly, for the T-plane circles

$$\bar{t}_1 = c + r_1 e^{j\theta_t} \tag{2.39}$$

and

$$\bar{t}_2 = c + r_2 e^{j\theta_t}. \tag{2.40}$$

The radius of the rotor can be written as

$$R_2 = |\bar{z}_2 - d|. \tag{2.41}$$

Since

$$\bar{t} = u + jv, \tag{2.42}$$

we can use the inversion to give

$$R_2 = \left| \frac{1}{u + jv} - d \right|. \tag{2.43}$$

Rearranging

$$\left( u - \frac{d}{d^2 - R_2^2} \right)^2 + v^2 = \left( \frac{R_2}{d^2 - R_2^2} \right)^2. \tag{2.44}$$

This is the equation of circle 2 in the T-plane, where

$$r_2 = \frac{R_2}{d^2 - R_2^2} \tag{2.45}$$

and

$$c = \frac{d}{d^2 - R_2^2}. \tag{2.46}$$

The equation for circle 1 can be obtained in a similar fashion

$$\left( u - \frac{d - D}{(d - D)^2 - R_1^2} \right)^2 + v^2 = \left( \frac{R_1}{(d - D)^2 - R_1^2} \right)^2 \tag{2.47}$$

where

$$r_1 = \frac{R_1}{(d - D)^2 - R_1^2} \tag{2.48}$$

and

$$c = \frac{d - D}{(d - D)^2 - R_1^2}. \tag{2.49}$$

The two equations for $c$ can be combined to give

$$d = \frac{D^2 + R_2^2 - R_1^2}{2D} \pm \sqrt{\left( \frac{D^2 + R_2^2 - R_1^2}{2D} \right)^2 - R_2^2}. \tag{2.50}$$

Of the two solutions for $d$, one will give $r_1 > r_2$. The stator windings are considered as point filaments on the outer circle and can be re-located in the T-plane using the simple inversion relationship. The T-plane circles can now be centred on the origin (by subtracting $c$) and the air-gap $g$ for the concentric rotor machine is then defined as $r_1 - r_2$.

The flux density distribution round the stator surface is different in the Z- and T-planes but, due to the re-location of the windings by the transform, the flux linkage between windings is the same whether it is in the T- or Z-plane. The machine now represented in the T-plane can be used to determine an impedance matrix linking the stator currents and terminal voltages.

### 2.3.3 Derivation of Coupling Impedances

The harmonic conductor density distribution can be found in the T-plane for each series winding using equation 2.1 producing the stator current density defined by equation 2.4. It should be noted that slot opening factors $k_s^n$ are taken as unity since the slots are represented as point filaments on the stator surface.

If we assume that the airgap is small compared to the diameter then we can assume that the flux crosses the air-gap radially (fig. 2.6) and applying Ampere's law in the T-plane gives

$$\frac{g}{\mu_o}\left(b(y,t) + \frac{\delta b(y,t)}{\delta y}\Delta y - b(y,t)\right) = j_s(y,t)\Delta y \tag{2.51}$$

from which

$$\mathrm{d}b(y,t) = \frac{\mu_o}{g} j_s(y,t).\mathrm{d}y \tag{2.52}$$

giving

$$b(y,t) = \mathrm{Re}\left[\sum_{n=-\infty}^{\infty}\sum_{b}\sum_{a}\overline{B}_{b,a}^{n} e^{j(\omega t - nky)}\right] \tag{2.53}$$

where

$$\overline{B}_{b,a}^{n} = -\frac{j\mu_o}{nkg}\overline{N}_{b,a}^{n}\overline{I}_{b,a}. \tag{2.54}$$

and $k$ is the inverse of the average T-plane airgap radius and $g$ is the T-plane airgap length.

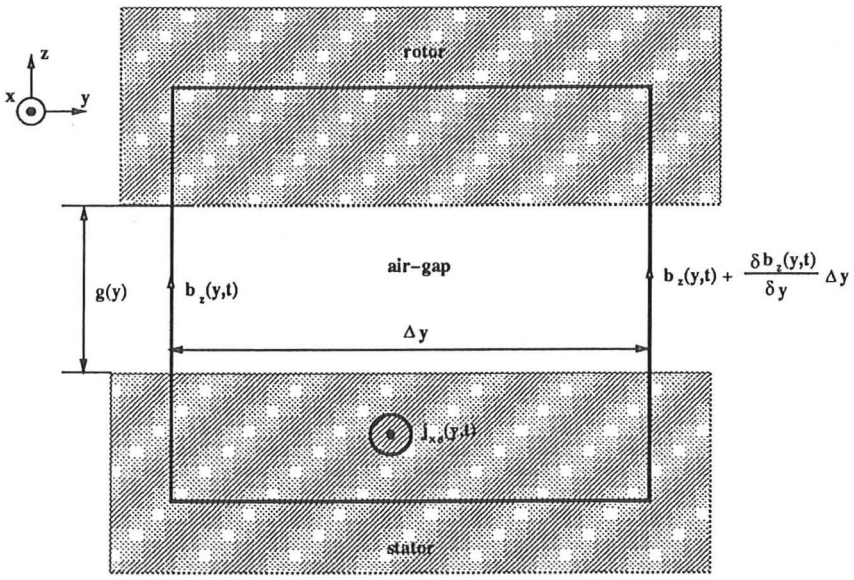


Figure 2.6: Ampere's Law

The flux density varies in the tangential direction and therefore the electric field varies axially. From

$$\mathrm{Curl}E = -\frac{\mathrm{d}b}{\mathrm{d}t} \tag{2.55}$$

then

$$e(y,t) = \int \frac{\mathrm{d}b}{\mathrm{d}t}.\mathrm{d}y. \tag{2.56}$$

Hence, the axial electric field strength in the air-gap is

$$e(y,t) = \mathrm{Re}\left[\sum_{n=-\infty}^{\infty}\sum_{b}\sum_{a}\overline{E}^{n}_{b,a}e^{j(\omega t - nky)}\right] \tag{2.57}$$

where

$$\overline{E}^{n}_{b,a} = -\frac{\omega\overline{B}^{n}_{b,a}}{nk}. \tag{2.58}$$

The back e.m.f. induced in the $b^{th}$ band of phase $a$ is

$$u(t) = \mathrm{Re}\int_{0}^{2\pi r} -e(y,t)\overline{n}_{b,a}(y)l.\mathrm{d}y \tag{2.59}$$

where $l$ is the effective stack length. The magnetising reactance of the $b^{th}$ phase band of phase $a$ can now be defined from equation 2.59 as follows

$$u_{ba,ba}(t) = \mathrm{Re}\left[jX_{ba,ba}\overline{I}_{b,a}e^{j\omega t}\right]. \tag{2.60}$$

In a similar fashion the mutual coupling between the $b^{th}$ phase band of phase $a$ by the $d^{th}$ phase band of phase $c$ is

$$u_{ba,dc}(t) = \mathrm{Re}\left[jX_{ba,dc}\overline{I}_{d,c}e^{j\omega t}\right]. \tag{2.61}$$

This defines the mutual reactance as follows

$$X_{ba,dc} = \sum_{n=-\infty}^{\infty} \frac{2\pi\omega\mu_o lr}{(nk)^2 g}\overline{N}_{d,c}^{n}\overline{N}_{b,a}^{*n}. \tag{2.62}$$

The self impedances have phase band resistance and leakage inductance terms added to them as shown in equation 2.21.

The phase band currents can now be calculated. However equation 2.53 gives the flux density distribution in the T-plane. In order to calculate the UMP it is necessary to know the flux density distribution in the Z-plane and a mapping technique has to be used to determine this. Hence an analytical solution UMP is not available when using the conformal technique. The mapping is given in chapter 3 where the UMP calculation methods are described.

## 2.4 Permeance Harmonic Analysis

### 2.4.1 Introduction

The permeance harmonic method is somewhat more involved than the conformal transformation method because of the inclusion of the rotor cage. Also, the stator model includes a double summation: a winding harmonic summation and a permeance harmonic summation. The conformal transformation stator model on the other hand only has a winding harmonic summation. However this drawback is offset by the fact that a conformal mapping technique is not required and that a direct expression for the airgap flux density is available.

It is first necessary to obtain an expression for the permeance harmonics in a convenient form. They can then be incorporated into the algorithm when applying Ampere's law, leading to an expression for the flux density and hence obtaining expressions for the coupling impedences. The field can be resolved not only into

distinct harmonics but also into distributions produced by either the stator currents or the rotor currents. This is important because of the influence of rotor skew on the field distribution. This is investigated further in chapter 3.

An added complication is the appearance of homopolar flux in the algorithm, i.e. flux density terms which vary in time only. This appears during the integration of the current density when applying Ampere's law. The two-dimensional analysis used for the conformal transformation gives no homopolar flux. The flow of homopolar flux relies on a good flux path between the rotor and stator which does not include the airgap. The analysis has to be developed to take this into account.

### 2.4.2 Airgap Permeance Harmonics

The air-gap can be described by the following equation (provided $D$ is much less than the stator radius)

$$g(\theta) = g_{av}\,(1 - \Lambda cos\theta) \tag{2.63}$$

as described in appendix C.

The angle $\theta$ is the angular distance from the point of narrowest airgap, $g_{av}$ is the average air-gap length and $\Lambda g_{av}$ is the distance between the rotor and stator axes.

The permeance is defined as the inverse of the airgap length and can be expressed as a Fourier series

$$\frac{1}{g_{av}(1 - \Lambda cos\theta)} = \frac{1}{g_{av}\sqrt{1-\Lambda^2}}\left[1 + 2\sum_{m=1}^{\infty} p^m cos(m\theta)\right] \tag{2.64}$$

where

$$p = \frac{1 - \sqrt{1-\Lambda^2}}{\Lambda}. \tag{2.65}$$

Putting this into exponential form

$$\frac{1}{g_{av}\,(1 - \Lambda cos\theta)} = \frac{1}{g_{av}}\sum_{m=-\infty}^{\infty} Q(m)e^{jm\theta} \tag{2.66}$$

where $m = -\infty, \cdots -1, 0, 1, \cdots \infty$, and

$$Q(m) = \frac{p^{|m|}}{\sqrt{1-\Lambda^2}}. \tag{2.67}$$

If the machine is linearised by replacing the angle $\theta$ by a distance $y$ around the air-gap then the permeance series can be described as follows

$$\overline{\Delta}(y) = \frac{1}{g_{av}} \sum_{m=-\infty}^{\infty} Q(m) e^{jmky}. \tag{2.68}$$

The permeance series also has to be expressed in rotor co-ordinates (from equation 2.6) so Ampere's law can be applied to the rotor cage using the rotor reference frame

$$\overline{\Delta}(y', t) = \frac{1}{g_{av}} \sum_{m=-\infty}^{\infty} Q(m) e^{jm\left(ky' + \frac{\omega_s(1-s)}{p}t\right)}. \tag{2.69}$$

### 2.4.3 Stator Airgap Flux Distribution

If Ampere's Circuital Law is applied to fig. 2.7 with the stator windings only then

$$\left(b_s(y,t) + \frac{\delta b_s(y,t)}{\delta y}\Delta y\right)\left(g(y) + \frac{\delta g(y)}{\delta y}\Delta y\right) - b_s(y,t)g(y) = \mu_o j_s(y,t)\Delta y \tag{2.70}$$

This assumes that the iron is infinitely permeable and that flux is considered to be flowing in the radial ($z$) direction only (as with the case of the conformal transformation method). Expanding and letting $\Delta y$ tend to zero we get

$$b_s(y,t)\frac{\delta g(y)}{\delta y} + \frac{\delta b_s(y,t)}{\delta y} g(y) = \mu_o j_s(y,t) \tag{2.71}$$

This equation can be applied to a machine with a non-uniform air-gap. Equation 2.71 can be written as

$$\frac{\mathrm{d}\left(b_s(y)g(y)\right)}{\mathrm{dy}} = \mu_o j_s(y,t) \tag{2.72}$$

which gives

$$b_s(y,t) = \frac{1}{g(y)}\left[\int \mu_o j_s(y,t)\mathrm{d}y + \overline{C}(t)\right] \tag{2.73}$$

where $\overline{C}(t)$ is the constant of integration. Using the permeance expression from equation 2.68

$$b_s(y,t) = \overline{\Delta}(y)\left[\int \mu_o j_s(y,t)\mathrm{d}y + \overline{C}(t)\right] \tag{2.74}$$

Combining equations 2.74 and 2.4 gives

$$b_s(y,t) = \mathrm{Re} \sum_{m=-\infty}^{\infty} \sum_{n=-\infty}^{\infty} \overline{B}_s^{m,n} e^{j(\omega t - k(n-m)y)} + \overline{\Delta}(y)\overline{C}(t) \tag{2.75}$$

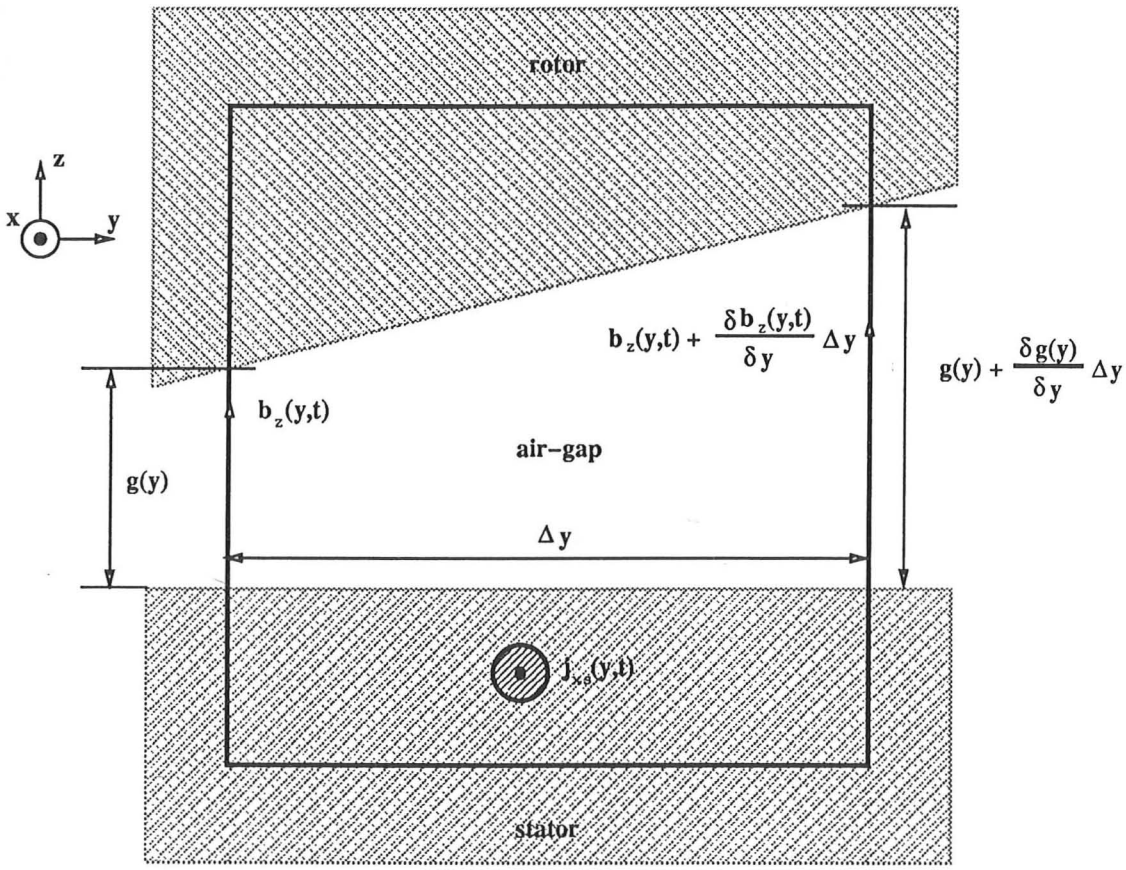


Figure 2.7: Amperes Law Applied to a Non-Uniform Air-Gap

where

$$\overline{B}_s^{m,n} = \frac{j\mu_o}{g_{av}} \sum_b \sum_a \frac{Q(m)}{kn} \overline{N}_{b,a}^n \overline{I}_{b,a}. \tag{2.76}$$

It can be seen that in equation 2.75 there exists a harmonic component of flux density which varies in time only. This crosses the air-gap only once and has to find an alternative path back to the stator. This is referred to as a "homopolar flux". The main path of the homopolar flux from the rotor to the stator is via the rotor shaft, bearings and machine casing. The reluctance of this circuit will be very dependent on the particular machine. The analysis therefore has to be extended to allow for this. This is done by choosing a suitable value for the constant of integration $\overline{C}(t)$. The conformal transformation method assumes this to be zero. To obtain no homopolar flux the first part of equation 2.75 is integrated with respect to $y$ over the interval $2\pi r$

$$\overline{\Phi}(t) = 2\pi r l \sum_{n=-\infty}^{\infty} \overline{B}_s^{m,n} e^{j\omega t}\Big|_{m=n} \tag{2.77}$$

where $l$ is the effective stack length.

This must be equal and opposite to the integral of the second part of equation 2.75

$$\frac{Q(0)\overline{C}(t)}{g_{av}} = -\sum_{n=-\infty}^{\infty} \overline{B}_s^{m,n} e^{j\omega t}\Big|_{m=n}. \tag{2.78}$$

It is interesting to note that, if equation 2.77 is re-arranged, then

$$\overline{F}_h(t) = R_g \overline{\Phi}(t) \tag{2.79}$$

where $\overline{F}_h(t)$ is an m.m.f. and $R_g$ is the magnetic reluctance of the homopolar flux path.

The integration constant $\overline{C}(t)$ will not change the reluctance but will control the driving m.m.f. of the homopolar flux. Considering the homopolar flux terms only, equation 2.75 can be expressed as follows

$$b_s(t) = \frac{\mu_o}{g_{av}} \left(\overline{F}_h(t) - \overline{F}'_h(t)\right) \tag{2.80}$$

where $b_s(t)$ is the airgap homopolar flux density, $\overline{F}_h(t)$ is the m.m.f. derived from the first term of equation 2.75 and $\overline{F}'_h(t)$ is the m.m.f. derived from the integration constant of equation 2.75. If $b_s(t)$ is zero then we can combine equations 2.77

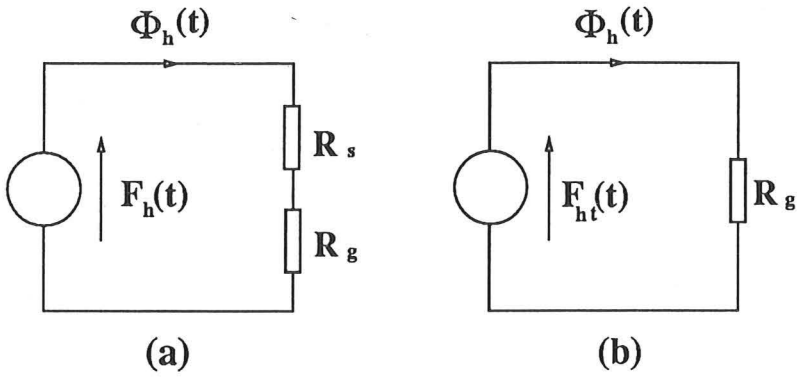


Figure 2.8: Homopolar Flux Magnetic Circuits

and 2.78

$$\overline{F}'_h(t) = \frac{g_{av}\overline{\Phi}(t)}{2\pi r l Q(0)\mu_o}. \tag{2.81}$$

$\overline{F}'_h(t)$ can be considered as a "back m.m.f." and must be equal to $\overline{F}_h(t)$ to prevent a homopolar flux. Equation 2.81 represents a magnetic circuit where the magnetic reluctance is

$$R_g = \frac{g_{av}}{2\pi r l Q(0)\mu_o}. \tag{2.82}$$

This is the magnetic reluctance of the air-gap. Considering figure 2.8(a), if there is an external reluctance $R_s$ in the homopolar flux path to represent the case, bearings etc. then this is equivalent to adjusting the driving m.m.f. of the flux in figure 2.8(b). If there is no homopolar flux then $\overline{F}_h(t) = \overline{F}'_h(t)$. If the homopolar flux path has a reluctance of $R_g$ and the external reluctance $R_s$ is zero then $\overline{F}'_h(t) = 0$. It is possible therefore, to relate $\overline{F}'_h(t)$ to $\overline{F}_h(t)$ as follows

$$\overline{F}'_h(t) = \alpha \overline{F}_h(t) \tag{2.83}$$

where $0 \leq \alpha \leq 1$.

The value of $\alpha$ is governed by $R_g$ and external reluctance $R_s$. In figure 2.8(a)

$$\overline{F}_h(t) = (R_g + R_s)\overline{\Phi}_h(t) \tag{2.84}$$

and figure 2.8(b)

$$\overline{F}_{ht}(t) = \overline{F}_h(t) - \alpha \overline{F}_h(t) = \overline{\Phi}_h(t) R_g. \tag{2.85}$$

Equating these gives

$$\alpha = \frac{R_s}{R_g + R_s}. \tag{2.86}$$

We can now define the air-gap flux density produced by the stator as

$$b_s(y,t) = \mathrm{Re} \sum_{m=-\infty}^{\infty} \sum_{n=-\infty}^{\infty} \left[ \overline{B}_s^{m,n} e^{j(\omega_s t - k(n-m)y)} + \overline{B}_{sh}^{m,n} e^{j(\omega_s t + kmy)} \right] \tag{2.87}$$

where

$$\overline{B}_{sh}^{m,n} = \frac{-\alpha Q(m) \overline{B}_s^{m',n}}{Q(0)} \qquad (m' = n) \tag{2.88}$$

The flux density distribution produced by the stator windings has now been completely defined.

### 2.4.4 Rotor Flux Density Distribution

Applying Ampere's law to equation 2.13, such that

$$b_r(x,y',t) = \overline{\Delta}(y',t) \left[ \int \mu_o j_r(x,y',t) \mathrm{d}y' + \overline{C}_r(t) \right] \tag{2.89}$$

this gives

$$b_r^{\nu}(x,y',t) = \mathrm{Re} \sum_{m=-\infty}^{\infty} \sum_{\mu=-\infty}^{\infty} \overline{B}_r^{m,\nu,\mu} e^{j((\omega^{\nu}+\omega^m)t + k(m-(\mu N_b+\nu))y' - k(\mu N_b+\nu)x\tan\delta)} + \overline{\Delta}(y',t)\overline{C}_r(t) \tag{2.90}$$

where

$$\overline{B}_r^{m,\nu,\mu} = \frac{j\mu_o Q(m)}{k g_{av} (\nu + \mu N_b)} N_b \overline{N}_r^{\nu,\mu} \overline{I}_r^{\nu} \tag{2.91}$$

and

$$\omega^m = \frac{m}{p}(1-s)\omega_s. \tag{2.92}$$

It can be seen that there may be homopolar fluxes produced which are not at supply frequency (when $\mu$ is not zero). They will be assumed to be negligible and will therefore be ignored. The only homopolar flux considered will be when $\nu = m$ and $\mu = 0$. Therefore, the complete equation can be expressed in a similar manner to equation 2.87

$$\begin{aligned} b_r^{\nu}(x,y',t) \;=\; & \mathrm{Re} \sum_{m=-\infty}^{\infty} \left[ \sum_{\mu=-\infty}^{\infty} \overline{B}_r^{m,\nu,\mu} e^{j((\omega^{\nu}+\omega^m)t + k(m-(\mu N_b+\nu))y' - k(\mu N_b+\nu)x\tan\delta)} \right. \\ & \left. + \overline{B}_{rh}^{m,\nu} e^{j((\omega_s+\omega^m)t+kmy')} \right] \end{aligned} \tag{2.93}$$

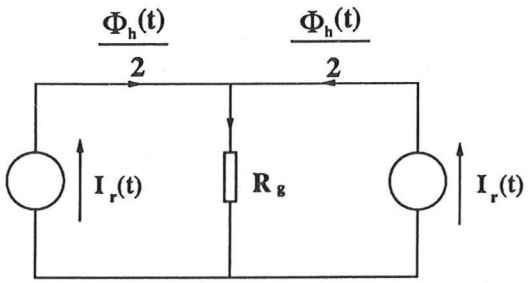


Figure 2.9: Magnetic Circuit of Rotor Homopolar Flux

where

$$\overline{B}_{rh}^{m,\nu} = \frac{-\alpha Q(m)\overline{B}_r^{m',\nu,\mu}}{Q(0)} \qquad (\mu = 0, m' = \nu). \tag{2.94}$$

It has already been shown that the stator and rotor produce homopolar fluxes by modulation of the poles by the permeance harmonics. These will link the rotor cage in such a manner that currents will be induced in the end-rings and not in the bars. This can be seen in figure A.2 and equation 2.9 where, if $\nu = 0$, the current in each rotor loop is the same. The result is that there will be no net current flow in the bars whilst there will be circulating currents in the end-rings. This represents current flowing in the $y'$ direction and the conductor density analysis has to be modified to take this into account. Consider figure 2.9, the path of the rotor homopolar flux can be represented by a magnetic circuit. The current $\overline{I}_r^0$ is the actual ring current but also includes other circulating currents in the core, shaft and casing. In addition there is the extra reluctance $R_s$ (as previously mentioned) to be taken into account (figure 2.8).

$$\overline{\Phi}_r(t) = \frac{\overline{I}_r^0}{R_g} \tag{2.95}$$

where $R_g$ is defined by equation 2.82. Therefore

$$\overline{B}_r(t) = \frac{\mu_o Q(0)\overline{I}_r^0(t)}{g_{av}}. \tag{2.96}$$

Including the permeance harmonics, this will give

$$b_r^\nu(y', t) = \mathrm{Re} \sum_{m=-\infty}^{\infty} \overline{B}_r^{m,\nu,\mu} e^{j((\omega_s+\omega^m)t+mky')} \qquad (\nu = \mu = 0) \tag{2.97}$$

Again, the external reluctance term can be added using $\alpha$ from equation 2.85. This gives

$$\overline{B}_r^{m,\nu,\mu} = \frac{(1-\alpha)\,\mu_o Q(m)}{g_{av}} \overline{I}_r^0 \quad (\nu = \mu = 0). \tag{2.98}$$

Equations 2.93 and 2.97 therefore define the rotor fields. The obvious constraint of equation 2.93 is that $\nu \neq 0$.

The airgap flux density distribution due to the stator and rotor currents has now been expressed and the coupling impedances can be found.

### 2.4.5 Stator-Stator Coupling Impedances

It can be seen from the previous section that the flux density distribution is described by a series including the homopolar flux terms. This leads to complicated expressions for the airgap electric field and hence the coupling impedences. However, the method of deriving these equations is still performed using

$$e(y,t) = \int \frac{\mathrm{d}b(y,t)}{\mathrm{d}t}.\mathrm{d}y. \tag{2.99}$$

This gives the airgap electric field due to the stator field as

$$e_s(y,t) = \mathrm{Re} \sum_{m=-\infty}^{\infty} \sum_{n=-\infty}^{\infty} \left[ \overline{E}_s^{m,n} e^{j(\omega_s t - k(n-m)y)} + \overline{E}_{sh}^{m,n} e^{j(\omega_s t + kmy)} \right] \tag{2.100}$$

where

$$\begin{aligned} \overline{E}_s^{m,n} &= \frac{\omega_s}{k(n-m)} \overline{B}_s^{m,n} \quad (n \neq m) \qquad (2.101) \\ &= j\omega_s \overline{B}_s^{m,n} y \quad (n = m) \end{aligned}$$

and

$$\begin{aligned} \overline{E}_{sh}^{m,n} &= \frac{\omega_s}{km} \overline{B}_{sh}^{m,n} \quad (m \neq 0) \qquad (2.102) \\ &= j\omega_s \overline{B}_{sh}^{m,n} y \quad (m = 0). \end{aligned}$$

From equation 2.59 the mutual coupling between the $b^{th}$ phase band of phase $a$ by the $d^{th}$ phase band of phase $c$ is

$$u_{ba,dc}(t) = \mathrm{Re}\left[ j X_{ba,dc} \overline{I}_{d,c} e^{j\omega t} \right]. \tag{2.103}$$

Defining the mutual reactance as in equation 2.18 using equations 2.100, 2.17, 2.102, 2.103, 2.76 and 2.88 we get

$$X_{ba,dc} = \frac{2\pi\omega_s r l \mu_o}{k^2 g_{av}} \sum_{m=-\infty}^{\infty} \sum_{n=-\infty}^{\infty} \left[ \frac{Q(m)}{n(n-m)} \overline{N}_{d,c}^{n} \overline{N}_{b,a}^{*(n-m)} \Big|_{n \neq m} \right.$$

$$- \alpha \frac{Q(m)Q(n)}{n(-m)Q(0)} \overline{N}_{d,c}^{n} \overline{N}_{b,a}^{*(-m)} \Big|_{m \neq 0}$$

$$\left. - (1-\alpha) \frac{Q(n)}{n} \sum_{n'=-\infty}^{\infty} \frac{1}{n'} \overline{N}_{d,c}^{n} \overline{N}_{b,a}^{*(n'-m)} \Big|_{n=m} \right]. \quad (2.104)$$

### 2.4.6 Rotor-Stator Coupling Impedances

The electric field produced by the stator currents will induce currents into the rotor. Equation 2.100 should be expressed therefore in rotor coordinates. The equation (2.17) used to calculate the back e.m.f.s induced into the rotor is modified to take into account rotor skew. The $\nu^{th}$ harmonic back e.m.f. induced into the $l = 0$ rotor loop by the $d^{th}$ band of the $c^{th}$ phase can be calculated from the equation

$$u^{\nu}(t) = \int_{-\frac{l}{2}}^{\frac{l}{2}} \int_{0}^{2\pi r} -e_s(y',t) n_{r0}(x,y').\mathrm{d}y'.\mathrm{d}x \quad (2.105)$$

where the stator electric field equation 2.100 is expressed in terms of the rotor co-ordinates $e(y',t)$ and skewing is included. Following the same procedure as described in the previous section gives

$$u^{\nu}(t) = \mathrm{Re}\left[ j X_{\nu,dc} \overline{I}_{dc} e^{j\omega^{\nu} t} \right] \quad (2.106)$$

where

$$X_{\nu,dc} = \frac{2\pi\omega_s \left(1 - \frac{\nu}{p}(1-s)\right) r l \mu_o}{k^2 g_{av}} \sum_{m=-\infty}^{\infty} \sum_{n=-\infty}^{\infty} \left[ \frac{Q(m) k_{sk}^{\nu}}{n\nu} \overline{N}_{d,c}^{n} \overline{N}_{r}^{*\nu} \Big|_{n \neq m}^{\nu=n-m} \right.$$

$$\left. - \alpha \frac{Q(m)Q(n)k_{sk}^{\nu}}{n\nu Q(0)} \overline{N}_{d,c}^{n} \overline{N}_{r}^{*\nu} \Big|_{m \neq 0}^{\nu=m} + (1-\alpha) \frac{jQ(n)}{2nr} \overline{N}_{d,c}^{n} \Big|_{n=m}^{\nu=0} \right] \quad (2.107)$$

This equation describes the mutual impedance between any stator winding and any rotor loop, including the end-rings.

The conclusion from this equation is that the harmonic currents induced in the rotor decrease as the pole number and skew increase. This will have an effect on the UMP since the stator harmonic fields are damped by the rotor.

### 2.4.7 Rotor-Rotor Coupling Impedances

The rotor-rotor coupling impedances can be calculated in a similar way to the stator-stator coupling impedances. Working in the rotor coordinate reference frame

$$e(x,y',t) = \int \frac{\mathrm{d}b(x,y',t)}{\mathrm{d}t}.\mathrm{d}y'. \tag{2.108}$$

Using the expressions derived in section 2.4.4 the rotor electric field is defined by

$$\begin{aligned} e_r^{\nu}(x,y',t) &= \mathrm{Re}\sum_{m=-\infty}^{\infty}\left[\sum_{\mu=-\infty}^{\infty}\overline{E}_r^{m,\nu,\mu}e^{j[(\omega^{\nu}+\omega^m)t+k(m-(\mu N_b+\nu))y'-k(\mu N_b+\nu)x\tan\delta]}\right. \\ &\left. + \overline{E}_{rh}^{m,\nu}e^{j((\omega_s+\omega^m)t+kmy')}\right]. \end{aligned} \tag{2.109}$$

where

$$\begin{aligned} \overline{E}_r^{m,\nu,\mu} &= -\frac{\omega^{\nu}+\omega^m}{k(\nu+\mu N_b-m)}\overline{B}_r^{m,\nu,\mu} \quad (\nu+\mu N_b \neq m) \\ &= j(\omega_s+\omega^m)\overline{B}_r^{m,\nu,\mu}y' \quad (\nu=m,\mu=0) \end{aligned} \tag{2.110}$$

and

$$\begin{aligned} \overline{E}_{rh}^{m,\nu} &= \frac{\omega_s+\omega^m}{km}\overline{B}_{rh}^{m,\nu} \quad (m\neq 0) \\ &= j\omega_s\overline{B}_{rh}^{m,\nu}y' \quad (m=0). \end{aligned} \tag{2.111}$$

The equation for the back e.m.f. induced in the $\nu' th$ loop harmonic is derived using the equation

$$u^{\nu'}(t) = \int_{-\frac{l}{2}}^{\frac{l}{2}}\int_0^{2\pi r} -e_r^{\nu}(x,y',t)n_{\nu'}(x,y').\mathrm{d}y'.\mathrm{d}x \tag{2.112}$$

The mutual reactance between the $\nu' th$ and the $\nu th$ rotor loop harmonics is then

$$
\begin{aligned}
X_{\nu',\nu} \;=\; & \frac{2\pi\omega_s\left(1-\frac{\nu'}{p}(1-s)\right) r l \mu_o}{k^2 g_{av}} \times \\
& \sum_{m=-\infty}^{\infty}\left[\sum_{\mu=-\infty}^{\infty}\frac{Q(m)k_{sk}^{m}}{(\nu'+\mu N_b)(\nu+\mu N_b)} N_b \overline{N}_r^{\nu,\mu}\overline{N}_r^{*\nu',\mu}\Bigg|_{\nu'+\mu N_b\neq 0,\nu+\mu N_b\neq 0}^{\nu'=\nu-m}\right. \\
& -\alpha\frac{Q(m)Q(\nu)k_{sk}^{(\nu'-\nu)}}{\nu'\nu Q(0)} N_b \overline{N}_r^{\nu}\overline{N}_r^{*\nu'}\Bigg|_{m\neq 0,\nu\neq 0}^{\nu'=-m} \\
& +(1-\alpha)\frac{jQ(m)k_{sk}^{m}}{2\nu r} N_b \overline{N}_r^{\nu}\Bigg|_{\nu=m\neq 0}^{\nu'=0} \\
& \left.+(1-\alpha)\frac{jQ(m)k_{sk}^{m}}{-\nu' r}\overline{N}_r^{*\nu'}\Bigg|_{\nu=0}^{\nu'=-m\neq 0} + (1-\alpha)\frac{Q(0)}{2r^2}\Bigg|_{\nu=0}^{\nu'=0}\right].
\end{aligned}
\tag{2.113}
$$

If $\nu' = \nu$ then a self inductance is defined. If $\nu \neq 0$ then the rotor loop impedance is modified by the effective bar and end-segment resistance and leakage reactance. Thus

$$
\overline{Z}_{\nu',\nu} = 2(R_b^{\nu} + R_{er}) + j(X_{\nu',\nu} + 2(X_b^{\nu} + X_{er})). \tag{2.114}
$$

The end-ring impedance becomes

$$
\overline{Z}_{0,0} = R_{er} + j(X_{0,0} + X_{er}). \tag{2.115}
$$

For any rotor harmonic loop current, the currents in the adjacent loops will have harmonic currents with equal magnitudes but with a phase shift of $\nu\lambda$. Using superposition of the loop currents the effective bar resistance and leakage reactance are defined by

$$
R_b^{\nu} = (1 - \cos(\nu\lambda))\, R_{bar} \tag{2.116}
$$

and

$$
X_b^{\nu} = (1 - \cos(\nu\lambda))\, X_{bar}. \tag{2.117}
$$

### 2.4.8 Stator-Rotor Coupling Impedances

The stator-rotor coupling impedances are determined using the reverse process of the rotor-stator impedance calculation and the equation

$$
u_{b,a}(t) = \int_{-\frac{l}{2}}^{\frac{l}{2}}\int_{0}^{2\pi r} -e_r^{\nu}(x,y,t) n_{b,a}(y).\mathrm{d}y.\mathrm{d}x. \tag{2.118}
$$

Equation 2.109 should be transposed to stator co-ordinates to obtain an expression for the rotor electric field $e_r^{\nu}(x,y,t)$ in the stator reference frame. The differential leakage components (i.e. when $\mu \neq 0$), which induce non-supply frequency harmonics are ignored in a similar manner to that of the non-supply frequency end-ring currents. This can be used to obtain an expression for the stator-rotor coupling impedances.

$$X_{ba,\nu} = \frac{2\pi\omega_s r l \mu_o}{k^2 g_{av}} \sum_{m=-\infty}^{\infty} \left[ \frac{Q(m)k_{sk}^{\nu}}{n\nu} N_b \overline{N}_r^{\nu} \overline{N}_{b,a}^{*n} \Big|_{\nu\neq m,\nu\neq 0}^{n=\nu-m} \right. \tag{2.119}$$
$$\left. - \alpha \frac{Q(m)Q(\nu)k_{sk}^{\nu}}{n\nu Q(0)} N_b \overline{N}_r^{\nu} \overline{N}_{b,a}^{*n} \Big|_{m\neq 0,\nu\neq 0}^{n=m} + (1-\alpha) \frac{jQ(n)}{-nr} \overline{N}_{b,a}^{*n} \Big|_{n=m}^{\nu=0} \right]$$

# Chapter 3

# Calculation of UMP

## 3.1 Introduction

The previous chapter derived expressions for the airgap flux density distribution of the machine. In the case of the conformal method this was in the plane containing the concentric rotor and stator. These expressions can be used to calculate the unbalanced magnetic pull of the machine by calculating the Maxwell stress round the surface of either the rotor or the stator. The Maxwell stress force acting normally to a point on the surface is

$$\sigma = \frac{1}{2\mu_o}\left(b_n^2 - b_t^2\right). \tag{3.1}$$

The tangential (shear) force is

$$\gamma = \frac{b_n b_t}{\mu_o}. \tag{3.2}$$

where $b_n$ is the flux density normal to the surface and $b_t$ is the flux density flowing at a tangent to the surface. It has been assumed that the flux density is normal to the surface. However, this is an approximation because it would lead to no torque being generated. If the square of the tangential component is still considered as negligible then

$$\sigma = \frac{1}{2\mu_o} b_n^2. \tag{3.3}$$

The influence of the shear stress on the UMP may be noticeable under high torque conditions.

## 3.2 Conformal Transformation Method

The flux density in the T-plane (concentric rotor, asymmetrical windings) is described analytically by equation 2.53. The flux density in the Z-plane (eccentric rotor) is obtained by mapping the flux density from one plane to another in a pointwise fashion. Any segment of the rotor surface $\delta\theta_z$ will have a flux $\delta\Phi_z$ crossing it. If this segment is mapped into the T-plane then the segment $\delta\theta_t$ will have a flux $\delta\Phi_t$ crossing it. By the nature of the mapping technique used

$$\delta\Phi_z = \delta\Phi_t. \tag{3.4}$$

We can then write

$$\frac{\delta\Phi_z}{\delta\theta_z} = \frac{\delta\Phi_t}{\delta\theta_t}\frac{\mathrm{d}\theta_t}{\mathrm{d}\theta_z} \tag{3.5}$$

or

$$b_z(y') = b_t(y)\frac{r_2\mathrm{d}\theta_t}{R_2\mathrm{d}\theta_z}. \tag{3.6}$$

where $y'$ is the distance around the rotor surface in the Z-plane.

Since

$$c + r_2e^{j\theta_t} = \frac{1}{d + R_2e^{j\theta_z}} \tag{3.7}$$

by rearranging and differentiating

$$\frac{\mathrm{d}\theta_t}{\mathrm{d}\theta_z} = -\frac{R_2e^{j\theta_z}}{r_2e^{j\theta_t}}\frac{1}{(d + R_2e^{j\theta_z})^2}. \tag{3.8}$$

Combining equations 2.53, 3.6, 3.7 and 3.8, the flux density can be found at any point on the rotor surface in the Z-plane.

Assuming the flux crosses the airgap radially and that there are no rotor currents, the Maxwell stress at any point on the rotor surface simplifies to

$$\sigma = \frac{b_z^2(y')}{2\mu_o}. \tag{3.9}$$

The net force along the x axis is then

$$F_x = \int_0^{2\pi r} \frac{b_z^2(y')}{2\mu_o} l\cos(k'y').dy'. \tag{3.10}$$

Similarly for the y axis

$$F_y = \int_0^{2\pi r} \frac{b_z^2(y')}{2\mu_o} l\sin(k'y').dy' \tag{3.11}$$

where $k'$ is the fundamental wave number in the Z-plane ( $\frac{1}{r}$ ).

Using Gaussian integration or by segmenting the surface and using linear approximations the UMP can then be calculated. In this study surface segmentation was used.

## 3.3 Permeance Harmonic Method

The permeance harmonic method leads to analytical expressions for the airgap flux density distribution. These can be manipulated to obtain expressions for the UMP. The tangential force can also be calculated by

$$\gamma = \frac{b_n b_t}{\mu_o}. \tag{3.12}$$

Consider figure 3.1, the tangential field strength on the stator surface is

$$\int \overline{H}.\mathrm{d}l = \overline{J}_s \Delta y \tag{3.13}$$

which becomes

$$-\overline{H_t}\Delta y = \overline{J}_s \Delta y \tag{3.14}$$

or

$$\frac{b_t(y,t)}{\mu_o} = -j_s(y,t). \tag{3.15}$$

This leads to the expression

$$\gamma = -b(x,y,t) j_s(y,t) \tag{3.16}$$

where $b(x,y,t)$ is the airgap flux density and is assumed to be normal to the stator surface. If the square of the tangential force is still assumed to be negligible then equation 3.1 simplifies to

$$\sigma = \frac{1}{2\mu_o} b^2(x,y,t) \tag{3.17}$$

The UMP is then calculated from

$$F_x = \int_{y=0}^{2\pi r} (\sigma \cos ky + \gamma \sin ky).\mathrm{d}y \tag{3.18}$$

and

$$F_y = \int_{y=0}^{2\pi r} (\sigma \sin ky - \gamma \cos ky).\mathrm{d}y \tag{3.19}$$

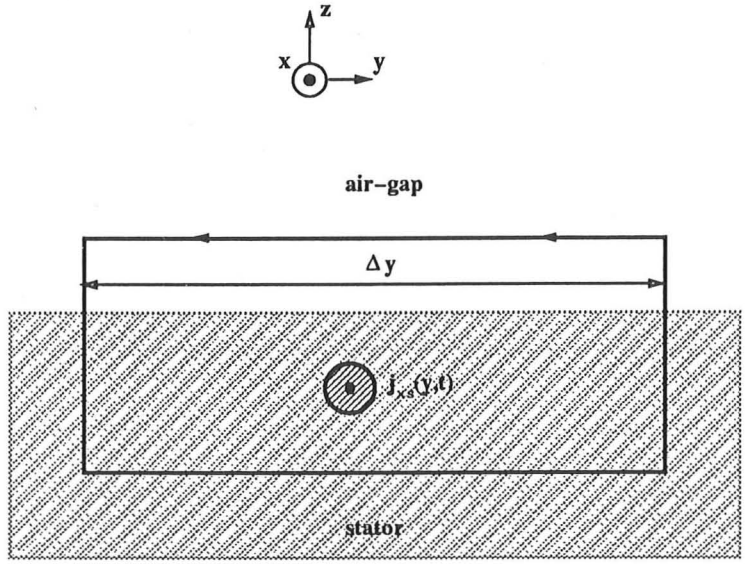


Figure 3.1: Tangential Field Strength

The airgap flux density is made up of rotor and stator fields such that

$$b(x,y,t) = b_s(y,t) + b_r(x,y,t) \tag{3.20}$$

therefore the force acting normally to the stator surface is

$$\sigma = \frac{1}{2\mu_o}\left(b_s^2(y,t) + b_r^2(x,y,t) + 2b_s b_r(x,y,t)\right) \tag{3.21}$$

$$= F_1 + F_2 + F_3 \tag{3.22}$$

where $F_1$, $F_2$ and $F_3$ the three force terms in the equation.

The stator field takes the form

$$b_s(y,t) = \mathrm{Re}\sum_{n=-\infty}^{\infty}\left[\overline{B}_s^n e^{j(\omega_s t - kny)}\right] \tag{3.23}$$

where $n = 0, \pm 1, \pm 2, \ldots$. The values of $\overline{B}_s^n$ can be calculated from equation 2.87. From this we get

$$b_s^2(y,t) = \mathrm{Re}\left[\frac{1}{2}\sum_{n=-\infty}^{\infty}\sum_{n'=-\infty}^{\infty}\left[\overline{B}_s^n \overline{B}_s^{n'} e^{j(2\omega_s t - k(n+n')y)} + \overline{B}_s^n \overline{B}_s^{*n'} e^{-jk(n-n')y}\right]\right]. \tag{3.24}$$

leading to the first force term $F_1$. Hence a steady state force plus a twice supply frequency vibrational force will be acting at any point on the stator surface. The

net force components of $F_1$ due to the stator field acting upon the stator in the direction of narrowest airgap and a direction perpendicular to this are therefore

$$\begin{aligned}
F_{1x} &= \int_{y=0}^{2\pi r} \frac{b_s^2(y,t)}{4\mu_o}\left(e^{-jky}+e^{jky}\right) l.\mathrm{d}y \\
&= \int_{y=0}^{2\pi r} \frac{l}{8\mu_o}\mathrm{Re}\left[\sum_{n=-\infty}^{\infty}\sum_{n'=-\infty}^{\infty} \times\right. \\
&\quad \left[\overline{B}_s^n \overline{B}_s^{n'} e^{j(2\omega_s t - k(n+n'+1)y)} + \overline{B}_s^n \overline{B}_s^{*n'} e^{-jk(n-n'+1)y}\right. \\
&\quad \left.\left. + \overline{B}_s^n \overline{B}_s^{n'} e^{j(2\omega_s t - k(n+n'-1)y)} + \overline{B}_s^n \overline{B}_s^{*n'} e^{-jk(n-n'-1)y}\right]\right].\mathrm{d}y \\
&= \frac{\pi r l}{4\mu_o}\mathrm{Re}\sum_{n=-\infty}^{\infty}\left[\left(\overline{B}_s^n \overline{B}_s^{-(n+1)} + \overline{B}_s^n \overline{B}_s^{-(n-1)}\right) e^{j2\omega_s t}\right. \\
&\quad \left. + \left(\overline{B}_s^n \overline{B}_s^{*(n+1)} + \overline{B}_s^n \overline{B}_s^{*(n-1)}\right)\right]. \qquad (3.25)
\end{aligned}$$

and

$$\begin{aligned}
F_{1y} &= \int_{y=0}^{2\pi R} \frac{b_s^2(y,t)}{4\mu_o}\left(je^{-jky} - je^{jky}\right) l.\mathrm{d}y \\
&= \frac{\pi r l}{4\mu_o}\mathrm{Im}\sum_{n=-\infty}^{\infty}\left[\left(\overline{B}_s^n \overline{B}_s^{-(n-1)} - \overline{B}_s^n \overline{B}_s^{-(n+1)}\right) e^{j2\omega_s t}\right. \\
&\quad \left. + \left(\overline{B}_s^n \overline{B}_s^{*(n-1)} - \overline{B}_s^n \overline{B}_s^{*(n+1)}\right)\right]. \qquad (3.26)
\end{aligned}$$

The general expression for UMP is also a steady force plus a twice supply frequency vibration in both directions.

The rotor field, when expressed in the stator co-ordinate system, produces components due to the differential fields leading to vibrations which are not at twice-supply frequency. These are of a much higher frequency and are assumed to negligible compared to the steady pull and twice-supply frequency vibration. Ignoring the differential fields, the rotor field is given by

$$b_r(x,y,t) = \mathrm{Re}\sum_{m=-\infty}^{\infty}\sum_{\nu=-\infty}^{\infty}\left[\overline{B}_r^{m,\nu} e^{j[\omega_s t + k(m-\nu)y - k\nu x\tan\delta]} + \overline{B}_{rh}^{m,\nu} e^{j(\omega_s t + kmy)}\right]. \qquad (3.27)$$

The rotor field components of the same pole number cannot be added together in the same way as the stator due to the skewing. However, this could be rewritten as

$$b_r(x,y,t) = \mathrm{Re} \sum_{\nu=-\infty}^{\infty} \sum_{m=-\infty}^{\infty} \left[ \overline{B}_r^{\nu',m} e^{j(\omega_s t - k\nu' y - k(\nu'-m)x \tan\delta)} \right] \tag{3.28}$$

which takes into account skewing of various fields with $m$ still representing the permeance harmonic series. The values of $\overline{B}_r^{\nu',m}$ can be calculated from equations 2.93 and 2.97. The UMP due to the second term is then defined as

$$\begin{aligned}
F_{2x} &= \int_{-\frac{l}{2}}^{\frac{l}{2}} \int_0^{2\pi r} \frac{b_r^2(x,y,t)}{4\mu_o} \left( e^{-jky} + e^{jky} \right) .\mathrm{d}y.\mathrm{d}x \\
&= \frac{\pi r l}{4\mu_o} \mathrm{Re} \sum_{\nu=-\infty}^{\infty} \sum_{m=-\infty}^{\infty} \sum_{m'=-\infty}^{\infty} \times \\
&\quad \left[ \left( \overline{B}_r^{\nu'} \overline{B}_r^{-(\nu'+1)} k_{sk}^{(m+m'+1)} + \overline{B}_r^{\nu'} \overline{B}_r^{-(\nu'-1)} k_{sk}^{(m+m'-1)} \right) e^{j2\omega_r t} \right. \\
&\quad \left. + \left( \overline{B}_r^{\nu'} \overline{B}_r^{*(\nu'+1)} k_{sk}^{(m-m'+1)} + \overline{B}_r^{\nu'} \overline{B}_r^{*(\nu'-1)} k_{sk}^{(m-m'-1)} \right) \right] .
\end{aligned} \tag{3.29}$$

and

$$\begin{aligned}
F_{2y} &= \int_{-\frac{l}{2}}^{\frac{l}{2}} \int_0^{2\pi r} \frac{b_r^2(x,y,t)}{4\mu_o} \left( je^{-jky} - je^{jky} \right) l.\mathrm{d}y.\mathrm{d}x \\
&= \frac{\pi r l}{4\mu_o} \mathrm{Im} \sum_{\nu=-\infty}^{\infty} \sum_{m=-\infty}^{\infty} \sum_{m'=-\infty}^{\infty} \times \\
&\quad \left[ \left( \overline{B}_r^{\nu} \overline{B}_r^{-(\nu-1)} k_{sk}^{(m+m'-1)} - \overline{B}_r^{\nu} \overline{B}_r^{-(\nu+1)} k_{sk}^{(m+m'+1)} \right) e^{j2\omega_s t} \right. \\
&\quad \left. + \left( \overline{B}_r^{\nu} \overline{B}_r^{*(\nu-1)} k_{sk}^{(m-m'-1)} - \overline{B}_r^{\nu} \overline{B}_r^{*(\nu+1)} k_{sk}^{(m-m'+1)} \right) \right] .
\end{aligned} \tag{3.30}$$

The UMP created by the third term can be derived in a similar manner to the first two terms

$$\begin{aligned}
F_{3x} &= \int_{-\frac{l}{2}}^{\frac{l}{2}} \int_0^{2\pi r} \frac{b_s(y,t) b_r(x,y,t)}{2\mu_o} \left( e^{-jky} + e^{jky} \right) .\mathrm{d}y.\mathrm{d}x \\
&= \frac{\pi r l}{2\mu_o} \mathrm{Re} \sum_{n=-\infty}^{\infty} \sum_{m=-\infty}^{\infty} \times
\end{aligned}$$

$$\left[\left(\overline{B}_s^n\overline{B}_r^{-(n+1)}k_{sk}^{(n+m+1)} + \overline{B}_s^n\overline{B}_r^{-(n-1)}k_{sk}^{(n+m-1)}\right)e^{j2\omega_r t}\right.$$

$$\left. + \left(\overline{B}_s^n\overline{B}_r^{*(n+1)}k_{sk}^{(n-m+1)} + \overline{B}_s^n\overline{B}_r^{*(n-1)}k_{sk}^{(n-m-1)}\right)\right] \tag{3.31}$$

and

$$F_{3y} = \int_{-\frac{l}{2}}^{\frac{l}{2}}\int_0^{2\pi r}\frac{b_s(y,t)b_r(x,y,t)}{2\mu_o}\left(je^{-jky} - je^{jky}\right).\mathrm{d}y.\mathrm{d}x$$

$$= \frac{\pi r l}{2\mu_o}\mathrm{Im}\sum_{n=-\infty}^{\infty}\sum_{m=-\infty}^{\infty}\times$$

$$\left[\left(\overline{B}_s^n\overline{B}_r^{-(n-1)}k_{sk}^{(n+m-1)} - \overline{B}_s^n\overline{B}_r^{-(n+1)}k_{sk}^{(n+m+1)}\right)e^{j2\omega_s t}\right.$$

$$\left. + \left(\overline{B}_s^n\overline{B}_r^{*(n-1)}k_{sk}^{(n-m-1)} - \overline{B}_s^n\overline{B}_r^{*(n+1)}k_{sk}^{(n-m+1)}\right)\right]. \tag{3.32}$$

These equations show that it is the interaction of two spatial harmonics with a pole-pair number varying by one which produce the UMP. The rotor and stator fields will be in near antiphase to each other, which means that the steady components of the first two terms will give UMP in the same direction. Hence these two terms will not give any UMP damping. The damping effects will be due to the third term since the UMP developed will act in the opposite direction to that of the first two terms. Bearing in mind that $m$ is the permeance harmonic number and can be expected to be zero or a low number, then skewing will not have a great effect on the second term. However, the third term has a skew factor which is a function not only of the permeance harmonic but also of a field harmonic number. This suggests that the higher stator harmonics will be damped by the skew to a lesser degree than the lower harmonics. However, it has to be remembered that the higher harmonic currents induced into the rotor will be negligible (even without skew) when the pole-pair number approaches the number of bars in the cage.

Similar methods can be used to work out the UMP due to the tangential forces using equations 3.12, 3.16, 3.18 and 3.19.

# Chapter 4

# Computer Implementation

## 4.1 Introduction

The implementation of the algorithms described in the previous two chapters involves the consideration of several important aspects. The infinite harmonic series used in the algorithms clearly have to be curtailed at a point when the solution has satisfied some predetermined convergence criterion. Estimations can be made by consideration of the permeance and winding harmonics, although the asymmetrical windings in the conformal transformation still relies on trial and error. Also, skin effect in the rotor bars has to be considered as well as slotting effects. Methods are detailed in this chapter to deal with these points.

## 4.2 Harmonic Convergence

### 4.2.1 Conformal Transformation Technique

The conformal transformation technique outlined in chapter two leads to a single winding harmonic series. However, the asymmetrical nature of the windings makes the length of the series required difficult to assess without resorting to a trial and error basis. Bearing in mind that the slot conductors are modelled as filamentary conductors, then the harmonic series is increased until convergence of the current and UMP is achieved. Problems may arise due to the infinitely small current filaments

producing significant harmonic components as the pole number approaches the slot number.

The mapping of the T-plane field to the Z-plane field can be done by either dividing the stator surface into segments and approximating the field to be uniform across each segment or by use of gaussian integration. The former method was chosen since the gaussian integration order would be quite high. The segment size required clearly depends upon the maximum winding harmonic. The segment size reduces as the harmonic number becomes higher. Again the number of segments is increased until convergence is obtained.

### 4.2.2 Permeance Harmonic Technique

The permeance harmonic technique contains two types of harmonic series, both tending to infinity. These are the winding harmonic and the permeance harmonic series. If the machine is series connected then conventional winding factors can give an indication of the number of winding harmonics required.

If the stator contains parallel paths then this approach may be inaccurate due to the non-uniform currents flowing in the parallel winding paths. In addition, series windings will lead to only odd harmonics of the machine pole number, which is not necessarily the case with parallel paths. A solution point is achieved by simply increasing the harmonic number until convergence is reached.

The first few terms of the permeance harmonic series $Q(m)$ are shown in figure 4.1. It can be seen that they decay quite quickly and only the first few need be considered, the actual number depending on the degree of eccentricity. If the harmonic is below a specified percentage of the fundamental then it is taken to be negligible. In this study it was set to 0.5 %.

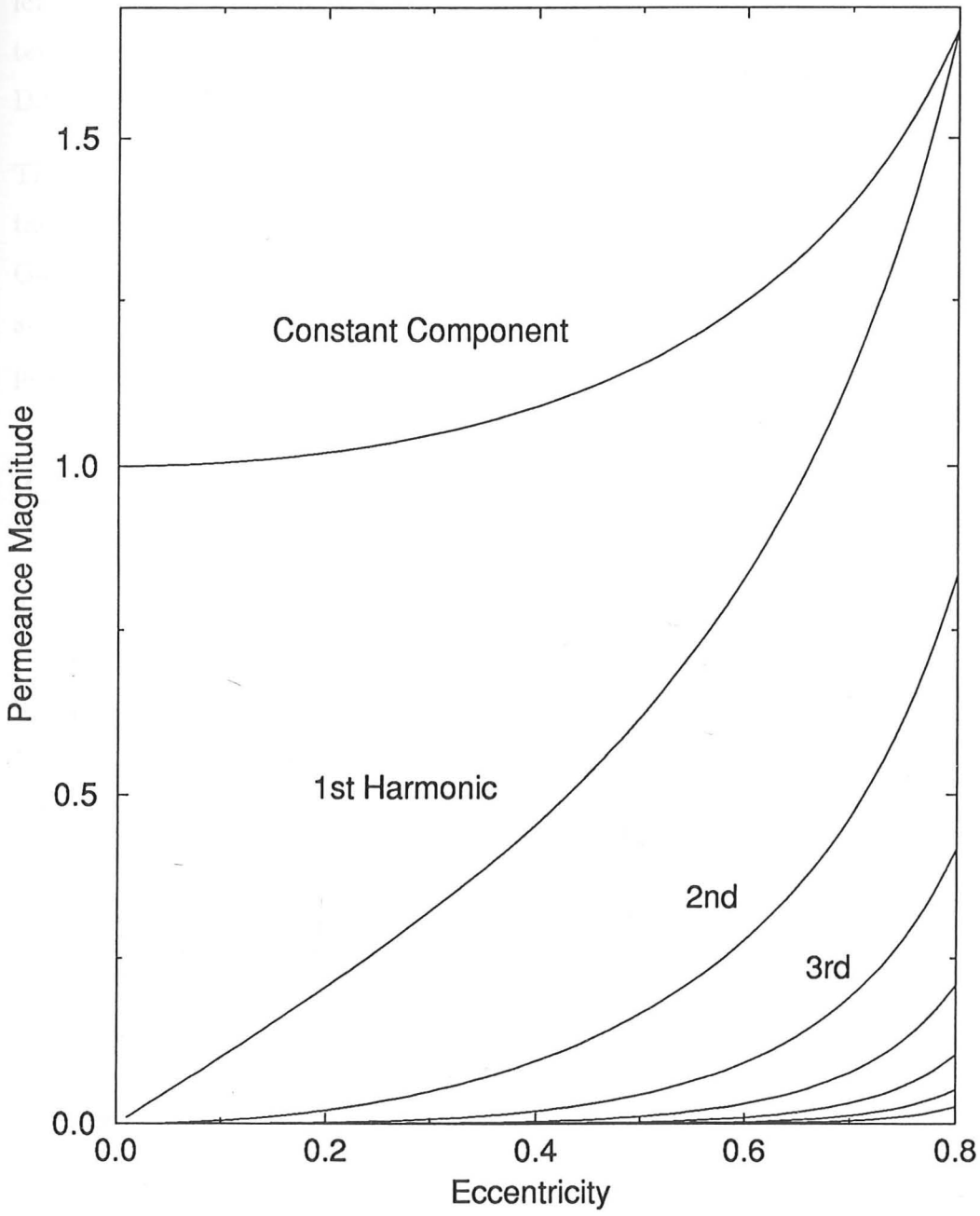


Figure 4.1: Permeance Harmonic Components

## 4.3 Stator Resistance and Leakage Inductance

The stator resistance depends on the temperature of the windings. Over a large part of the operating range of the motor it tends have only a small influence on the load current although it can have a significant effect near stall conditions when the terminal impedance is low. The simplest approach is to incorporate the measured D.C. winding resistance (taken when the machine is hot).

The stator leakage reactance is made up of the slot leakage and the end-winding reactance. The slot leakage can be calculated using the equations derived by Liwschitz-Garik and Whipple [4]. The end-winding reactance has proved difficult to calculate accurately [71], values quoted when the machine was used in a previous study [59] proved to be satisfactory.

## 4.4 Rotor Resistance and Leakage Inductance

The D.C. resistance of a rotor bar can be calculated to a reasonable degree of accuracy simply from the bar dimensions. The leakage inductance can be calculated using the same method described in the previous section. These two parameters however are not constant due to skin effect. This can be accounted for using frequency dependent correction factors as derived by Liwschitz-Garik [8]. This gives

$$r_{ac} = \phi r_{dc} \tag{4.1}$$

$$l_{ac} = \theta l_{dc} \tag{4.2}$$

where

$$\phi = \frac{\delta}{2}\left[\frac{\sinh\delta + \sin\delta}{\cosh\delta - \cos\delta}\right], \tag{4.3}$$

$$\theta = \frac{3}{\delta}\left[\frac{\sinh\delta - \sin\delta}{\cosh\delta - \cos\delta}\right] \tag{4.4}$$

and

$$\delta = 3.95 \times 10^{-3} d_r \sqrt{\frac{f}{\rho} s^n}. \tag{4.5}$$

$d_r$ is depth of the rotor bar, $f$ is the supply frequency, $\rho$ is the rotor bar resistivity and $s^n$ is the slip of the $nth$ harmonic.

## 4.5 Carter Factor Correction

The effects of slotting can be incorporated using the standard Carter correction factor as derived by Heller and Hamata [42]. The Carter factor $k_c$ however, is a function of the airgap as well as the slot opening. This leads to the apparent eccentricity being less than the actual as illustrated in figure 4.2. This characteristic is for a ten-pole machine with only the stator slots being considered. Since the airgap length varies in the circumferential direction then the effective airgap will also vary. However, the relationship between the actual airgap and the effective airgap is not exactly linear. Using the example of the ten-pole machine investigated in the experimental work (when fitted with the blank rotor), the airgap length is 1.5mm. When the machine is 40 % eccentricity the minimum airgap is 0.9mm and the maximum on the other side of the machine is 2.1mm. At 40 % eccentricity the apparent decrease in maximum airgap and the apparent increase in minimum airgap are about 5 % and 6 % respectively. The characteristic is almost linear between these two points, we can therefore approximate the apparent eccentricity to be 5.5 % less then the actual. The solid line on figure 4.2 is a plot of actual airgap against effective airgap $k_c(g)g$ taking into account the variation of the Carter factor with airgap length. The dotted line is a straight line passing though the origin and the point of the actual average airgap $g_{av}$ (airgap length when concentric) against the effective average airgap $k_c(g_{av})g_{av}$.

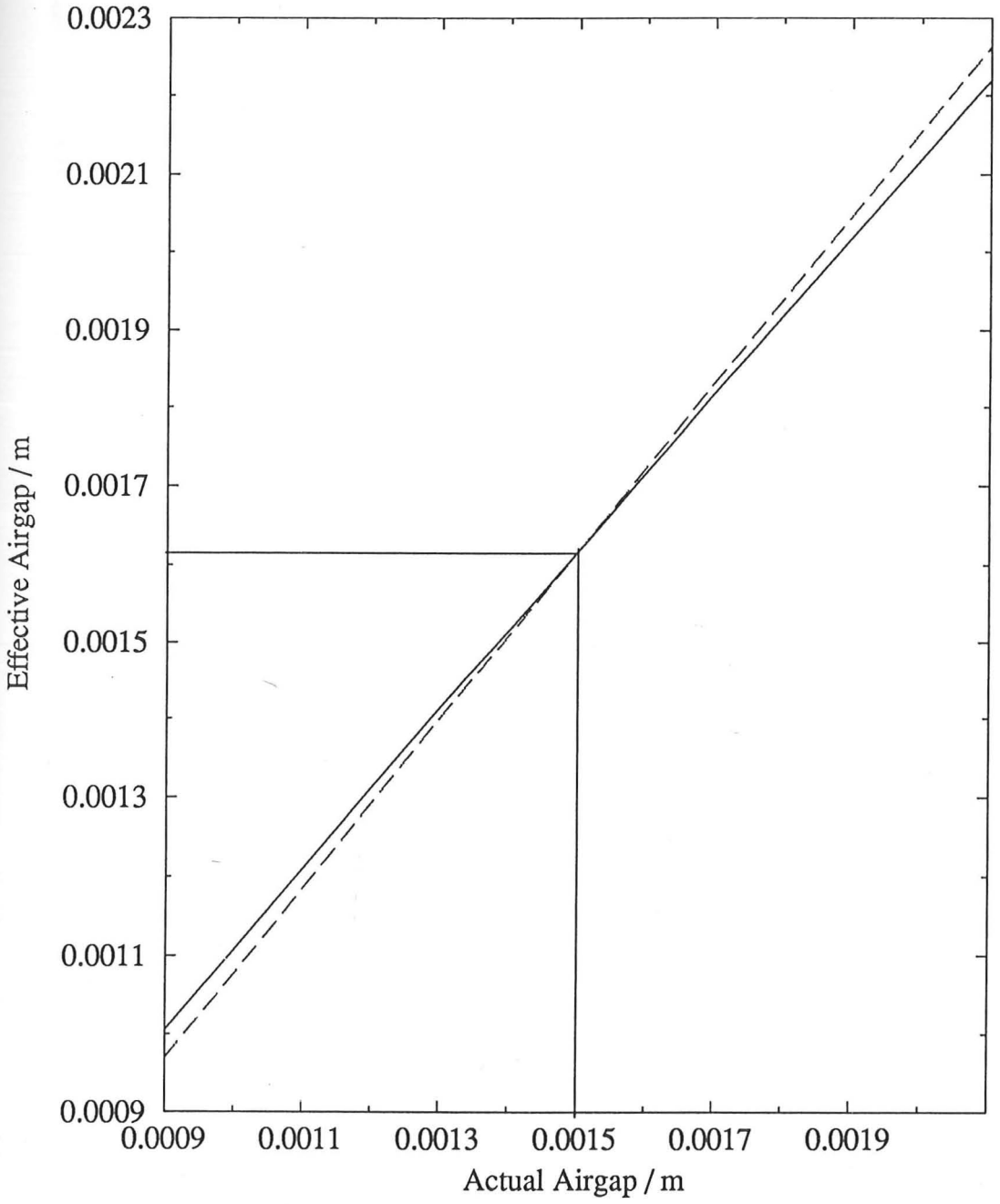


Figure 4.2: Carter Factor Correction

# Chapter 5

# Experimental Equipment

## 5.1 Introduction

The experimental investigation was carried out on two different machines. The first machine used was a 35 kW ten-twelve pole change cage motor which had been rewound so that each coil came out to its own pair of terminals. This could allow the influence of the stator winding connection (e.g. parallel paths) on the UMP to be examined. The rotor had a copper cage with open slots and the stator winding was double layered.

The second machine was a 4 KW two-pole motor with a cast aluminium rotor cage with closed slots. The stator was single layered with a concentric winding. The machine was used to further verify the model which used the permeance harmonic method and incorporated the cage rotor. This was important since many authors assume that the two-pole machine is a special case since the field can be modulated to produce homopolar fluxes. It was envisaged that this rig could be used to investigate in detail the influence of homopolar flux on UMP. However, the homopolar flux proved to be negligible due to the removal of the end-caps. Since this phenomenon has already been investigated in some detail by Kovacs [41] and Belmans [62], [63] it was decided not to examine this area in any great depth. The experimental investigation using this rig was therefore much less detailed.

Both machines had additional laminated blank rotors fabricated in order to verify

# Chapter 5

# Experimental Equipment

## 5.1 Introduction

The experimental investigation was carried out on two different machines. The first machine used was a 35 kW ten-twelve pole change cage motor which had been rewound so that each coil came out to its own pair of terminals. This could allow the influence of the stator winding connection (e.g. parallel paths) on the UMP to be examined. The rotor had a copper cage with open slots and the stator winding was double layered.

The second machine was a 4 KW two-pole motor with a cast aluminium rotor cage with closed slots. The stator was single layered with a concentric winding. The machine was used to further verify the model which used the permeance harmonic method and incorporated the cage rotor. This was important since many authors assume that the two-pole machine is a special case since the field can be modulated to produce homopolar fluxes. It was envisaged that this rig could be used to investigate in detail the influence of homopolar flux on UMP. However, the homopolar flux proved to be negligible due to the removal of the end-caps. Since this phenomenon has already been investigated in some detail by Kovacs [41] and Belmans [62], [63] it was decided not to examine this area in any great depth. The experimental investigation using this rig was therefore much less detailed.

Both machines had additional laminated blank rotors fabricated in order to verify

the computer models for the stator windings only. It was realised that a cage model could be inaccurate due to the effects not included in the model (e.g. heating of the machine, skin effect on the bars, interbar currents, miscalculation of resistances and leakage, etc). It was therefore important to be able to identify the source of model inaccuracies. Separate stator and rotor measurements would be useful in this area.

## 5.2 Ten-Pole Machine

The initial verification required the use of a laminated blank rotor. Since the test motor was not in current production a second rotor was not available and hence a new shaft and laminations were used to fabricate a blank rotor. The rotor was not required to rotate so no bearings were fitted. The shaft was turned to the right size and threaded so that large locking nuts could be used to compress the stack (again these needed fabricating). At each end of the stack, between the end laminations and the locking nut, tough non-metallic plates (1/2 inch thickness) were placed in order to prevent splaying out of the end laminations. The laminations were manufactured by stamping out centre holes in square lamination sheets and roughly rounding on a guillotine. The rotor was then assembled and turned down to the correct diameter.

Advantage was taken of this opportunity to turn the blank rotor down to a smaller diameter than the cage rotor. The original airgap with the cage rotor was 0.5 mm and this was considered too small to set a particular eccentricity with any accuracy. The airgap with the blank rotor was set to 1.5 mm. The blank rotor was mounted without bearings because rotation was not required.

The end-caps of the motor were removed and the stator mounted on a piezo-electric force table. This is shown in figure 5.1. The rotor was suspended separately by means of pillar supports which did not come into contact with the force table. These were attached to the bed-plate by means by four bolts. The bolts went though oversized holes to enable lateral movement and hence allowed horizontal positioning of the rotor. At each side of the pillar supports were tapped holes which allowed bolts to be screwed against the bed-plate and the pillars to be raised slightly. This permitted instrument shims to be placed underneath the pillars and hence accurate

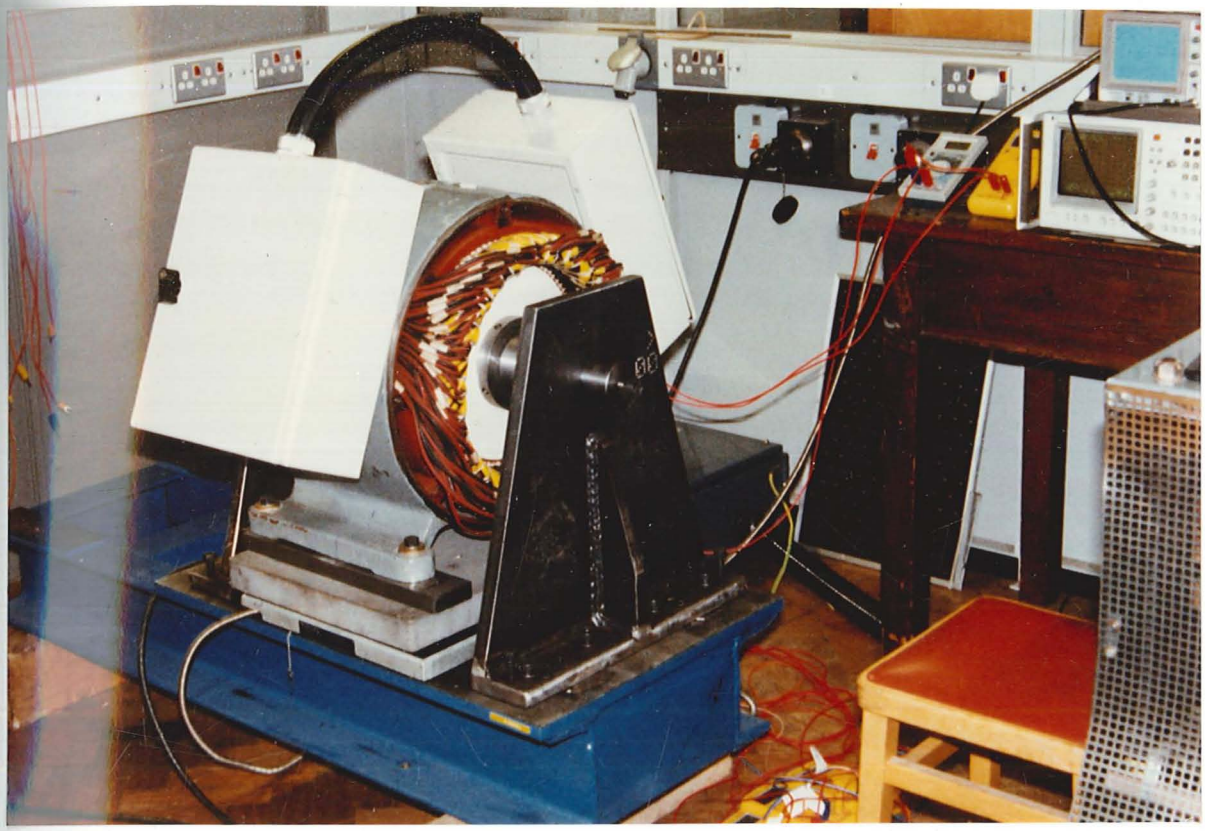

Figure 5.1: Ten-pole machine fitted with blank rotor

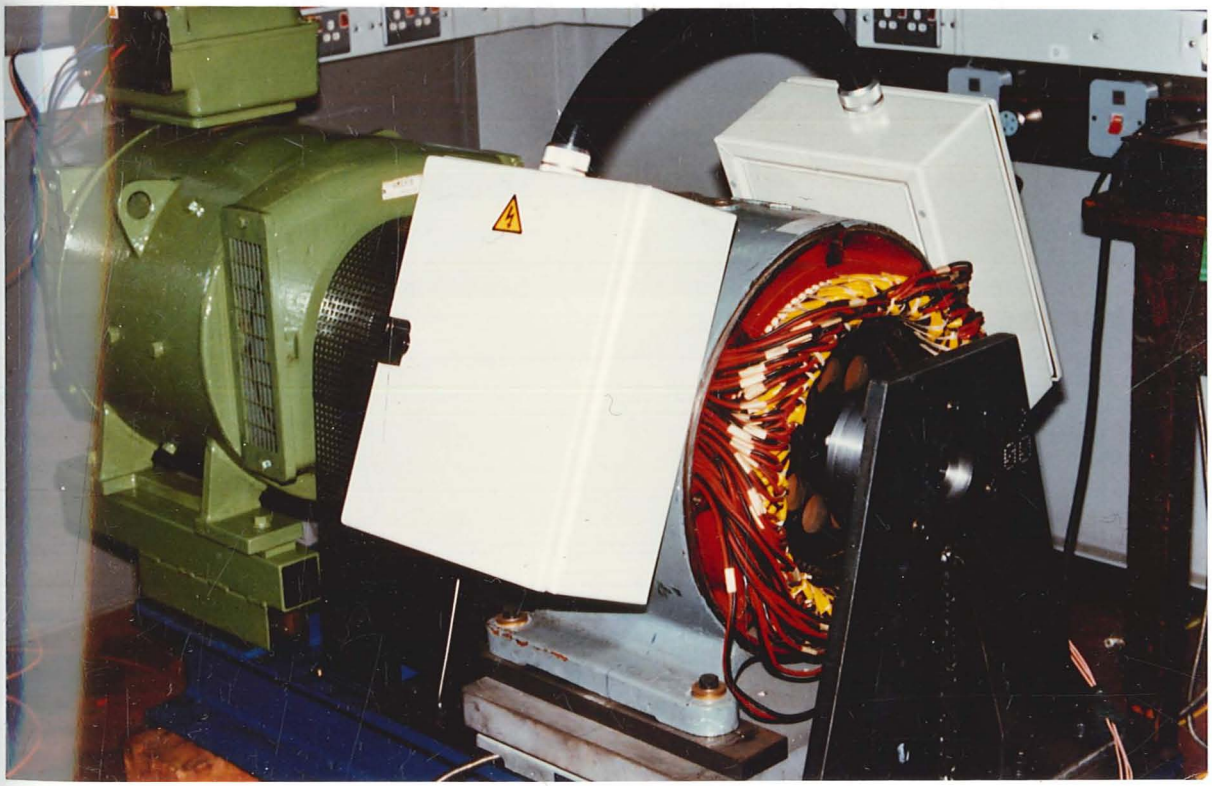

Figure 5.2: Ten-pole machine fitted with cage rotor

vertical positioning of the rotor was possible. Final positioning of the rotor was done using feeler gauges slid into the airgap at each end of the machine in both horizontal and vertical positions in order to measure the eccentricity. This approach was initially considered not to be accurate and was the main reason for increasing the airgap with the blank rotor. However the results from the blank rotor tests appeared to be very good and this method of measuring the airgap proved to be successful.

The success of measuring the eccentricity of the blank rotor with feeler gauges suggested that the cage rotor need not be modified to give a larger airgap. The positioning of the rotor did prove more difficult but reasonable positioning could be obtained with careful handling. Once the blank rotor tests were completed the pillar supports were modified and bearing housings made in order to accommodate the cage rotor. This is shown in figure 5.2. The motor was coupled to a D.C. machine through a flexible coupling in order to make alignment easier. It also allowed a degree of movement of the rotor, enough to cover the range of eccentricities investigated, without having to re-align the D.C. machine. The D.C. machine then provided a load for the test motor by use of a Ward-Leonard arrangement.

Each stator coil in the machine was bought out to a patch-board. There were ninety coils in total so two boxes were required to fit all the terminals in. These were fitted to the top of the motor and were joined by a flexible hose to allow connection between the two boards. It was expected that the homopolar flux in the machine would be negligible due to the high pole number (so that the m.m.f. generating any homopolar flux would be small) and the removal of the end-caps (so that the reluctance path though the shaft is high). However, two coils were made which would fit over the shaft at each end of the blank rotor. These allowed the shaft reluctance to be measured and any homopolar flux to be observed. It was not felt necessary to fit these to the cage rotor since the shaft reluctance had already proved to be very high.

The stator was connected to an autotransformer rated at 200 A. This was necessary in order to allow parallel connection of the phase bands where the line voltage will be reduced but the current will be increased. i.e. if the machine is series connected

with a line voltage of 415 V and a line current of 17 A then connecting all ten bands of each phase in parallel will reduce the line voltage required to produce the same field (when the machine is concentric) to 41.5 V but the line current drawn will be 170 A.

## 5.3 Two-Pole Machine

The two-pole machine was mounted in a similar way to the ten-pole machine with the stator mounted on the piezo-electric force table and the rotor separately suspended. The small size of the motor meant that the rotor bearing housings were attached to cross members, these in turn were supported by pillars at the sides of the force table. This can be seen in figure 5.3. The bearing housings had to be fabricated and bearings were fitted to both the blank and cage rotors.

The blank rotor was fabricated from a complete cage rotor by dissolving the aluminium cage in a sodium hydroxide solution. The rest of the rotor was made from steel and was unaffected except for parting of some of the laminations at each end of the stack. These were stuck back together using resin adhesive and the residue removed by turning in a lathe.

The two rotors were theoretically identical but it was found that the radii were slightly different, with the rotor used to produce the blank rotor having a smaller radius. The fabrication technique used for this type of machine often leads to airgaps being quoted only as nominal values because the rotor is turned down when the cage has been cast.

The motor was finally connected mechanically to a converter fed D.C. machine which was capable of running at 3000 rpm.

The alignment of the machine proved very difficult and time consuming. The blank rotor gave an airgap of 0.26mm and the cage rotor 0.22mm (compared to the nominal airgap of 0.18mm). Positioning was possible by placing instrument shim under the stator feet and by lateral stator movement due to oversized mounting holes. The alignment was again by use of feeler gauges placed in the airgap though this proved

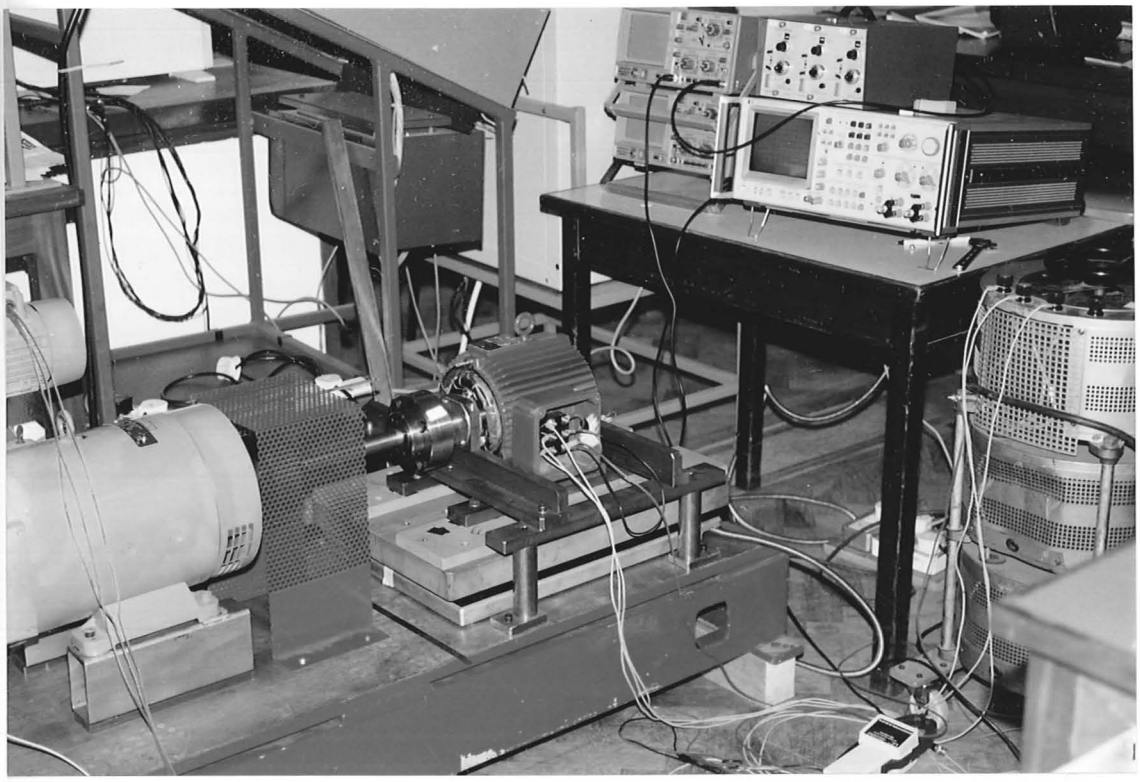

Figure 5.3: Two-pole machine rig used for both blank and cage rotors

more difficult due to stator movement when tightening fixing bolts. Adjustment was eventually possible by placing the correct thickness of shim under the stator feet to obtain the same airgap at the top and bottom and adjusting in the horizontal direction. The feeler gauges were left in at each side of the machine when being bolted down, the gauges spanning the length of the core stack. These could then be removed if the stator was correctly positioned.

## 5.4 Force Table

The force table on which the stators were mounted used piezo-electric transducers in four positions under the surface in order to detect the forces acting in three dimensions. These were connected to charge amplifiers which produce voltages proportional to the forces and could be displayed on an oscilloscope or spectrum analyser. There were three charge amplifiers, one for each direction, though only two were required at any one time. The charge amplifiers also had facilities for filtering, allowing low pass filters to be used to extract the steady forces with more accuracy.

# Chapter 6

# Ten-Pole Machine with Blank Rotor

## 6.1 Machine Parameters

The ten-pole machine had the following specification.

| | |
|---|---|
| Number of stator slots | 90 |
| Coil pitch ( slots ) | 9 |
| Number of turns per coil | 9 |
| Resistance per coil | 0.0427 Ω |
| Leakage reactance per coil | 0.13 Ω |
| Supply frequency | 50 Hz |
| Connection | Star |
| Effective machine length ($l$) | 0.203 m |
| Effective airgap radius ($r$) | 0.1485 m |
| Effective airgap length ($g_{av}$) | 1.62 mm |
| Rated voltage ( line ) | 415 V |

## 6.2 Measurement of Shaft Reluctance

It was expected that the ten-pole machine would normally have negligible homopolar flux since modulation of the ten-pole field by the fifth permeance harmonic would be very small unless the rotor is very eccentric. The construction of the rig should also lead to a very high shaft reluctance because of the removal of the end-caps. The blank rotor tests were conducted at stand-still (no bearings were fitted) since no torque was being generated. The machine could then be connected safely as a six or two-pole machine. This is because if the machine was running at the synchronous speed with a six or two pole winding connection then it would be running dangerously overspeed (the machine was originally designed as a ten-twelve pole-change motor). Since the two-pole configuration could lead to significant homopolar flux if the shaft reluctance is low, it was necessary to verify that the shaft reluctance is high and that the homopolar flux is negligible. This was done using two coils mounted on either end of the shaft. These were connected in series, with opposite polarities so that a homopolar flux could be created. The rotor was concentric for this and the homopolar flux could then be measured using the voltage induced into one of the stator winding coils. This is also a useful way of checking that the rotor is concentric by ensuring the open-circuit voltages of the stator coils are equal.

The airgap reluctance is defined as follows

$$\begin{aligned} R_g &= \frac{g_{av}}{2\pi r \mu_o l} \\ &= 66059 \text{ AT/Wb} \end{aligned} \tag{6.1}$$

where the dimensions are given in section 6.1.

The average voltage induced by the homopolar flux in one stator coil is 0.113 V. There are nine turns per coil, therefore

$$\frac{\mathrm{d}\phi}{\mathrm{d}t} = \frac{0.113}{9} \sin \omega t. \tag{6.2}$$

Hence the peak magnitude of the flux $\Phi = 4 \times 10^{-5}$ Wb/coil. Since the coils span one tenth of the stator surface and the homopolar flux is divided equally between

the two shaft paths, the flux flowing through one shaft coil is $2 \times 10^{-4}$ Wb. The total reluctance is therefore the shaft coil amp turns divided by the shaft flux. The shaft coils have 300 turns and if the coil resistance is considered negligible, for a coil current of 2 Amps the total reluctance is $R_{tot} = 3 \times 10^7$ AT/Wb. From equation 2.84

$$R_{tot} = R_{ex} + 2R_g \tag{6.3}$$

the shaft reluctance is therefore $R_{ex} = 2.99 \times 10^7$ AT/Wb.

i.e. $R_{ex} \gg R_g$ and from equation 2.86: $\alpha \simeq 1$.

This was expected since the end-caps have been removed and the rotor and stator mounted separately on the bed-plate.

## 6.3 Ten-pole Tests

### 6.3.1 Series Connection

The UMP was measured for a variety of voltages and eccentricities, with rotor displacement in both vertical and horizontal directions. It was found that the 100 Hz vibrational components were negligible and that the steady pull was directed towards the point of narrowest airgap.

The variation of current and UMP with eccentricity are shown in figures 6.1 and 6.2. The agreement between the theoretical predictions from the conformal and permeance methods and the actual results was very good. The slight divergence between the current predictions is caused by the use of infinitely small current filaments in the conformal model but finite conductor widths in the permeance method. This subsequently leads to a slight decrease in the machine reactances and a decrease in flux density levels in the airgap. The UMP predictions for the conformal and permeance methods are therefore so close that they cannot be distinguished from each other on the graph. The currents appear as a balanced three phase set with the magnetising reactances decreasing as the eccentricity increases. Up to about 40 % the UMP characteristic appears virtually linear but at large eccentricities it becomes nonlinear.

Figure 6.3 shows the variation of UMP with voltage at 40 % and 53.3 % eccentricity. As expected, it is proportional to the square of the voltage since it is a function of the square of the flux density. The magnetising current (figure 6.4) was found to be linear, showing no saturation at the voltage levels used. This is because the machine has been rewound with a different coil pitch and no longer operates at the same flux levels. In addition, the machine was initially built as a ten-twelve pole-changing machine, the ten-pole connection was star and the twelve-pole connection was delta, the ten-pole connection could then be operating in the unsaturated region even at rated voltage because of this.

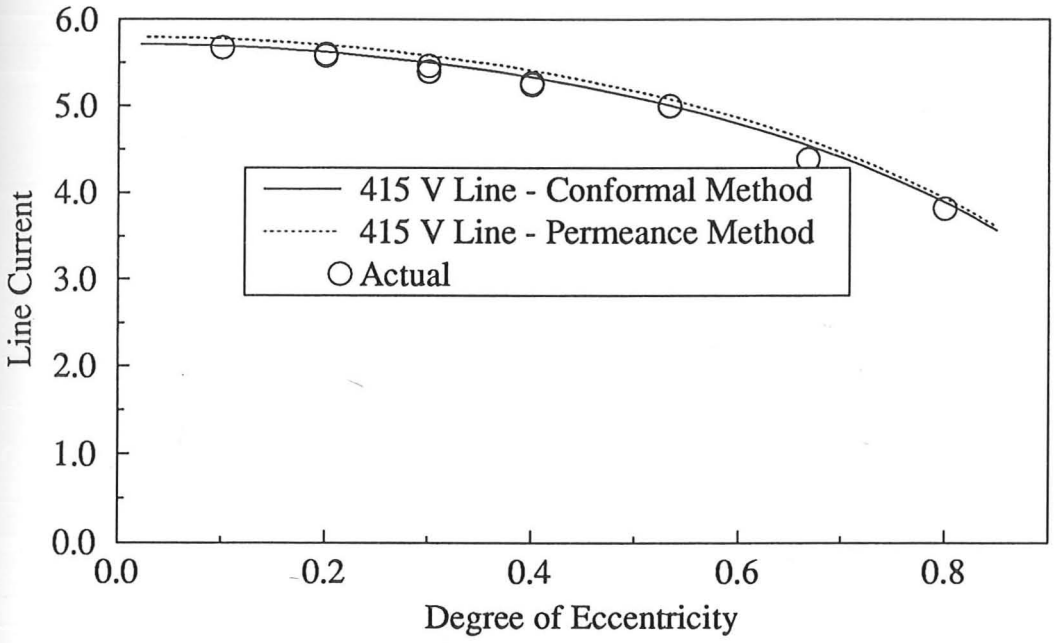


Figure 6.1: Variation of Line Current with Eccentricity for a 10-Pole, Series-Connected Machine with a Blank Rotor

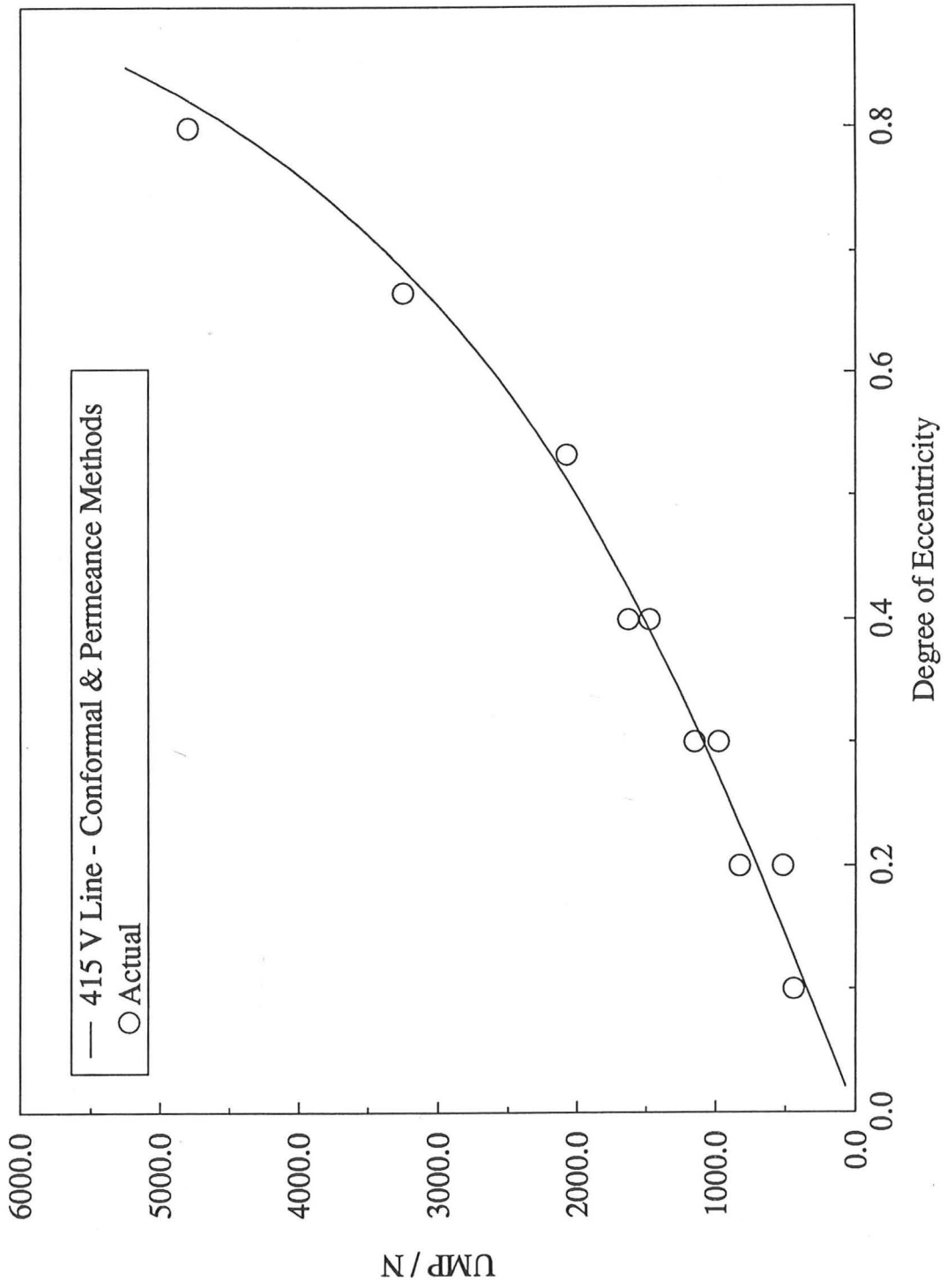


Figure 6.2: Variation of UMP with Eccentricity for a 10-Pole, Series-Connected Machine with a Blank Rotor

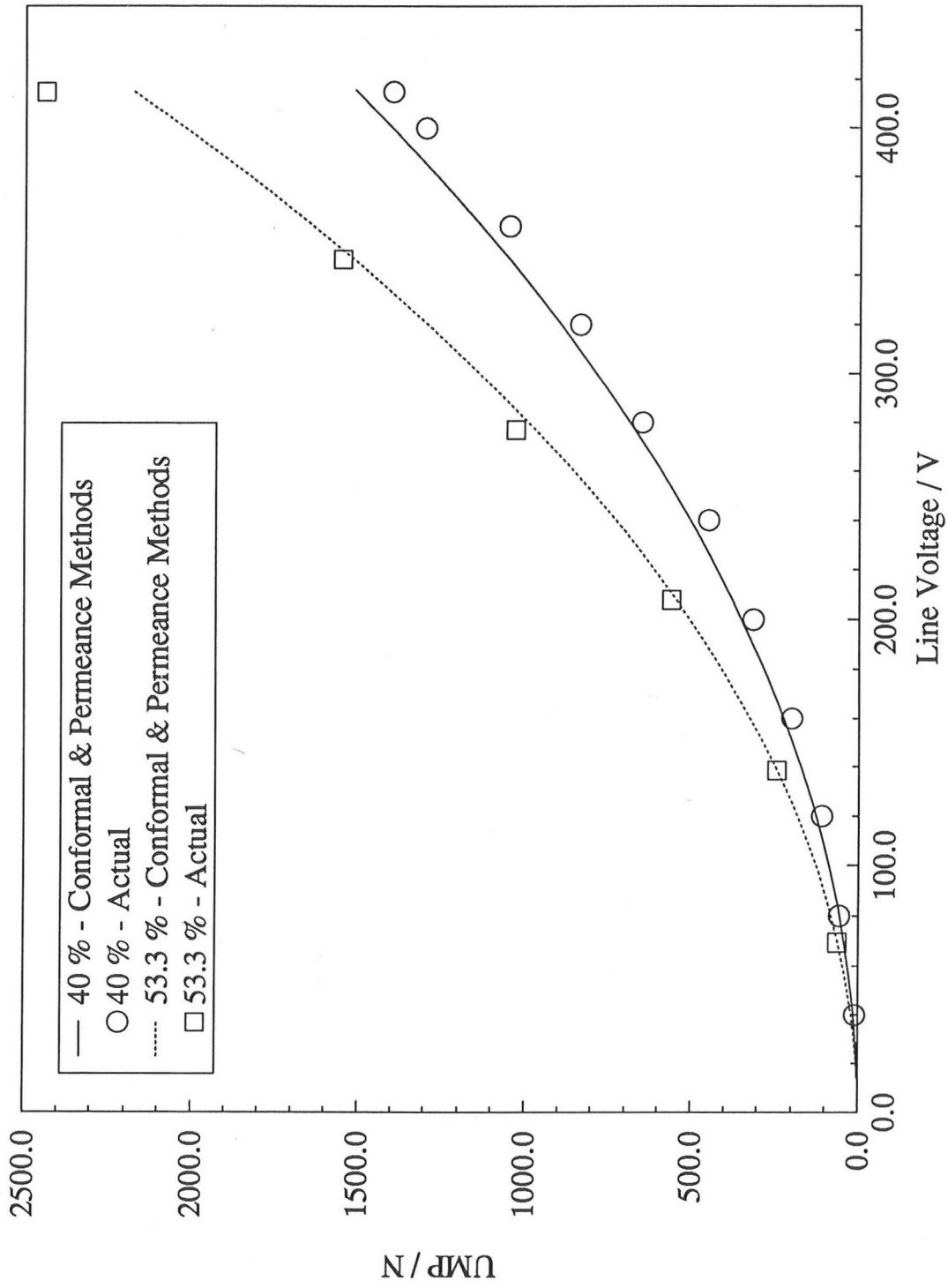


Figure 6.3: Variation of UMP with Voltage for a 10-Pole, Series-Connected Machine with a Blank Rotor

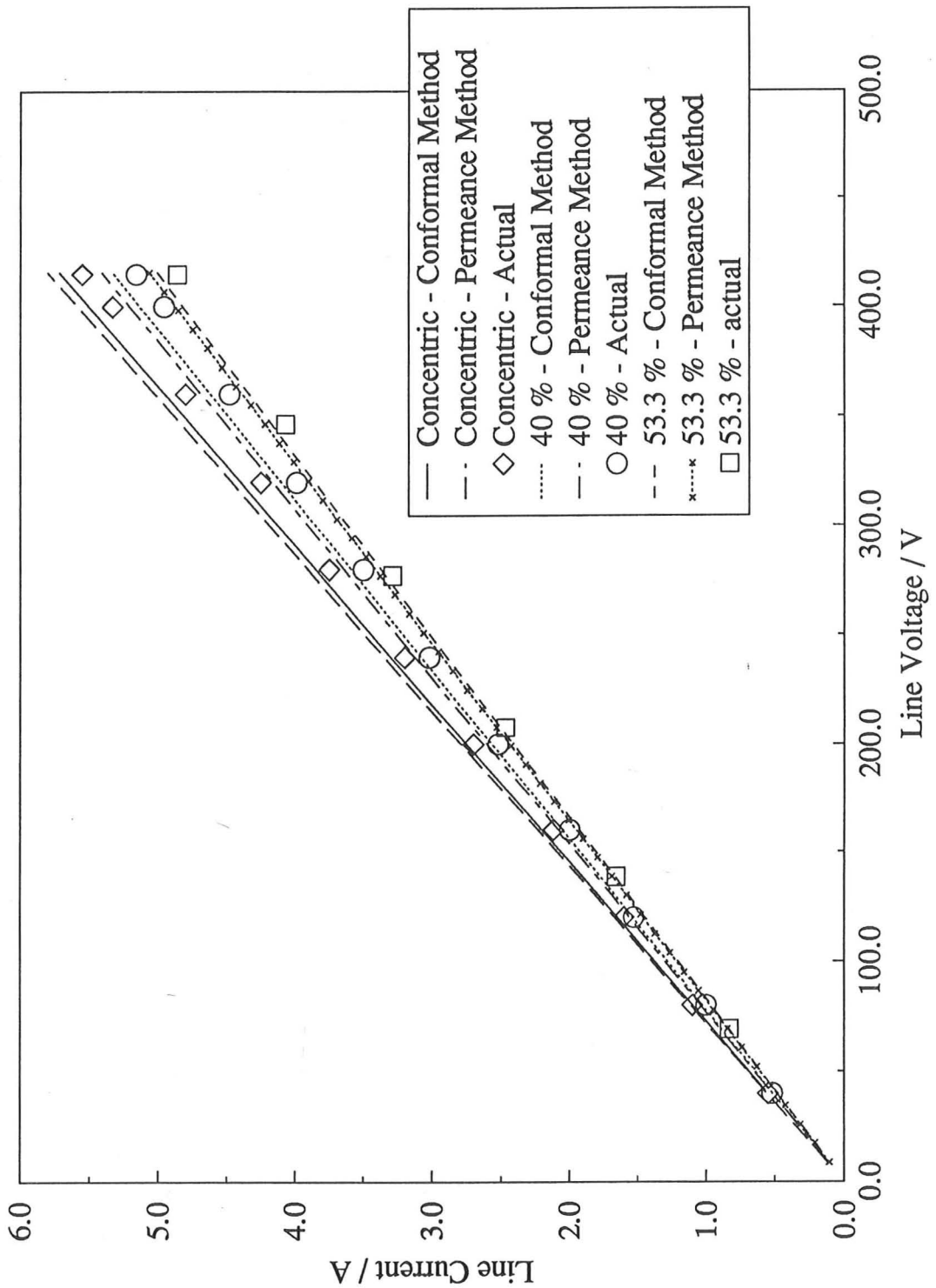


Figure 6.4: Variation of Line Current with Voltage for a 10-Pole, Series-Connected Machine with a Blank Rotor

### 6.3.2 Parallel Connection

If the phase bands are connected in parallel then the voltage has to be reduced in order to maintain constant flux levels in the machine (assuming the rotor is concentric). For example, if there are ten phase bands in parallel then the voltage should be reduced by ten. However, the current taken from the supply would correspondingly increase by the same amount. The 200 A autotransformer used to supply such a high current had a limited voltage variational capacity and the nearest test voltage to 41.5 V line was 44.1 V line.

The variation of UMP with eccentricity can be seen in figure 6.5. It remains linear up to 80 % eccentricity. It can also be seen that the UMP no longer acts in the direction of narrowest airgap but is a few degrees away as shown by the fact that the force has a vertical as well as a horizontal component. The general equation for UMP in the permeance method suggests that this can happen since forces can occur which are perpendicular to the direction of narrowest airgap. Hence, if the airgap fields are phase shifted slightly by the use of parallel paths then the direction of UMP may well not act in the direction of minimum airgap. Again, the agreement between the conformal and permeance methods was good. The reduction of UMP due to the use of parallel paths is obvious, the UMP being over ten times less using parallel paths. This ratio is even higher at extreme values of eccentricity when the UMP characteristic becomes non-linear for the series case.

The current distribution for one phase is shown in figure 6.6. This shows a wide distribution of currents within the machine when the rotor is eccentric depending on the location of the phase band. When the phase band is located near the point of narrowest airgap the current required is somewhat less than that of a phase band on the opposite side of the machine. It can be seen that good agreement was found between the predicted and measured results.

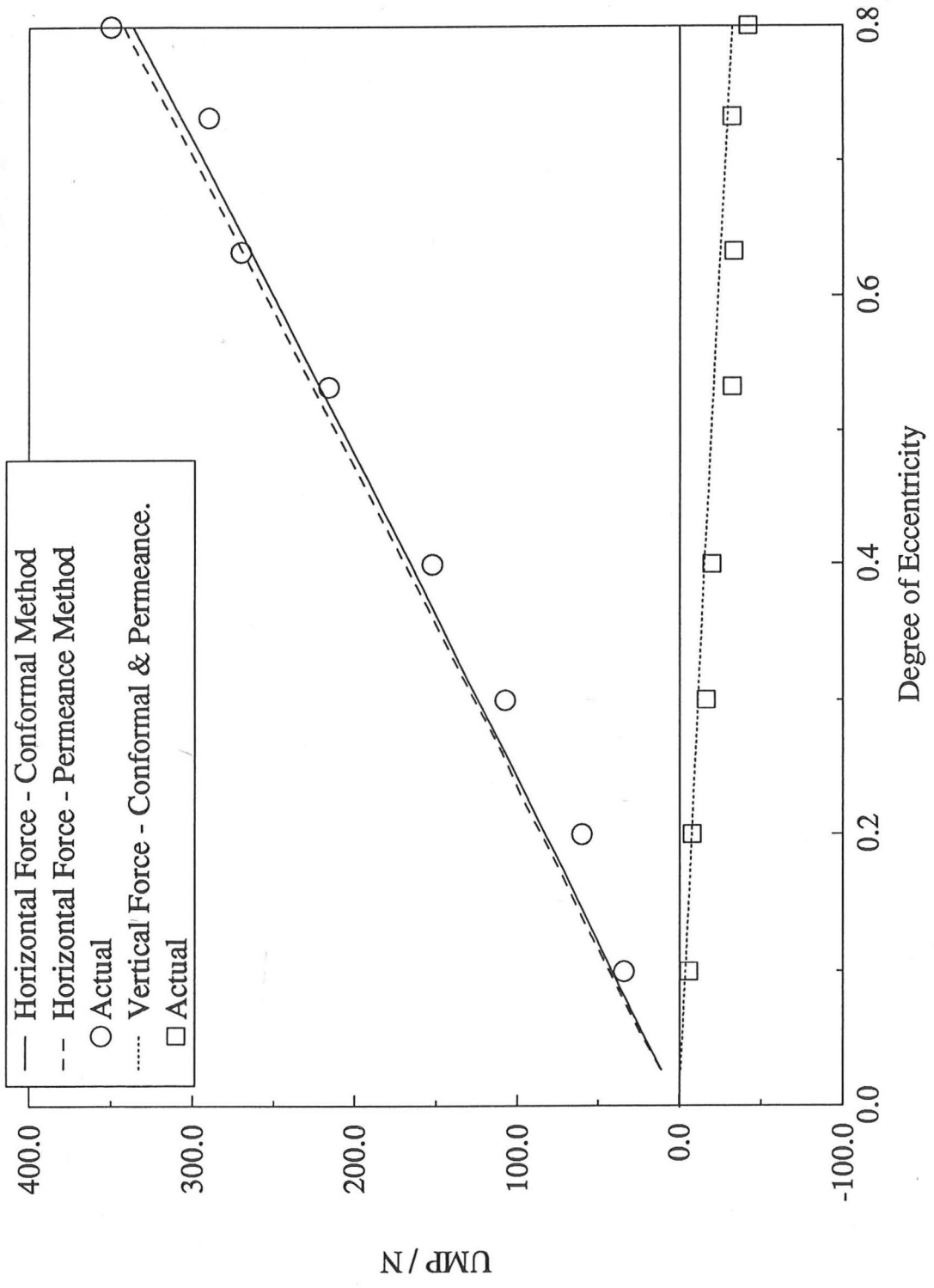


Figure 6.5: Variation of UMP with Eccentricity for a 10-Pole, Parallel-Connected Machine with a Blank Rotor at 44.1 V Line

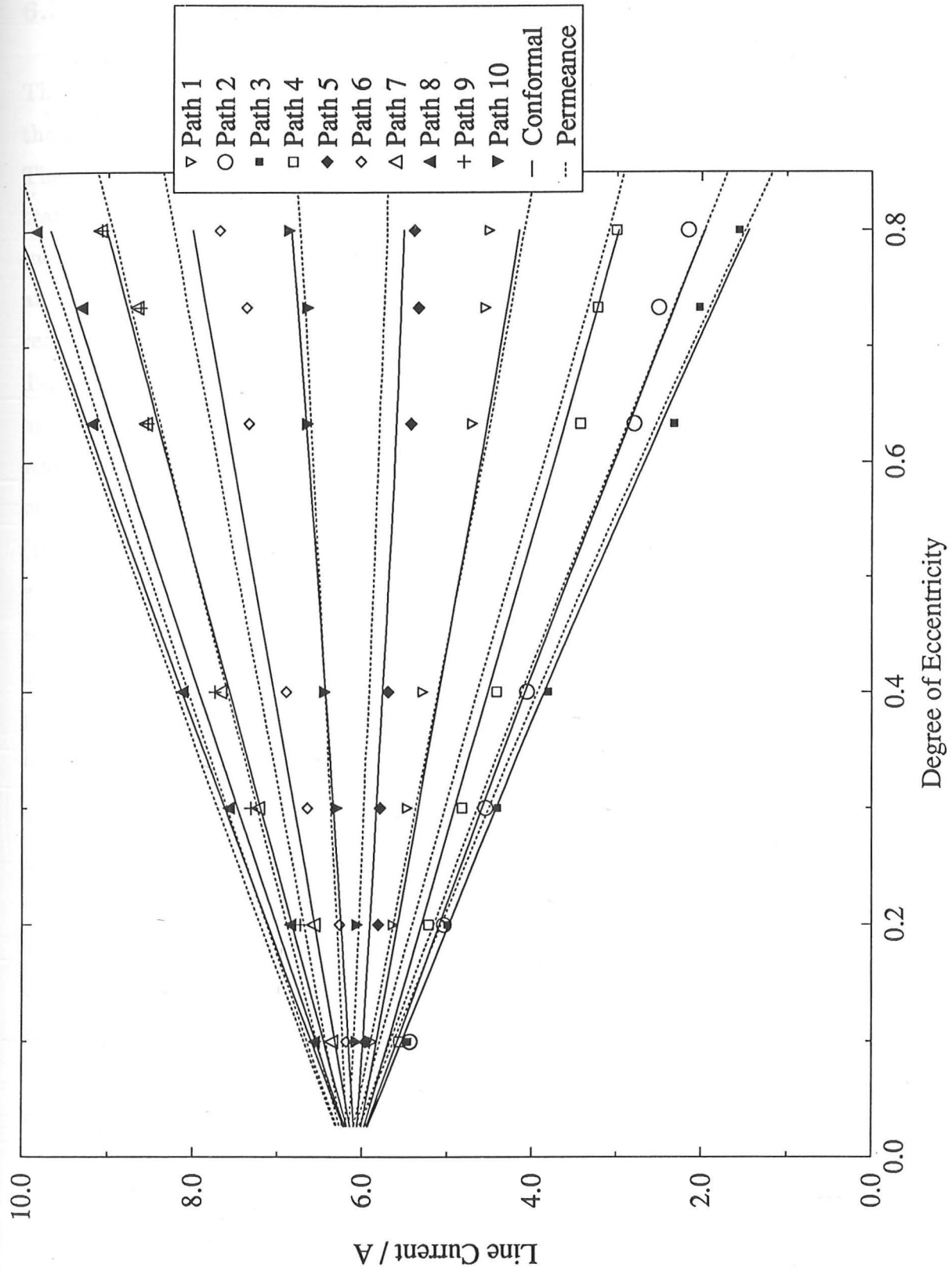


Figure 6.6: Variation of the Phase Band Currents of One Phase with Eccentricity for a 10-Pole, Parallel-Connected Machine with a Blank Rotor at 44.1 V Line

### 6.3.3 Convergence Rates

The conformal transformation technique contains one winding harmonic series whereas the permeance technique requires two: the winding and permeance harmonic series. The convergence rates of the winding series are shown in figure 6.7. The conformal transformation method achieves satisfactory convergence using nine winding harmonics at 40 % eccentricity and using sixteen at 80 % eccentricity for both parallel and series connections. This demonstrates clearly that more harmonic terms are required if the eccentricity is increased because the winding configuration in the T-plane becomes more asymmetrical (the fundamental pole number of the machine has a winding harmonic number of five). In the case of the permeance method, where the winding is symmetrical, there is immediate convergence with series connections indicating that higher winding harmonics have negligible effect on the UMP (the second winding harmonic would be twenty-five pole-pairs. If the star point is earthed and zero order currents can flow then it would be fifteen). The winding series for the parallel connection converges after six harmonics. The parallel nature of the windings means this winding harmonic has 6 pole-pairs and exists for each phase band. At this harmonic the currents have virtually converged and hence so has the UMP.

The permeance harmonic series for the results already given had converged (using a permeance series which went up to the seven harmonic). Figure 6.8 shows the effect of varying the maximum harmonic number. It can be seen that for even 40 % eccentricity the first harmonic dominates and higher harmonics have little effect for both series and parallel connections. At extreme eccentricities (80 %) the second harmonic begins to have a substantial effect. The UMP for series connection increases with the second harmonic but decreases with parallel connection. This can be explained by considering the phase band currents. The currents in the series case converge after the first harmonic and there are no higher winding harmonics linked by the field produced by the fundamental since the next winding harmonic will need a field with twenty-five pole-pairs to induce a net e.m.f. into it. However, for parallel windings, the fundamental winding harmonic will produce both lower and higher field harmonics (third, fourth, sixth, seventh, etc. when the fundamental

is taken as five) which will induce e.m.f.s into the phase band windings. Hence the current never fully converges until the full permeance series has been considered.

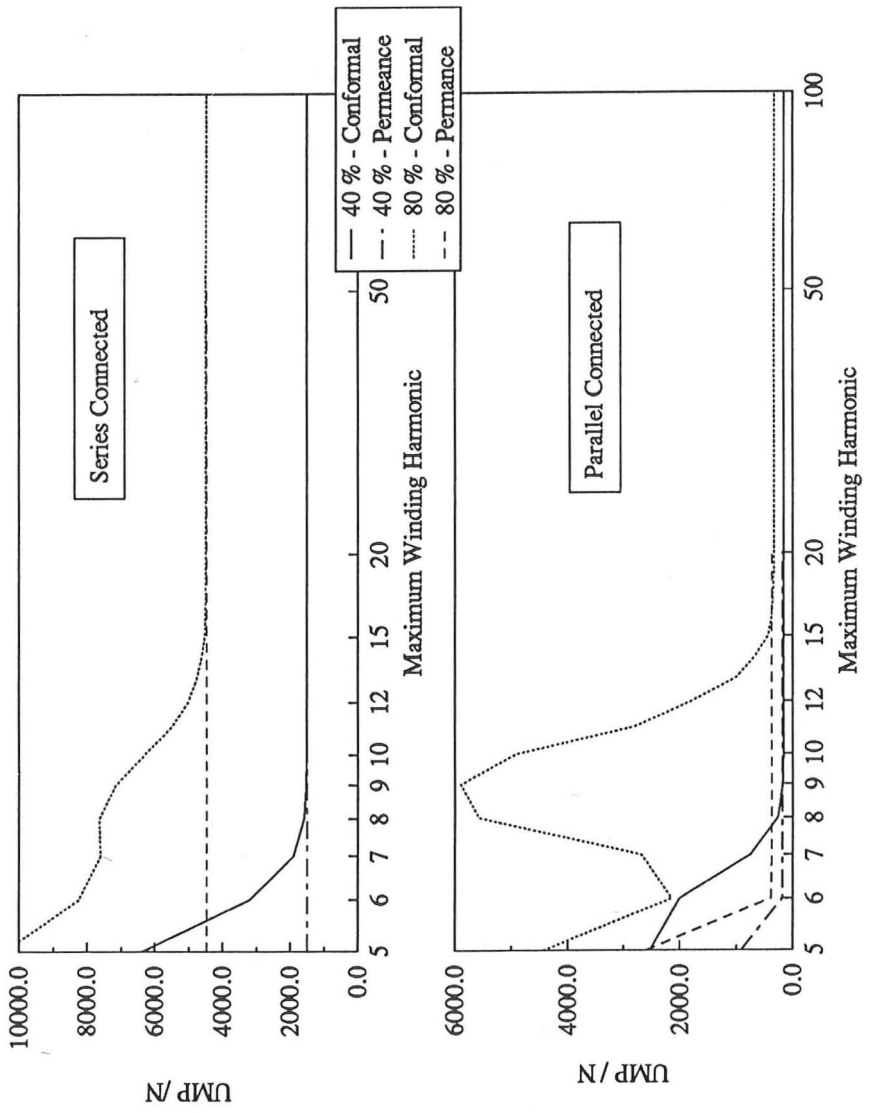


Figure 6.7: Variation of UMP with Winding Harmonic for a 10-Pole, Series and Parallel Connected Machine with a Blank Rotor at 415 V Line and 44.1 V Line Respectively

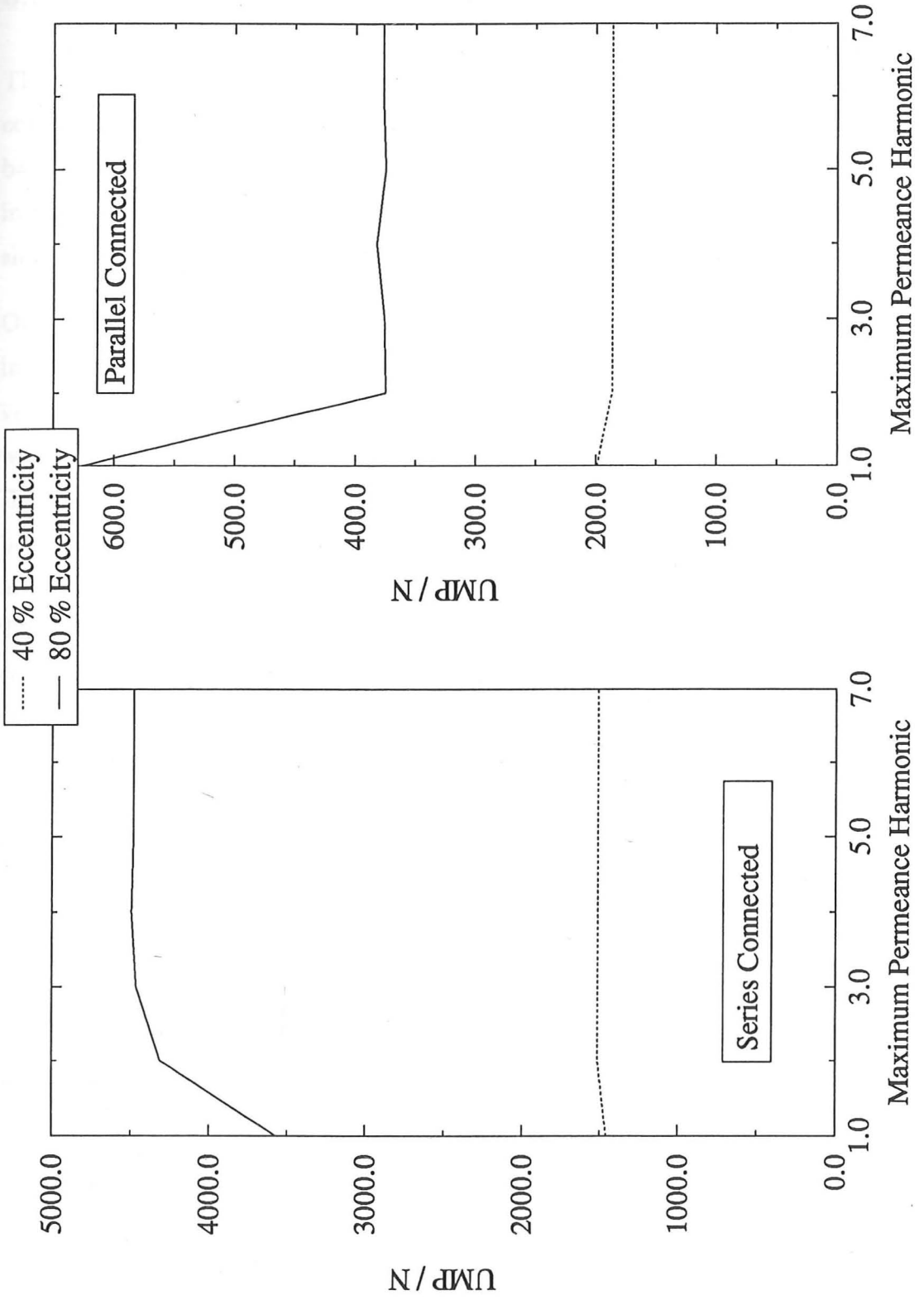


Figure 6.8: Variation of UMP with Permeance Harmonic for a 10-Pole, Series and Parallel-Connected Machine with a Blank Rotor at 415 V Line and 44.1 V Line Respectively

### 6.3.4 Five Parallel Path Connection

The series and parallel connected winding configurations exhibit negligible vibrating components. If the windings are connected with five parallel paths with adjacent bands connected in series then some 100 Hz component is exhibited. This is shown in figure 6.9. The pulsations act in the direction of minimum airgap only and are shown to be substantial when compared to the steady force.

One problem which appeared during the measurements was the reduction of rigidity in the machine when the end caps were removed. When the machine was shimmed vertically the computational and measured results compared favourably. If the rotor was moved horizontally the vibrational component increased substantially whilst the steady pull remained as in the vertical case. From the analytical model it can be shown that rotating the winding position with respect to the point of narrowest airgap should have negligible effect on both the steady pull and vibrating pulsations. This phenomenon appeared in several subsequent tests, where the steady pull was correct but horizontal vibration was much exaggerated. It was most evident when the machine was connected in a two pole configuration and there was a very large 100 Hz horizontal component due to the rotating radial pressure wave, even when the rotor was concentric. This can be explained by considering the construction of the experimental rig. The rotor and stator are separately mounted on the test bed, the stator being mounted on the force table and the rotor being supported by pillars at each end. These can pivot on the test bed, the rotor axis being some 41 cm above the surface of the test bed plate. The test bed will flex under extreme conditions if the horizontal force between the rotor and stator is large. There appeared to be a resonant frequency of the rig at 100 Hz so that any vibration in the horizontal direction was amplified. This produced higher values of 100 Hz vibratory force than expected. This is shown later in the two-pole section.

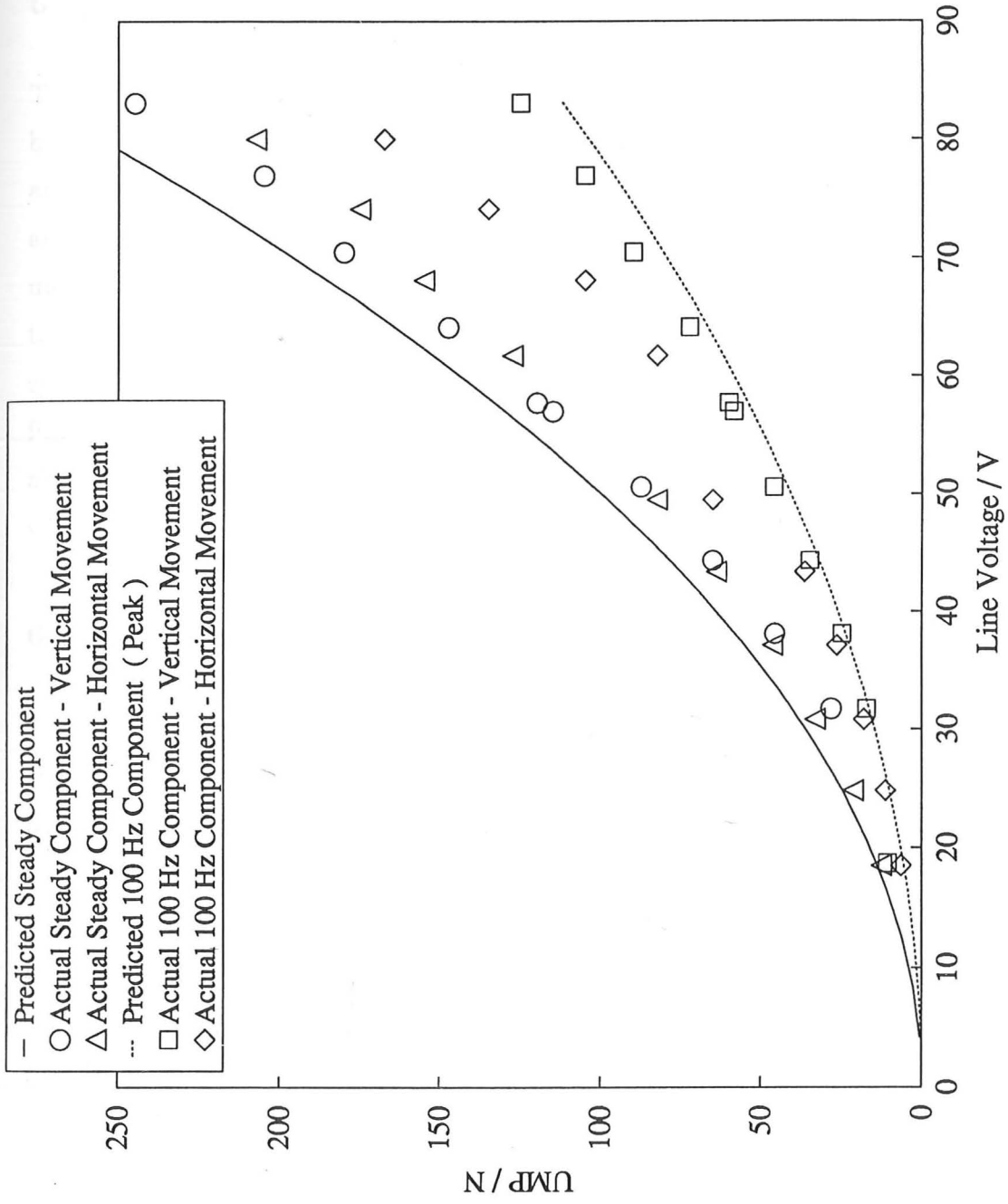


Figure 6.9: Variation of UMP with Line Voltage with 40 % Eccentricity for a 10-Pole Machine with a Blank Rotor and Five parallel Paths per Phase with Adjacent Bands Connected in Series

## 6.4 Six-Pole Configuration

### 6.4.1 Series Connection

The windings can be connected as a six-pole motor with the coils being short pitched by six slots (full pitch corresponded to fifteen slots). The variation of current and UMP against line voltage for several eccentricities can be seen in figures 6.10 and 6.11. These show good agreement between the predicted values and actual measurements. The predictions using the conformal technique and the permeance technique are almost identical. Convergence for the six-pole configuration with respect to the winding harmonics in the permeance case again indicated that the fundamental pole number harmonic dominates and higher harmonics can be virtually ignored. The pull was steady and acting in the direction of narrowest airgap with negligible 100 Hz pulsating components.

### 6.4.2 Parallel Connection

The machine was reconnected with six phase bands in parallel. The results are shown in figure 6.12. Again the UMP is seen to be considerably damped using parallel paths. The line voltage again has to be divided by six in order to maintain the normal fundamental flux level. There was a slight shift in the direction of the pull but this is only really detectable at high eccentricity (the magnitude only being shown for 20 % and 40 % eccentricities). The pulsating components were negligible.

### 6.4.3 Three Parallel Path Connection

The results so far given show very little variation of UMP due to the geometrical orientation of the coils with respect to the point of minimum airgap. If three parallel paths are used with two adjacent phase bands in series then geometrical orientation becomes important. This is shown in figure 6.13. The rotor could be shimmed upwards or moved horizontally in either direction. This produced three rotor positions with a spatial variation of 90 degrees between each. The measured variations

are shown in figure 6.13. It can be seen the results are very sensitive to even a slight variation in the direction of minimum airgap. A very high eccentricity was used to illustrate this phenomena. The vibrational components in the horizontal direction still seem to be greater than predicted (this phenomenon was discussed in section 6.3.4).

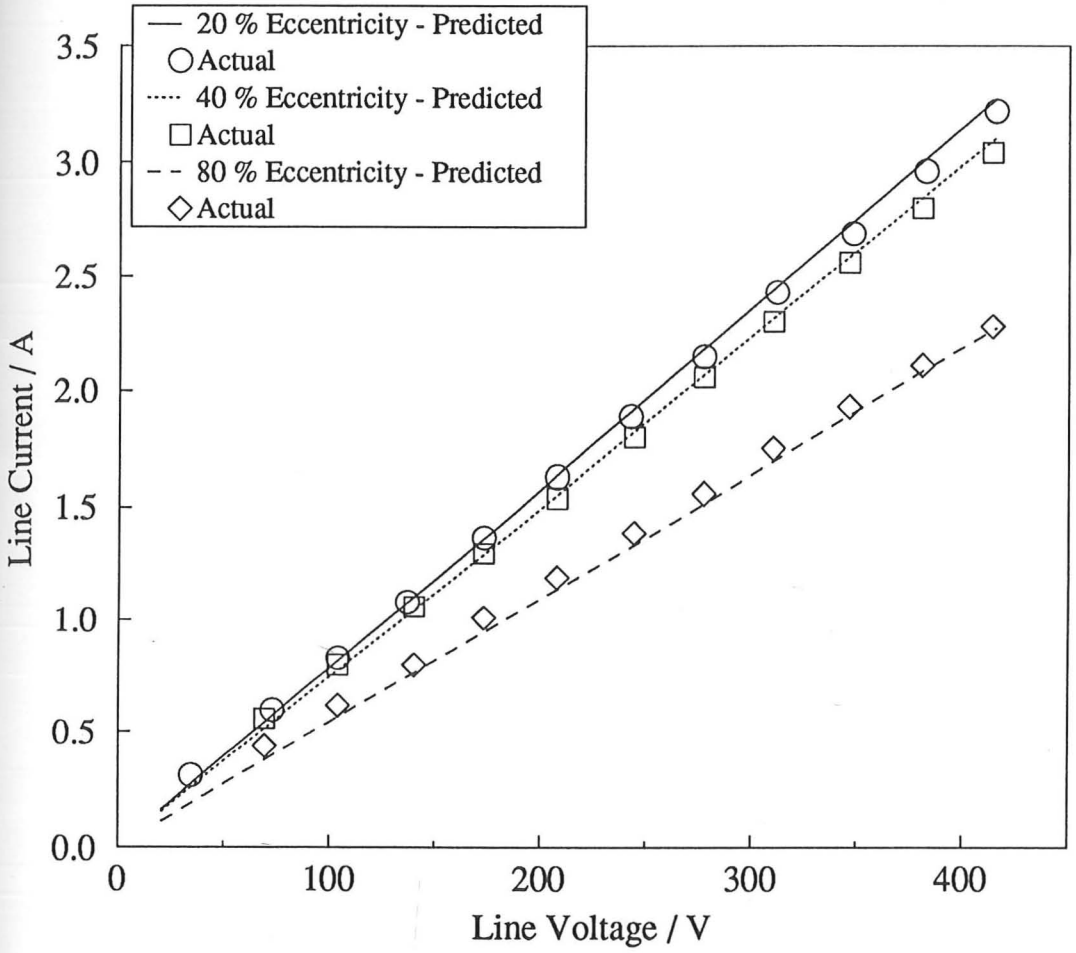


Figure 6.10: Variation of Line Current with Line Voltage for Several Eccentricities of a Six-pole Series-Connected Winding Configuration

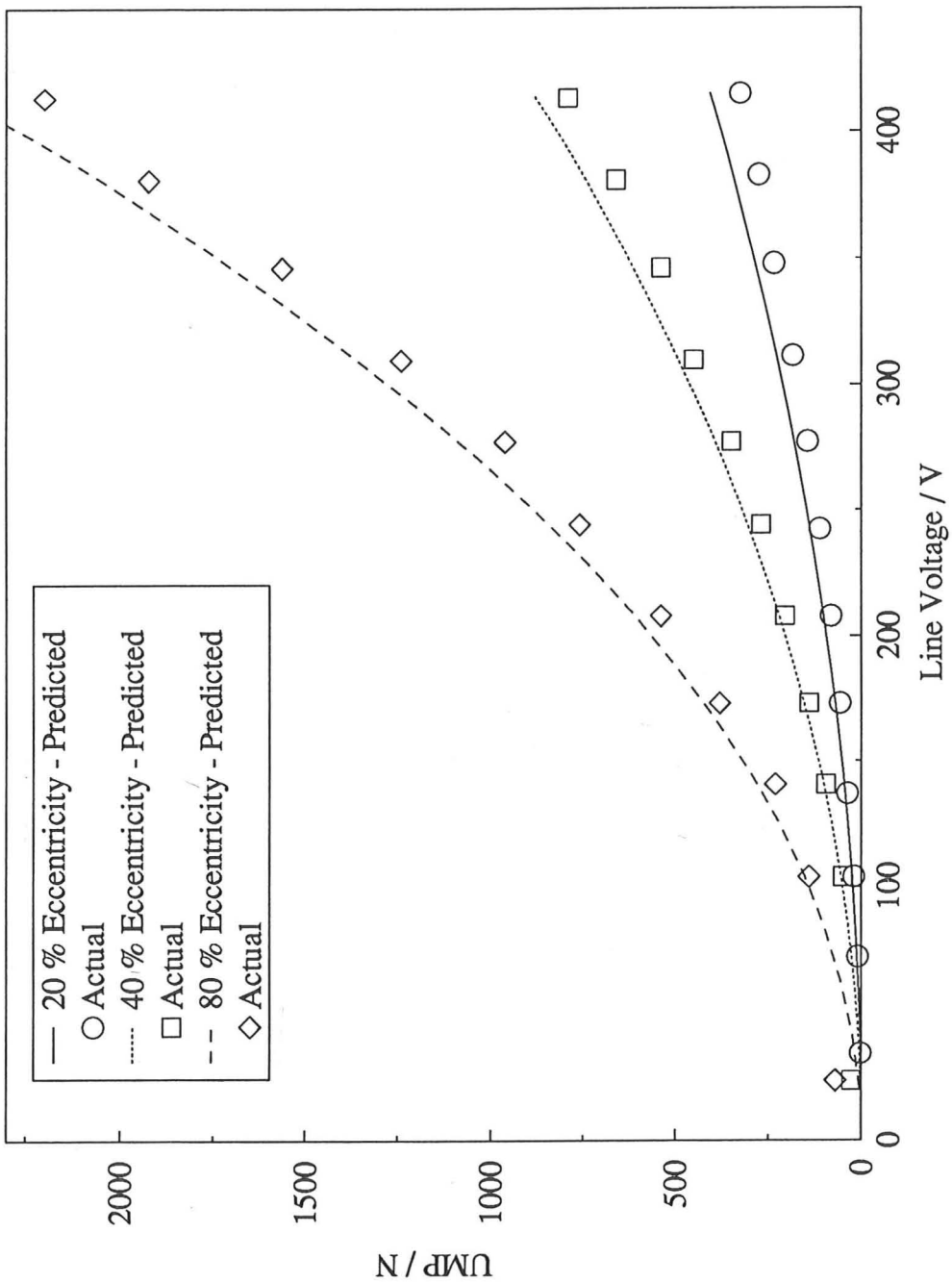


Figure 6.11: Variation of UMP with Line Voltage for Several Eccentricities of a Six-pole Series-Connected Winding Configuration

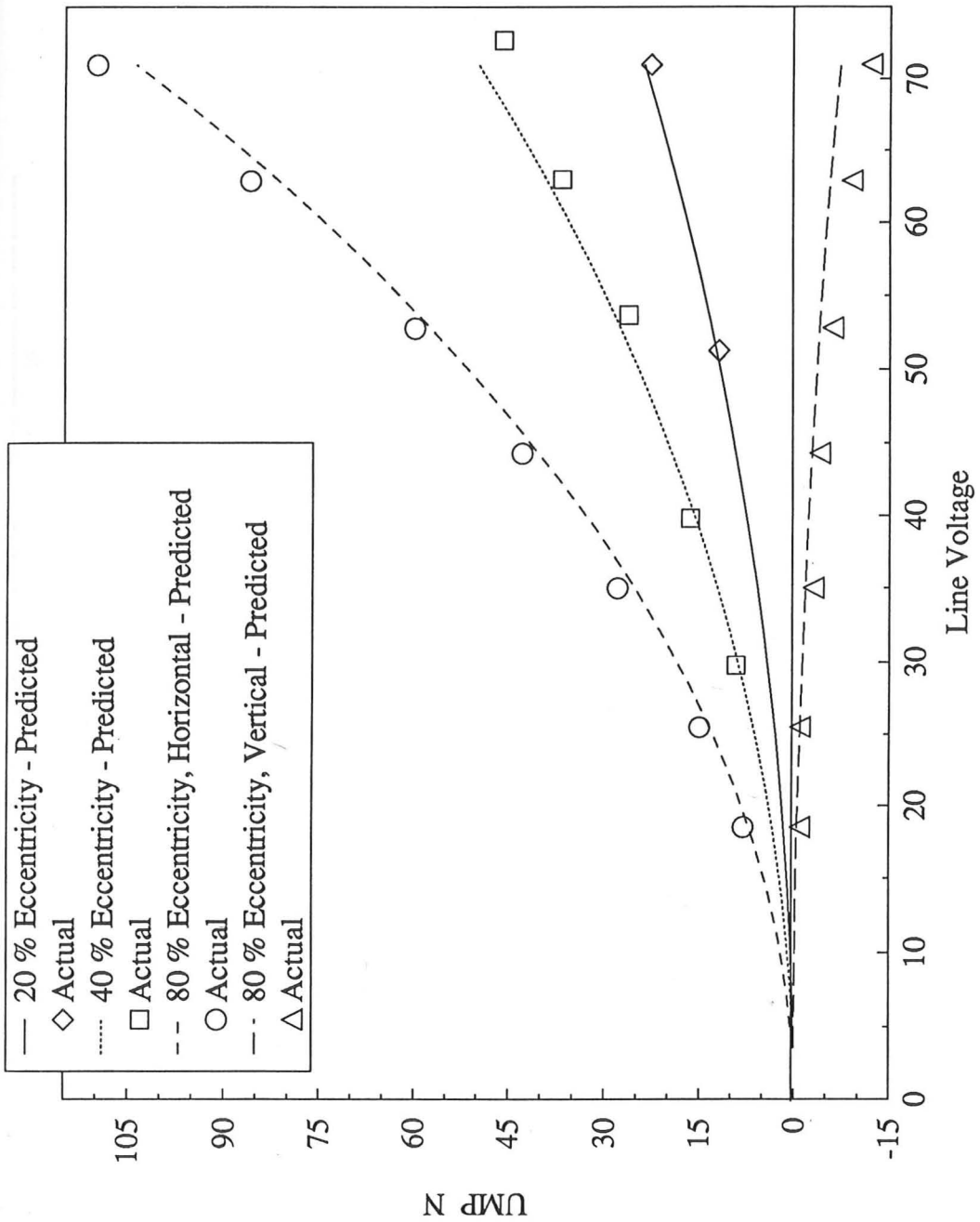


Figure 6.12: Variation of UMP with Line Voltage for Several Eccentricities of a Six-pole Parallel-Connected Winding Configuration

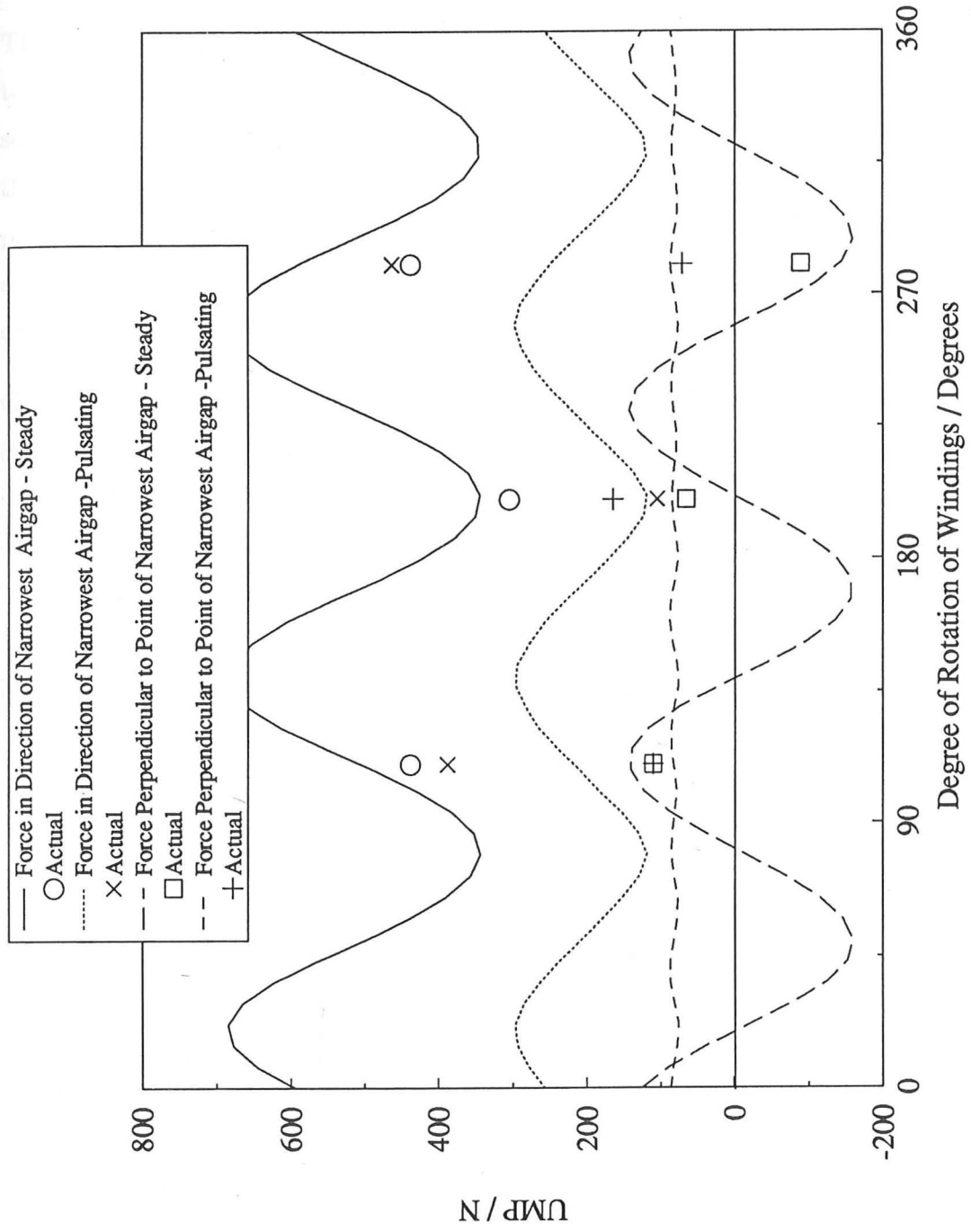


Figure 6.13: Variation of UMP with Rotation of Windings with Respect to the Point of Narrowest Airgap for a Six-Pole Machine with Three Parallel Paths per Phase and Two Adjacent Bands of One Phase Connected in Series. Eccentricity is 80 % and Line Voltage is 80 V.

## 6.5 Two-Pole Configuration

The windings were reconnected in a two-pole configuration. Full pitch corresponded to forty-five slots therefore the coils were short pitched by thirty-six slots. Only a series winding connection was considered. The main problem which occurred with this winding configuration was the excessive vibration at 100 Hz. Other components present had frequencies of 50 Hz and 200 Hz. These frequency components existed even when the rotor was concentric. They were however damped to some degree by earthing the star point. This will be discussed in detail in this section.

Good agreement was found between the predicted UMP and the measured values (figure 6.14). It can be seen that the 100 Hz component when the rotor was moved in the horizontal direction was much higher than predicted. This has already been discussed in section 6.3.4; a fuller explanation for this is also given in appendix E. The measured major vibrational components are shown in figure 6.15. It can be seen that there is a major 100 Hz horizontal component even when the machine is concentric. This component is therefore difficult to predict with any accuracy. Some geometrical variation was also found with the series connection (as shown in figure 6.16). This phenomenon did not occur with the six and ten-pole series connections.

The currents are still close to being a balanced three-phase set but the agreement between the predicted currents and the measured values initially appeared to be poor. However it has to be noted that, for the ten-pole and six-pole machines the core-back MMF drop was insignificant and no noticeable iron loss component was found. When the windings are connected in a two-pole configuration then there is significant core-back MMF drop which ought to be taken into account. Iron losses will as a result also be significant. This is because the machine was not designed as a two-pole machine and the core-back is relatively thin. Using a typical B-H curve and the machine dimensions, an approximate value of the amp-turns around the core-back can be made and an additional reactive component added in parallel to the magnetising reactance. For a peak flux density $B_{pk}$ in the airgap then the peak

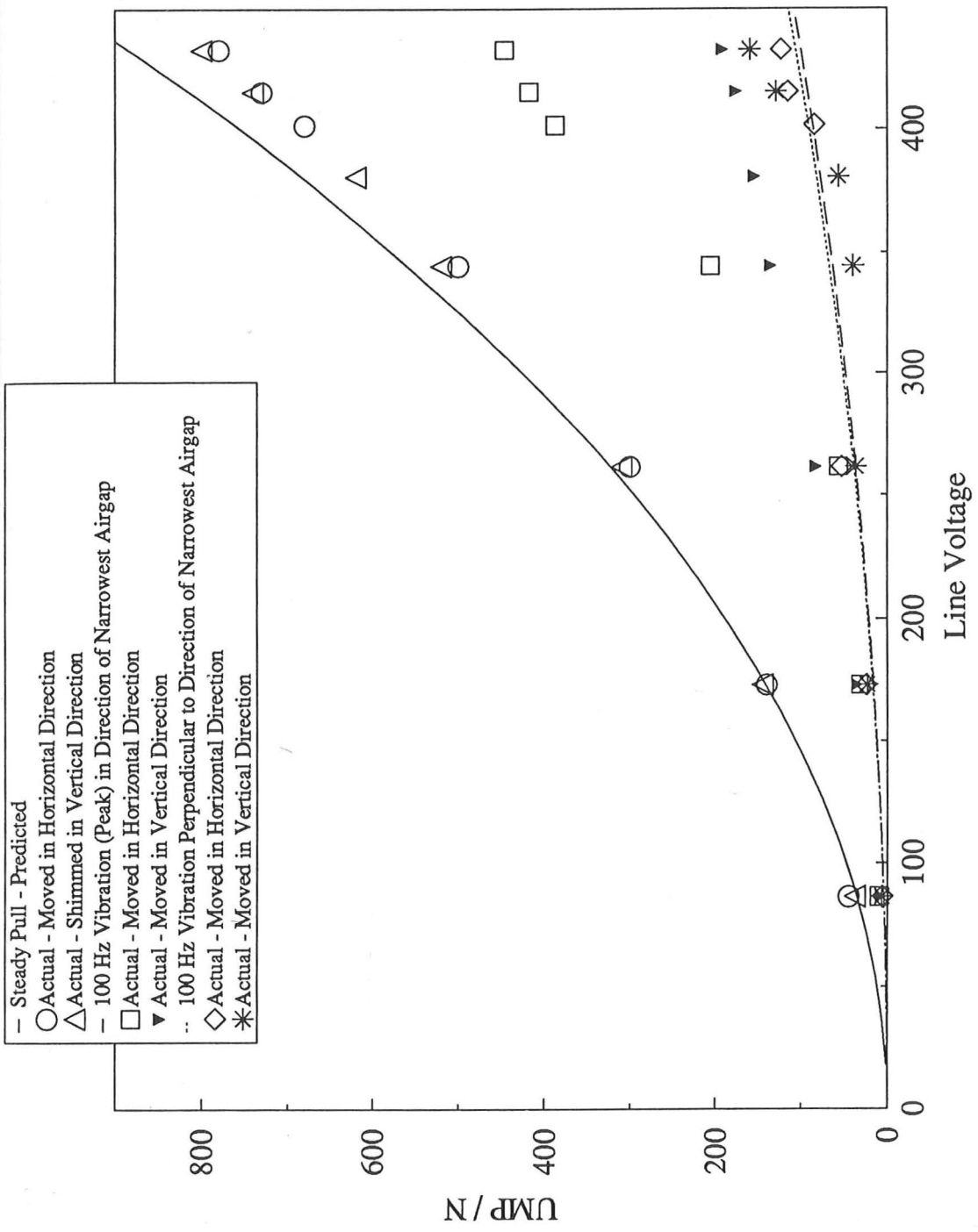


Figure 6.14: Variation of UMP with Line Voltage for a Two-Pole Series Winding at 80 % Eccentricity.

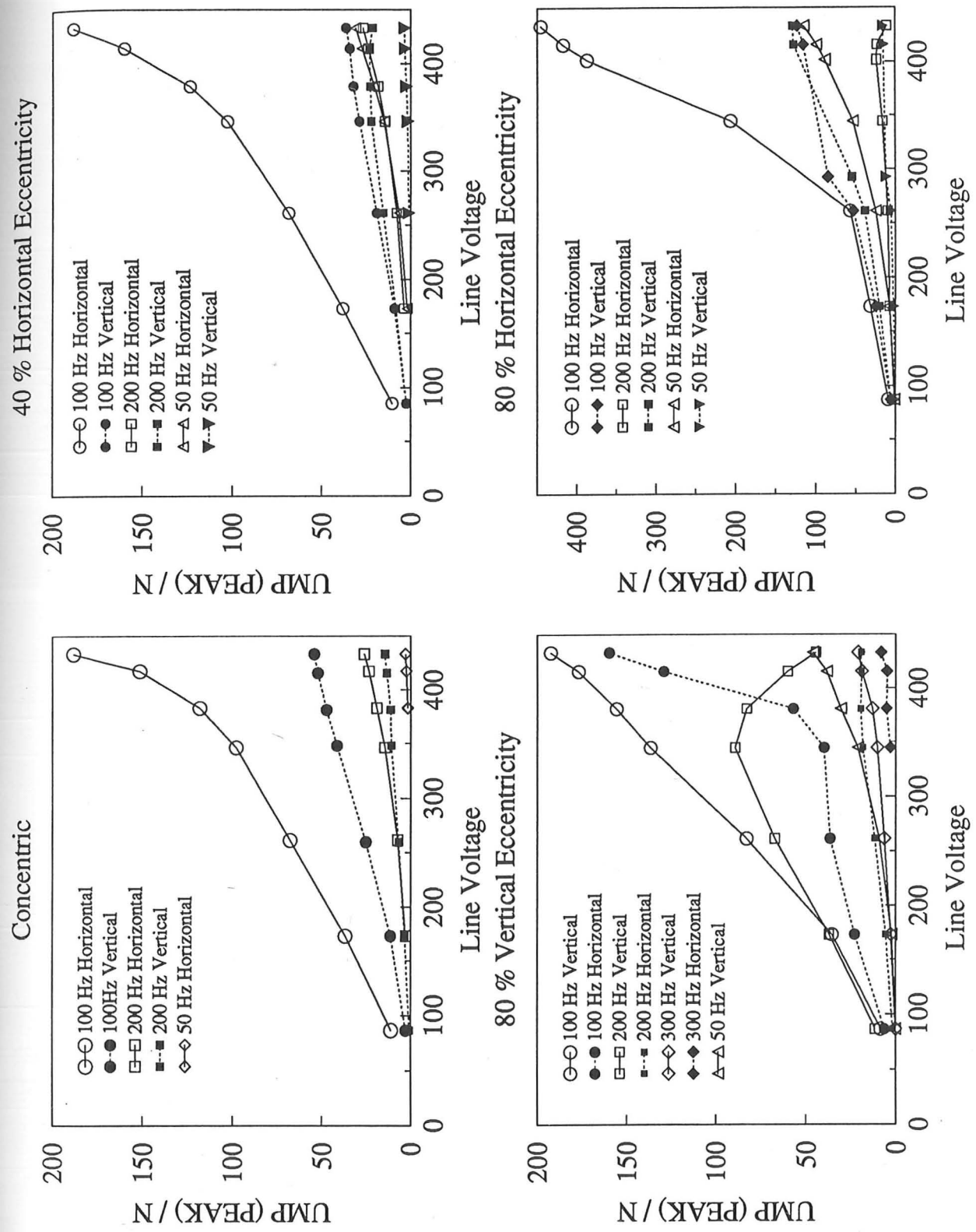


Figure 6.15: Variation of Measured 50Hz, 100 Hz and 200 Hz Vibrating UMP Components with Line Voltage for a Two-Pole Series Winding at Different Eccentricities.

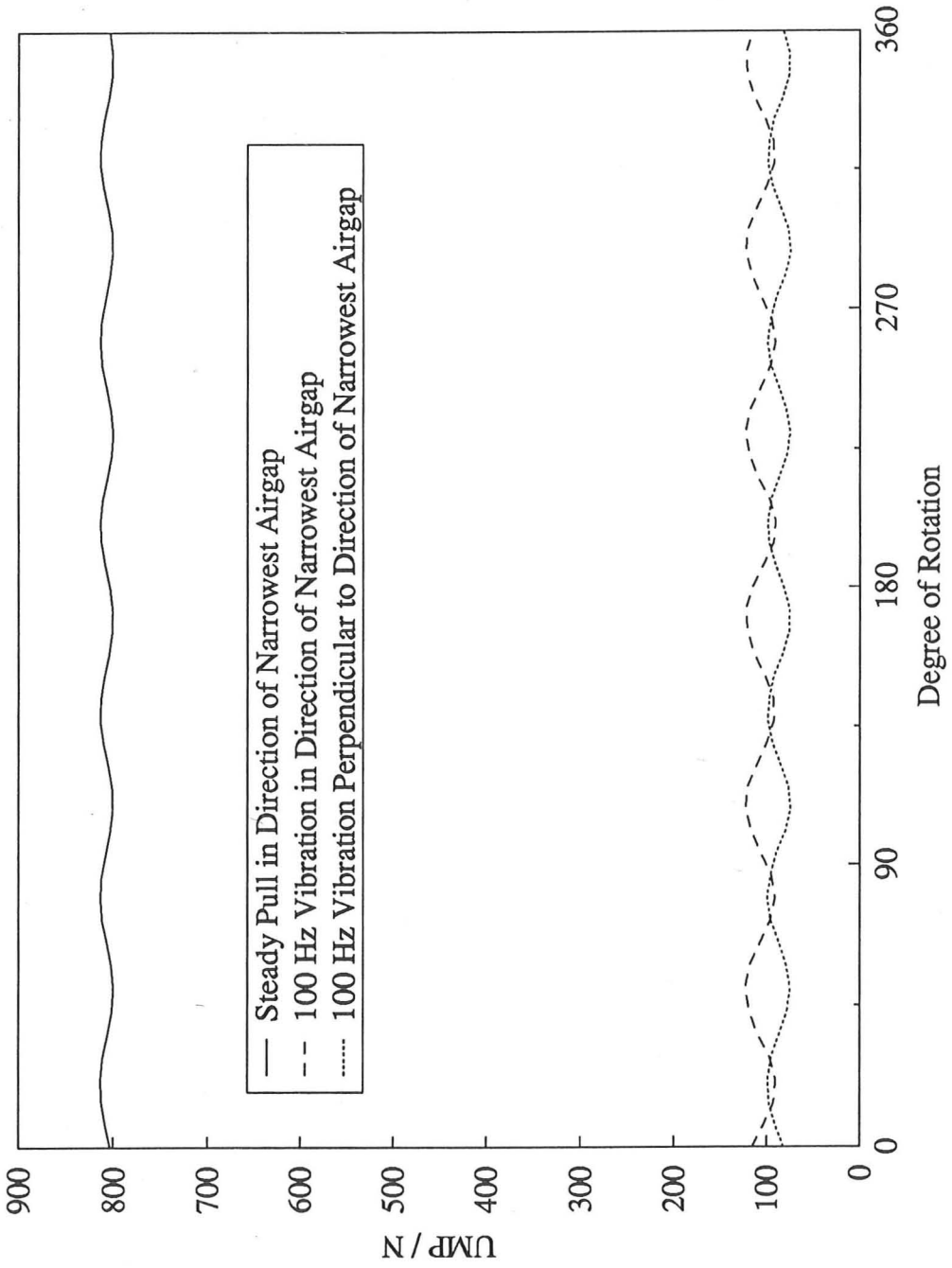


Figure 6.16: Predicted Variation of UMP with Coil Rotation with Respect to Point of Narrowest Airgap for a Two Pole Series Connection, Eccentricity is 80 % and Line Voltage 240 V.

ampere-turns across the airgap is

$$F_{ag} = \frac{B_{pk}}{\mu_o} g_{av} = 1297 B_{pk}. \tag{6.4}$$

The outside diameter of the core-back is 0.42 m with a core depth of 25 mm, therefore the average core-back diameter is 0.395 m. The approximate half distance travelled round the core back by a flux line passing through the pole peaks is then

$$l_{core} = \frac{\pi 0.395}{2 \times 2} + \frac{0.025}{2} = 0.323 \text{ m}. \tag{6.5}$$

The peak flux density in the core-back can be related to the peak airgap flux density by the equation

$$B_{core} = \frac{r B_{pk}}{\text{pole pairs} \times \text{core depth}} = 6 B_{pk}. \tag{6.6}$$

Therefore the ampere-turns around half the core-back length is

$$F_{core} = H_{core} \times l_{core} = 0.323 \times 173 \times 6 B_{pk} = 335 B_{pk} \tag{6.7}$$

where 173 represents the reluctivity of the material in the unsaturated region. Considering the MMF of the two pole field only (i.e. considering the machine to be concentric), the airgap magnetising reactance is approximately

$$X_{airgap} = \frac{V_{line}}{I_{line}} = \frac{433}{\sqrt{3} \times 2.63} = 95 \ \Omega. \tag{6.8}$$

Therefore the core-back magnetising component can be calculated to be approximately

$$X_{core-back} = \frac{F_{core}}{F_{airgap}} X_{airgap} = 368 \ \Omega. \tag{6.9}$$

This reactance assumes negligible iron and copper losses, however only an approximation is being attempted. The almost linear current characteristic of the measured currents in figure 6.17 suggests that saturation in the core-back can be ignored although some non-linearity is evident at higher voltages. The total magnetising reactance is then the parallel combination of $X_{airgap}$ and $X_{core-back}$

$$X_{mag} = \frac{X_{airgap} X_{core-back}}{X_{airgap} + X_{coreback}} \tag{6.10}$$

The two-pole series connection exhibits some different characteristics from the six and ten-pole series connections. The latter connections virtually converge with

consideration of only the fundamental winding harmonic when using the permeance method. When the rotor is very eccentric however this is not the case with the two-pole connection. The characteristic is closer to that of the parallel connection of the six and ten-pole configurations. This is due to the presence of winding harmonics within the permeance series range (in a similar manner to the parallel connections). e.g. The fundamental winding harmonic will produce 2-pole, 4-pole, 6-pole, etc. airgap fields due to the permeance harmonics. Hence the fundamental will link with the third harmonic at high eccentricities. From simple machine theory, a third harmonic should not exist for a balanced three phase winding. In reality, a six-pole field will induce zero order e.m.f.s in the windings producing currents with equal magnitude and phase. If the windings are connected in a star then zero order currents cannot flow. In previous tests the currents were found to be a virtually balanced three phase set and earthing of the star point made no difference. When the two-pole configuration was first used it was found that there was excessive vibration so the star point was earthed and this reduced the vibration. This was probably due to the zero order currents setting up a field to counteract the six-pole field generated by the fundamental winding harmonic i.e. damping the six-pole field.

Connection of the earth to the star point makes quite a difference to the predicted values of UMP as shown in figure 6.18. If there is no earth on the star point then zero order currents cannot flow and hence convergence of the winding harmonics is immediate. If there is an earth on the star point then the zero order currents will oppose the six-pole field inducing them and hence the UMP is reduced and convergence of the steady pull occurs by including the third harmonic. The 100 Hz components converge after the seventh winding harmonic, showing there is some interaction with the higher winding harmonics.

Convergence of the current as the number of winding harmonics considered is increased is shown in figure 6.19. The current are steady after the third harmonic is included while, with the earth disconnected, currents are almost steady after inclusion of the fundamental only (the fifth and seventh harmonics having some minor effect). When the earth is disconnected the currents are predicted to be almost balanced. This shows that the current is essentially a forwards rotating current set with little backwards rotating component.

The effect of the zero order currents becomes less as the eccentricity is reduced. At 40 % eccentricity the steady pull is 343 N and the line currents are 2.56, 2.44 and 2.42 A when the winding and permeance harmonics series have converged (star point earthed and line voltage of 415 V). If the fundamental winding and one permeance harmonic only are considered then the steady pull is now 358 N and the line currents balanced at 2.52 A which is only slightly different from the earthed star point case. This is because the second permeance harmonic is quite small and therefore the six-pole field generated in the airgap will also be small.

The effect of the shaft reluctance coefficient $\alpha$ can also be studied. The effects of varying $\alpha$ are shown in figures 6.20 and 6.21. While it seems to make little difference to the steady pull, the 100 Hz components can vary greatly. The line currents also show a big variation. It is doubtful that the lower values of $\alpha$ would ever be achieved in practice due to the lack of laminations in the path (i.e. eddy currents etc. would damp the homopolar flux, effectivly creating a high reluctance path), poor magnetic material, etc.. The variation of $\alpha$ was not pursued experimentally and the results are computer predictions only.

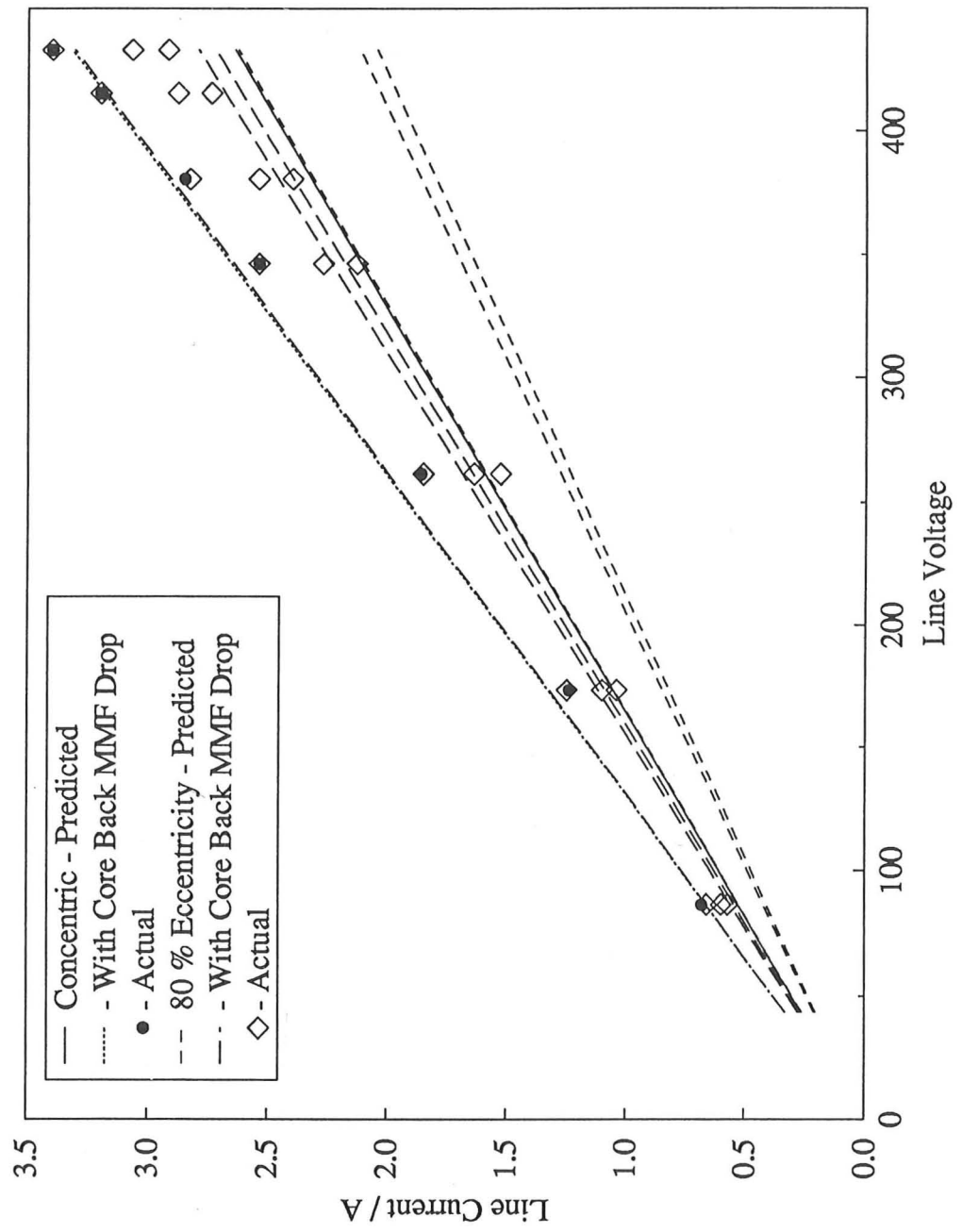


Figure 6.17: Variation of Line Current with Line Voltage for Concentric and 80 % Eccentric Rotor for a Two-Pole Configuration. The rotor was moved in a vertical direction.

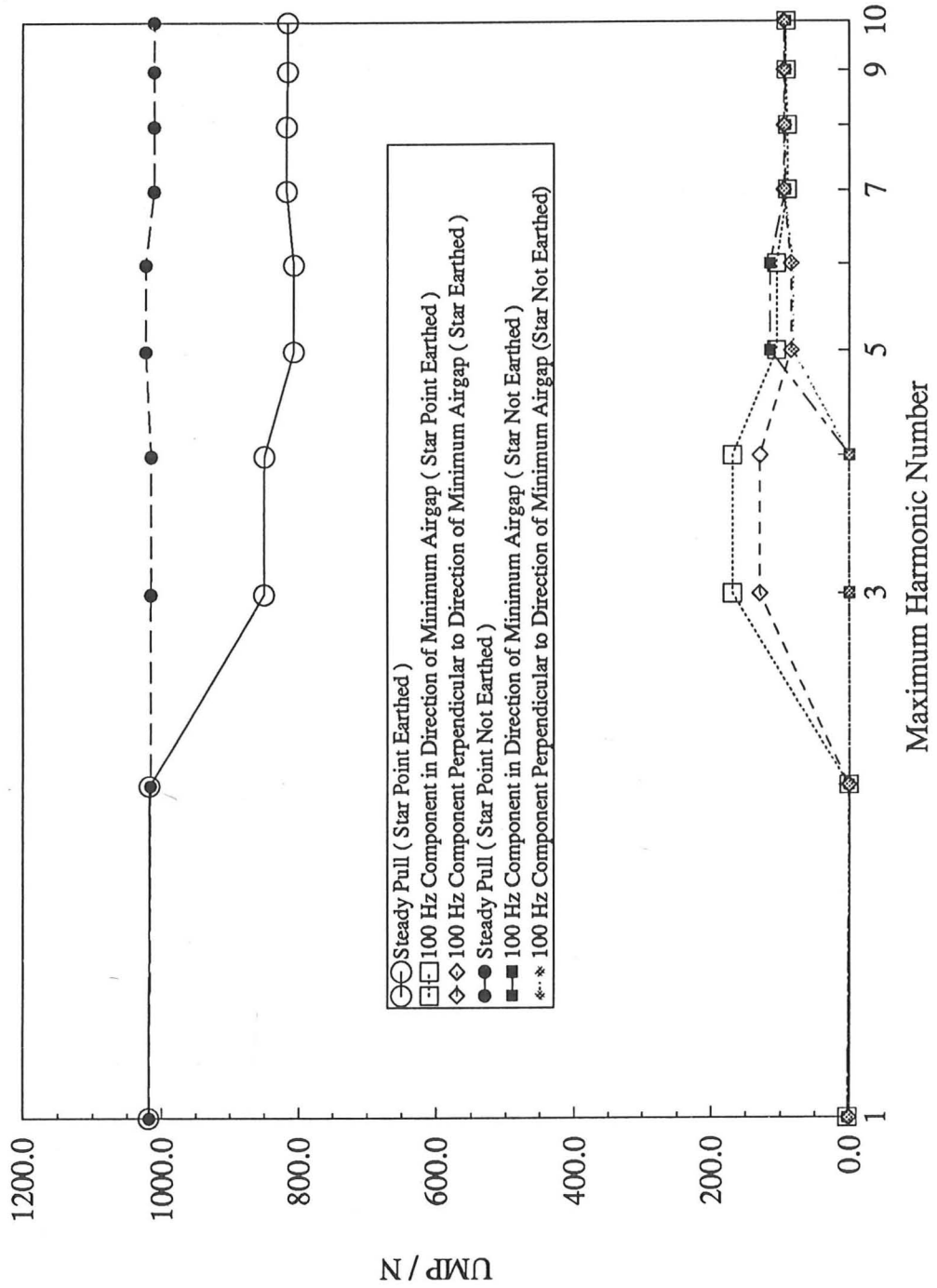


Figure 6.18: Predicted Variation of UMP with Winding Harmonic of a Two-Pole Configuration With and Without the Earthing of the Star Point. Line Voltage is 415 V and Eccentricity is 80 %.

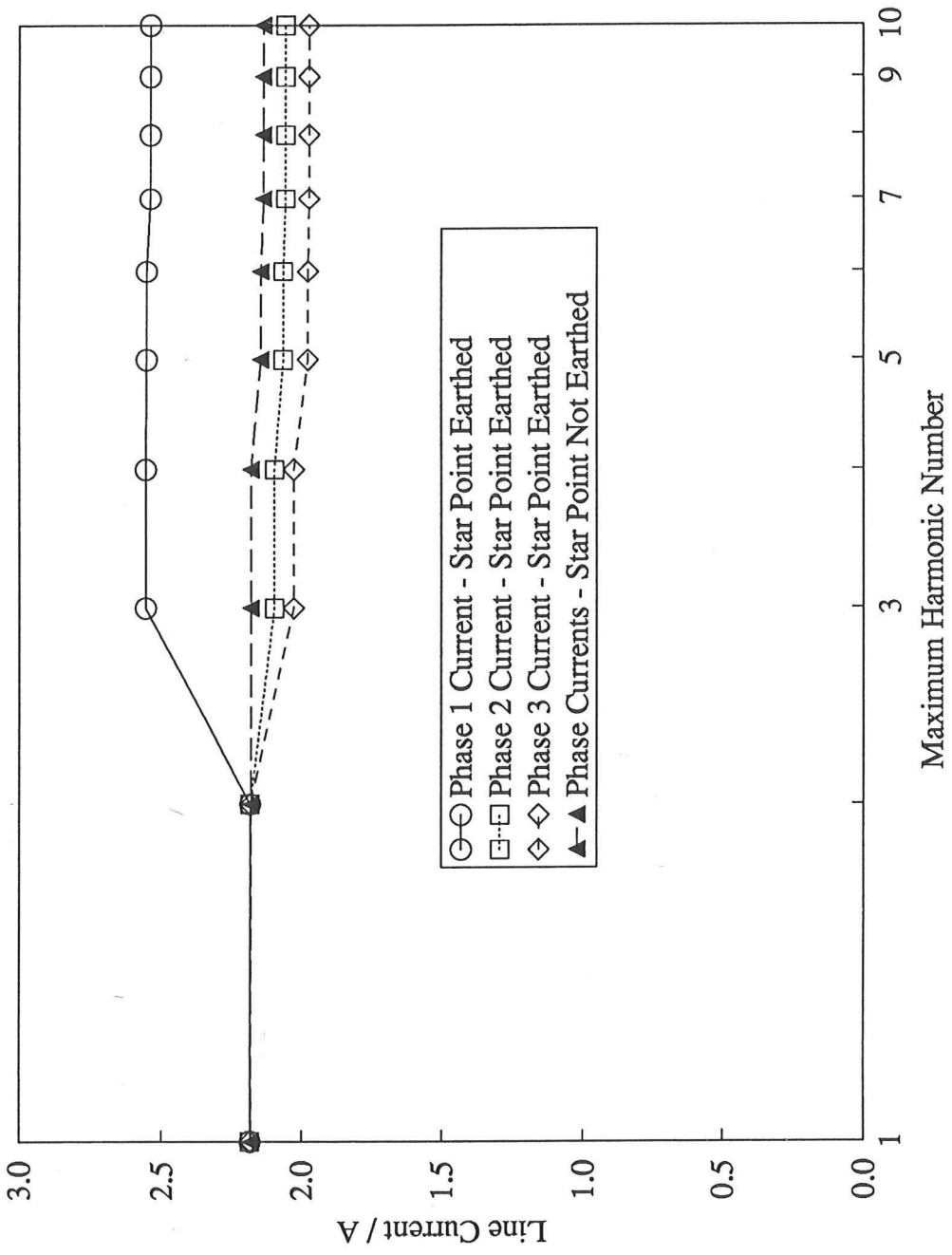


Figure 6.19: Predicted Variation of Line Current with Winding Harmonic of a Two-Pole Configuration With and Without the Earthing of the Star Point. Line Voltage is 415 V and Eccentricity is 80 %.

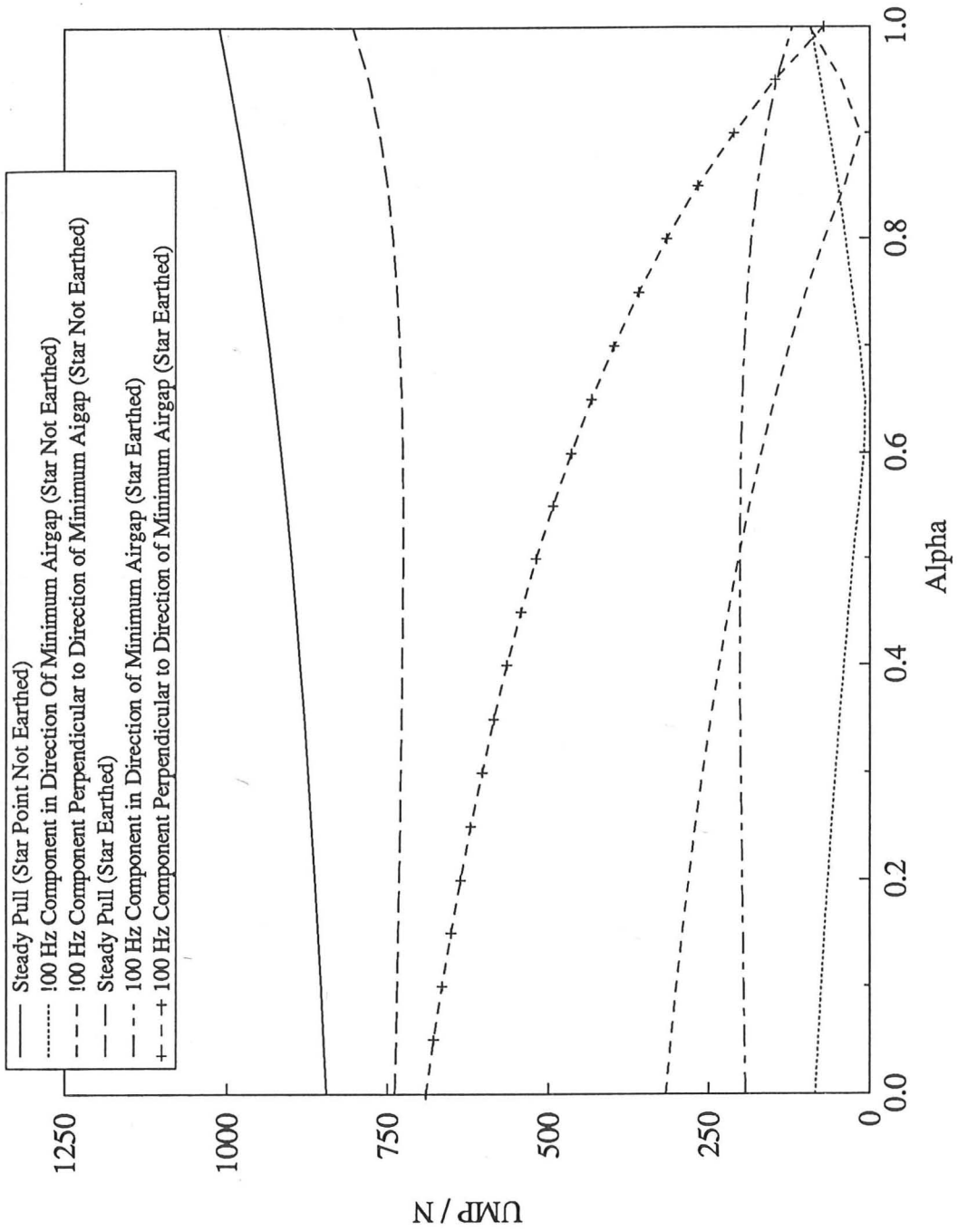


Figure 6.20: Predicted Variation of UMP with $\alpha$ of a Two-Pole Configuration With and Without the Earthing of the Star Point. Line Voltage is 415 V and Eccentricity is 80 %.

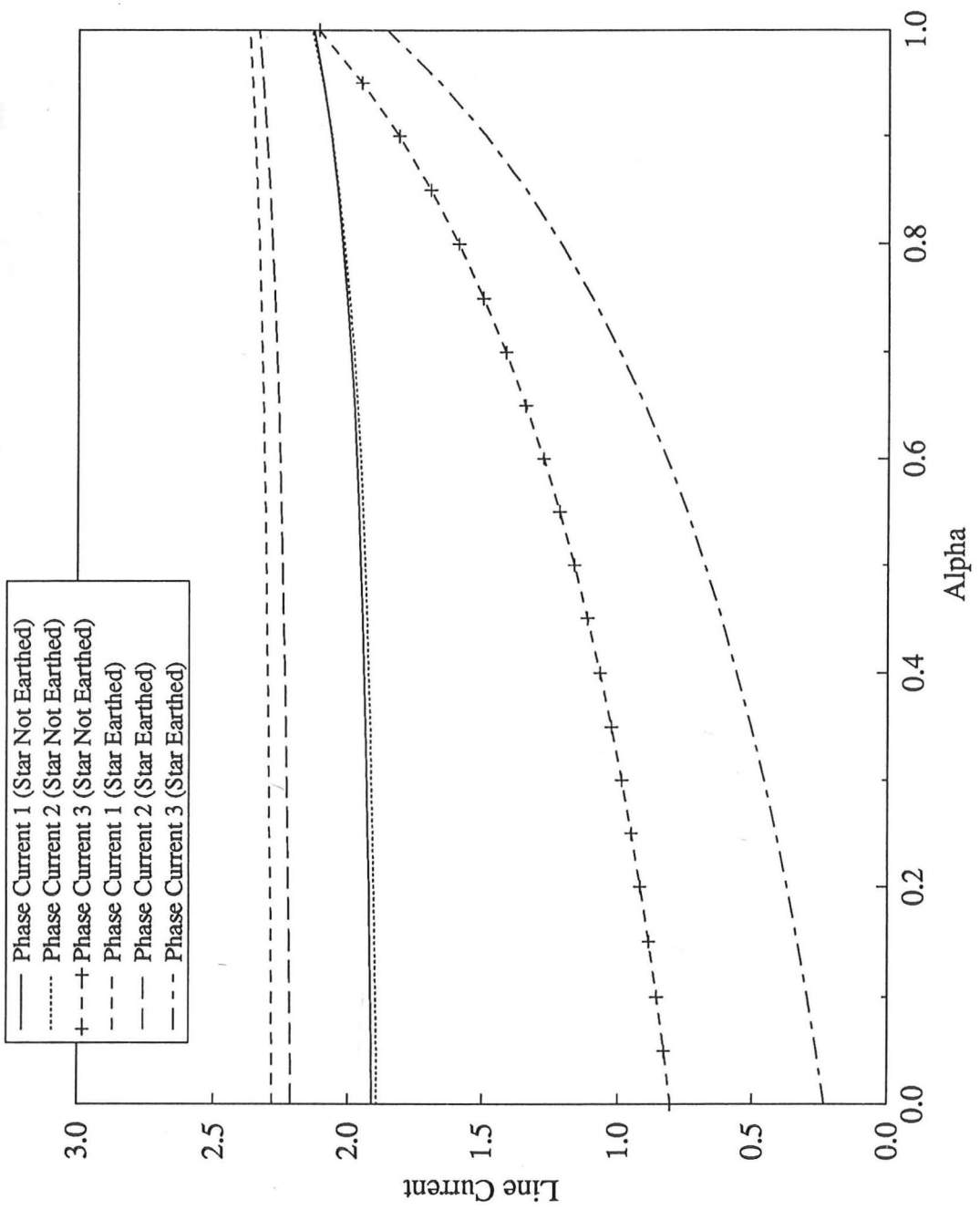


Figure 6.21: Predicted Variation of Line Current with $\alpha$ of a Two-Pole Configuration With and Without the Earthing of the Star Point. Line Voltage is 415 V and Eccentricity is 80 %.

# Chapter 7

# Ten-Pole Cage Machine

## 7.1 Introduction

The cage rotor reduced the airgap to 0.5 mm (giving an effective airgap of 0.62 mm when taking into account Carter's factors), which made alignment difficult but possible with care. The machine was not used with the six and two-pole winding configurations because of the danger of running the machine so far over-speed. Only the permeance harmonic method was developed to include a rotor model, this enabled the investigation of the influence of various winding harmonics on the UMP. Tests were carried at various eccentricities and loads. Due to the small airgap and vibration problems discussed in the previous chapter, speed/UMP curves were obtained at a reduced voltage in order to minimise the possibility of damage being caused by rotor and stator touching when there is excessive vibration. Additional information necessary is given below.

| | |
|---|---|
| Stator slot opening | 2.798 mm |
| Average airgap $g_{av}$ | 0.62 mm |
| Number of rotor slots (cage) | 80 |
| Rotor slot opening (cage) | 1.524 mm |
| Rotor slot depth (cage) | 10.7 mm |
| Rotor bar D.C. resistance (hot) | 0.103 m$\Omega$ |
| Rotor end-ring D.C. resistance (hot) | 0.0912 m$\Omega$ |
| Rotor bar D.C. leakage inductance | 0.316 $\mu$H |
| Rotor Skew | 0.89 Stator Slots |

## 7.2 Series Connection

### 7.2.1 Variation of UMP with Slip for Several Eccentricities

The variation of the line current and UMP with slip are shown in figures 7.2 and 7.3 over the slip range 0 to 0.8 and figures 7.4 and 7.5 over the slip range 0 to 0.15 for several different eccentricities at a line voltage of 208 V. The currents appeared to be a balanced three phase set and the correlation between the predicted and measured was very good. The UMP is steady and directed towards the point of minimum airgap, the 100 Hz components of UMP were negligible. It can be seen that the theoretical predictions and the measured values of UMP match well. The only divergence is at high eccentricity and high slip but the results prove excellent over the low slip range where the machine would normally operate.

The small peak in the curves at a slip of 0.167 corresponds to rotation of the rotor at the synchronous speed of the twelve-pole field. The rotor will not damp this field and therefore there is a slight increase in UMP about this point.

The results at high eccentricity and high slip in figure 7.3 seem poor. However, if the UMP is displayed as varying against eccentricity for certain values of slip then the results appear to be quite good. Figure 7.6 shows the variation of UMP against eccentricity for slips of 0.1 and 0.4. The steep rise of the UMP at high eccentricity for a slip of 0.4 leads to the large error between the predicted and measured results. Figure 7.7 shows that there is not the decrease in current with increase in eccentricity predicted, hence the measured UMP results are higher than predicted.*

There are several factors which are not considered in the theoretical solution which will affect the calculation of the line currents and the UMP. Classical per-phase machine circuits suggests that a component of the magnetising reactance $X_m$ is in series with the rotor reactances if the machine is skewed [44]. The rotor branch according to reference [44] is shown in figure 7.1, which considers the equivalent circuit for the



* The calculation of harmonic distributions includes a slot mouth width factor. It is possible that as the current increases at high values of slip, increased tooth saturation reduces this factor to such an extent that the harmonic fields are significantly reduced. This could also affect UMP.

fundamental, forwards rotating field only. The rotor branch is therefore

$$\overline{Z}_r = j\left(\left(\frac{1}{K_s}\right)^2 - 1\right) X_m + j\left(\frac{1}{K_s}\right)^2 X_2' + \left(\frac{1}{K_s}\right)^2 \frac{R_2'}{s} \tag{7.1}$$

where $K_s$ is the skew factor, $X_2'$ is the referred rotor leakage reactance and $R_2'$ is the referred rotor resistance. The magnetising reactance can be considered as consisting of three components (in parallel) caused by the airgap m.m.f., the core-back m.m.f. and the tooth m.m.f. The latter two, for a well designed machine, should be negligible when the machine is near synchronous speed. As the slip increases saturation in various parts of the core will occur and hence $X_m$ may reduce. Since no account is taken of core-back and tooth saturation, the predicted line currents may be less than the measured. The initial value of $X_1$ was calculated without taking saturation into account. In addition, the end-winding component of $X_1$ is substantial (nearly 30 %) and it has been shown that this component substantially reduces as the slip increases [71]. The effect of $X_1$ is greatest when the slip is unity and the current is high, as the slip approaches zero the equivalent circuit input impedance is much higher and $X_1$ become negligible . More accurate results would therefore be obtained by using a value of $X_1$ derived from a locked rotor test. This led to a reduction in $X_1$ of 30 %.

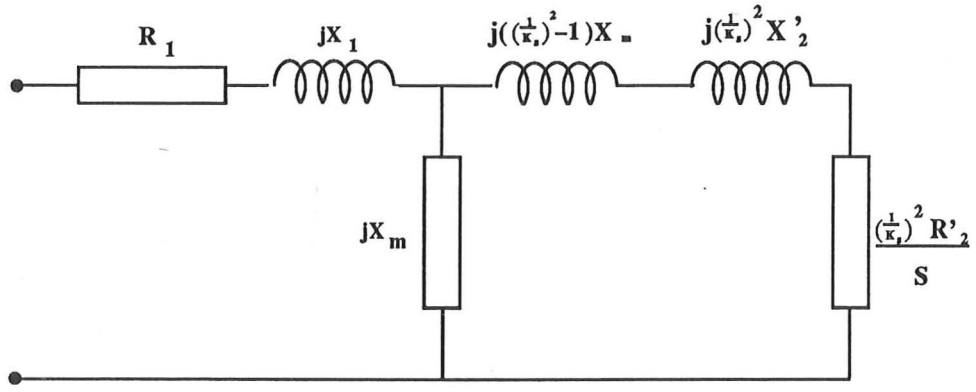


Figure 7.1: Equivalent Circuit with the Skew Factor Considered.

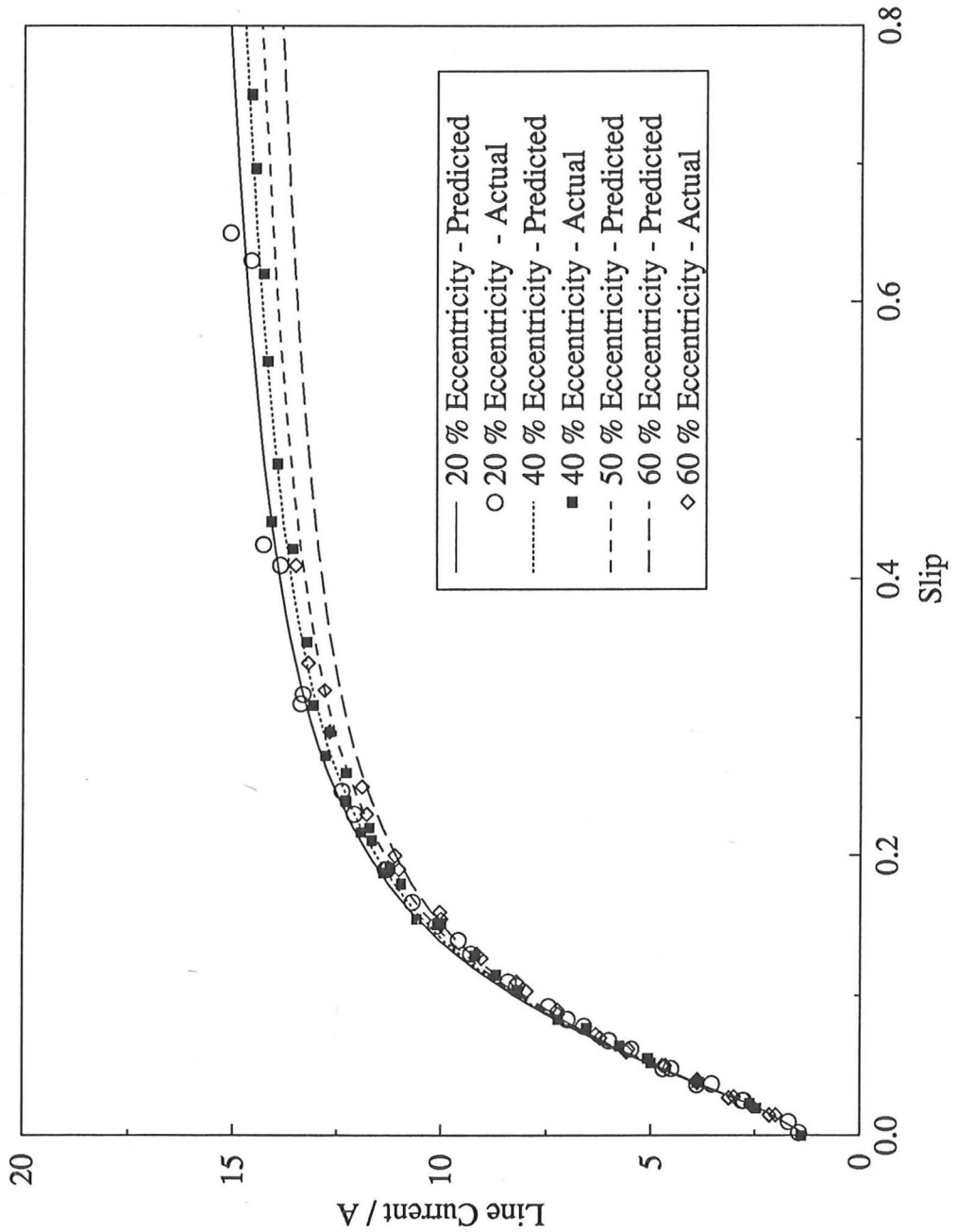


Figure 7.2: Variation of Line Current with Slip at Several Eccentricities and a Line Voltage of 208 V for the Ten-Pole Series Connected Machine with Cage Rotor

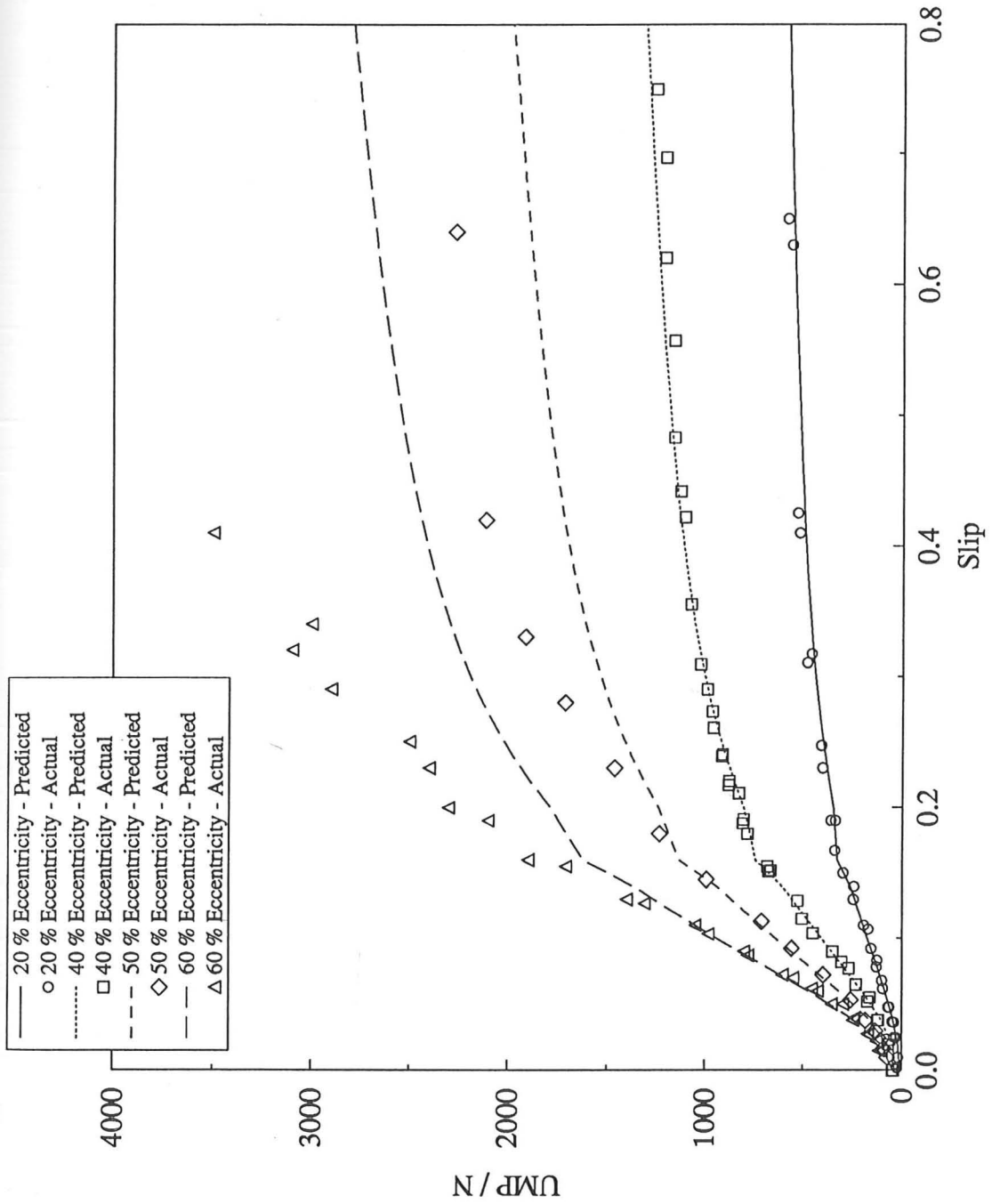


Figure 7.3: Variation of UMP with Slip at Several Eccentricities and a Line Voltage of 208 V for the Ten-Pole Series Connected Machine with Cage Rotor

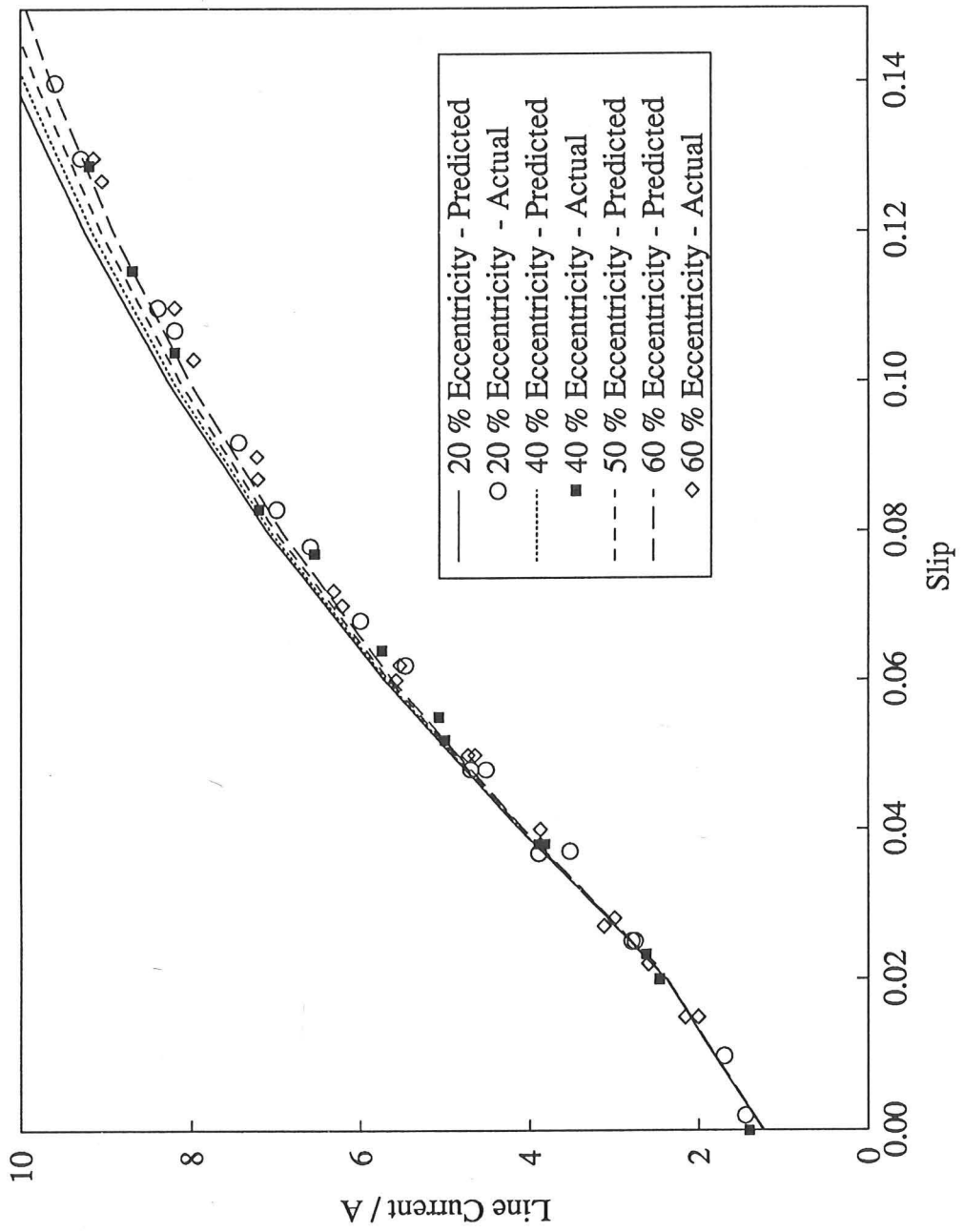


Figure 7.4: Variation of Line Current with Slip at Several Eccentricities and a Line Voltage of 208 V for the Ten-Pole Series Connected Machine with Cage Rotor

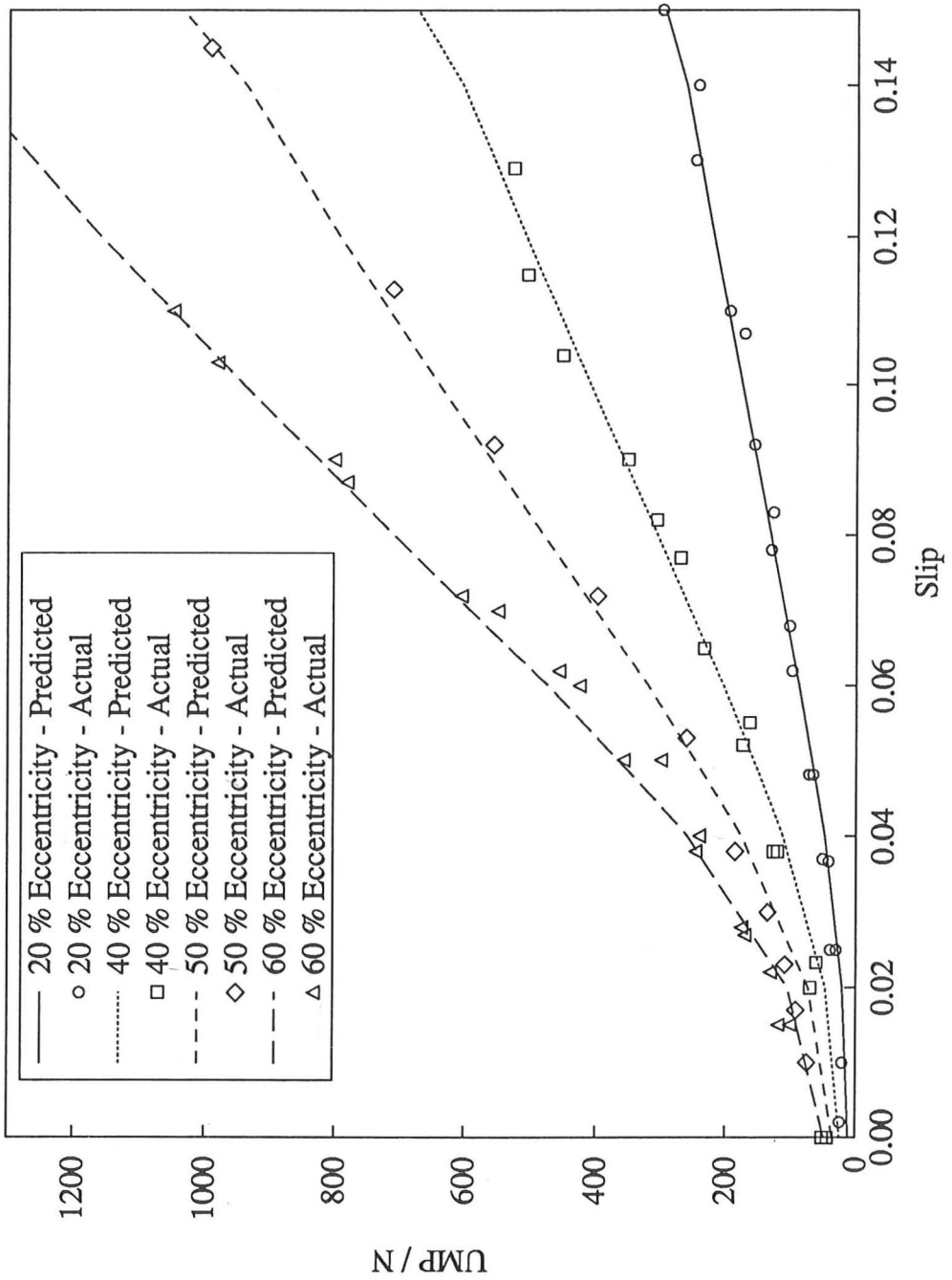


Figure 7.5: Variation of UMP with Slip at Several Eccentricities and a Line Voltage of 208 V for the Ten-Pole Series Connected Machine with Cage Rotor

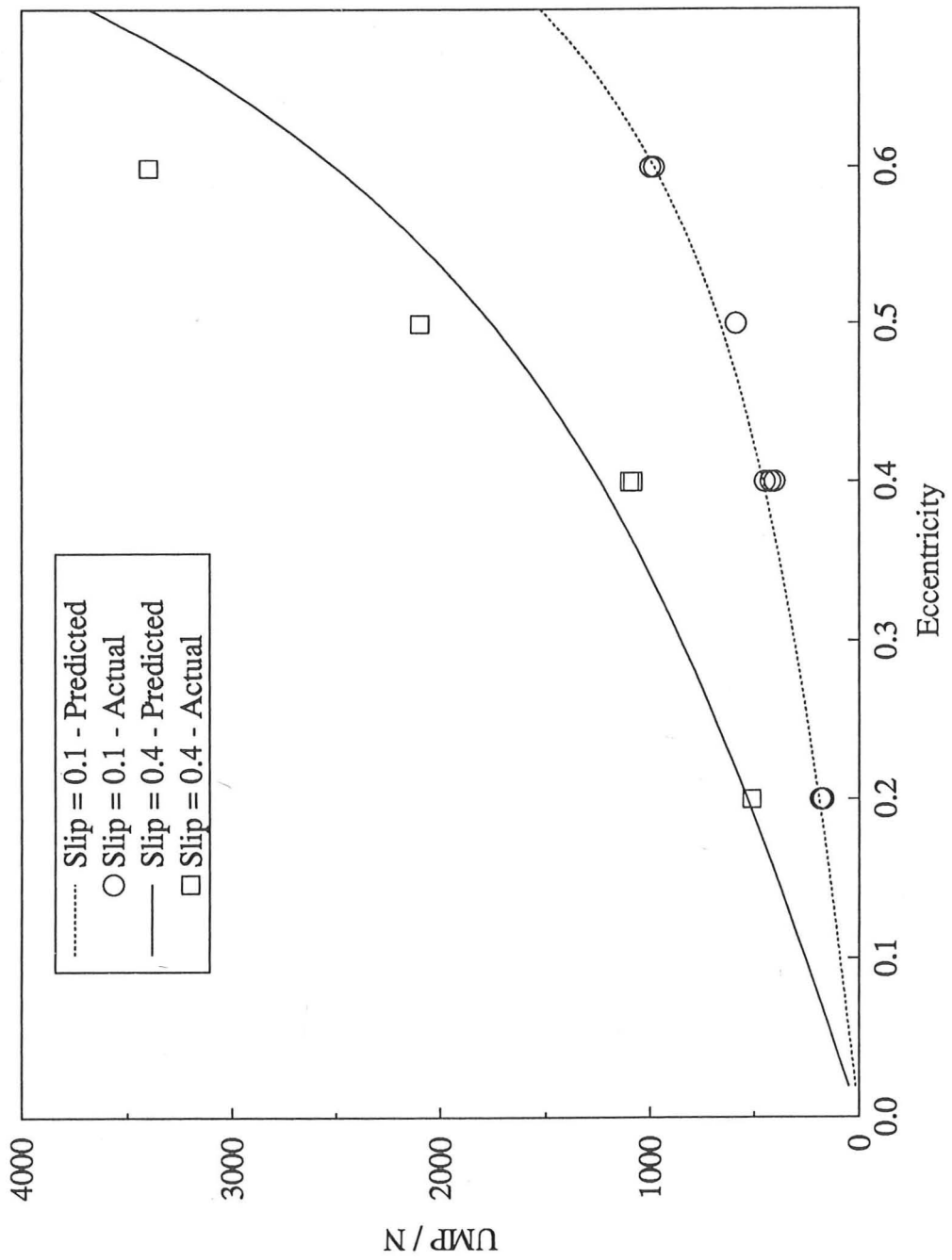


Figure 7.6: Variation of UMP with Eccentricity for Slips of 0.1 and 0.4 and a Line Voltage of 208 V for the Ten-Pole Series Connected Machine with Cage Rotor

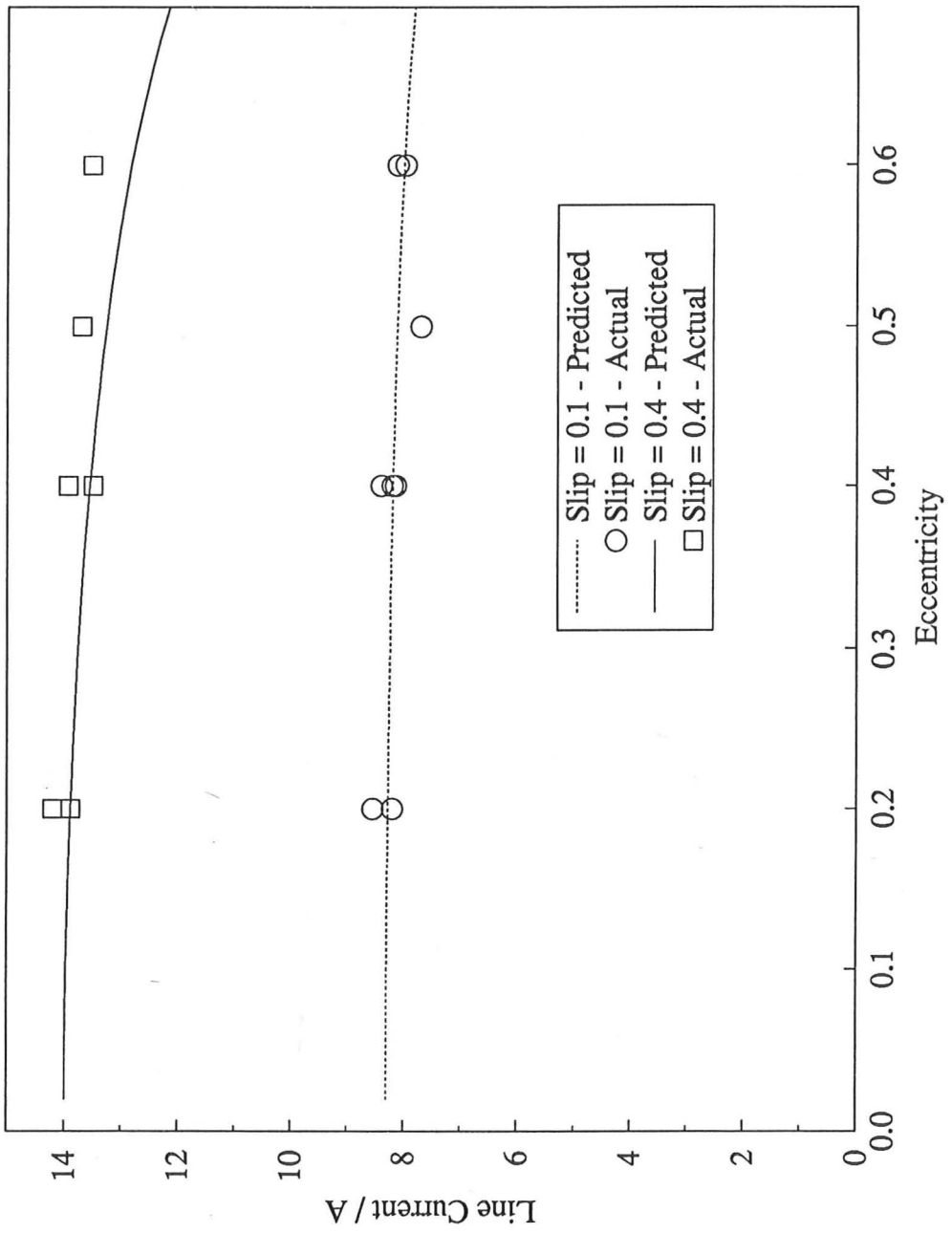


Figure 7.7: Variation of Line Current with Eccentricity at for Slips of 0.1 and 0.4 and a Line Voltage of 208 V for the Ten-Pole Series Connected Machine with Cage Rotor

### 7.2.2 Effect of the Winding Harmonic Series on UMP

The effect of the winding harmonic on the line current and UMP can be seen in figures 7.8, 7.9 and 7.10. The series is shown to stop at a winding harmonic number of 110. The winding harmonic series has converged at this point with no variation in current and UMP, the series was actually taken up to 400.

There is a significant contribution to the UMP by the higher harmonics. For a series connected ten pole machine where the fundamental is the fifth winding harmonic then the 85th and 95th winding harmonics correspond to the 17th and 19th ten-pole series winding harmonics. The reason for using a fundamental base winding harmonic of one on these graphs is to illustrate that these lie near the number of rotor bars. Any field which has a pole-pair number equal to the number of bars will not induce any currents in the rotor cage. Similarly any field with a pole-pair number close to the number of rotor bars will induce only small currents in the cage. Hence if there are any significant winding harmonics close to the number of bars their fields will not be damped by the rotor cage. Whilst the magnitudes of these stator fields may seem insignificant compared to the fundamental stator field, the absence of induced rotor currents is such that the 85th and 95th winding harmonics can make a significant contribution. As the slip and currents increase then the contribution to the UMP of these higher harmonics also increases. This is because the higher harmonic fields increase and are not opposed by any fields set up by the rotor currents.

This phenomenon represents an important aspect of UMP in cage induction motors but has not been previously studied. At a slip of 0.4 and 40 % eccentricity the higher field harmonics contribute nearly a third of the total UMP of the machine.

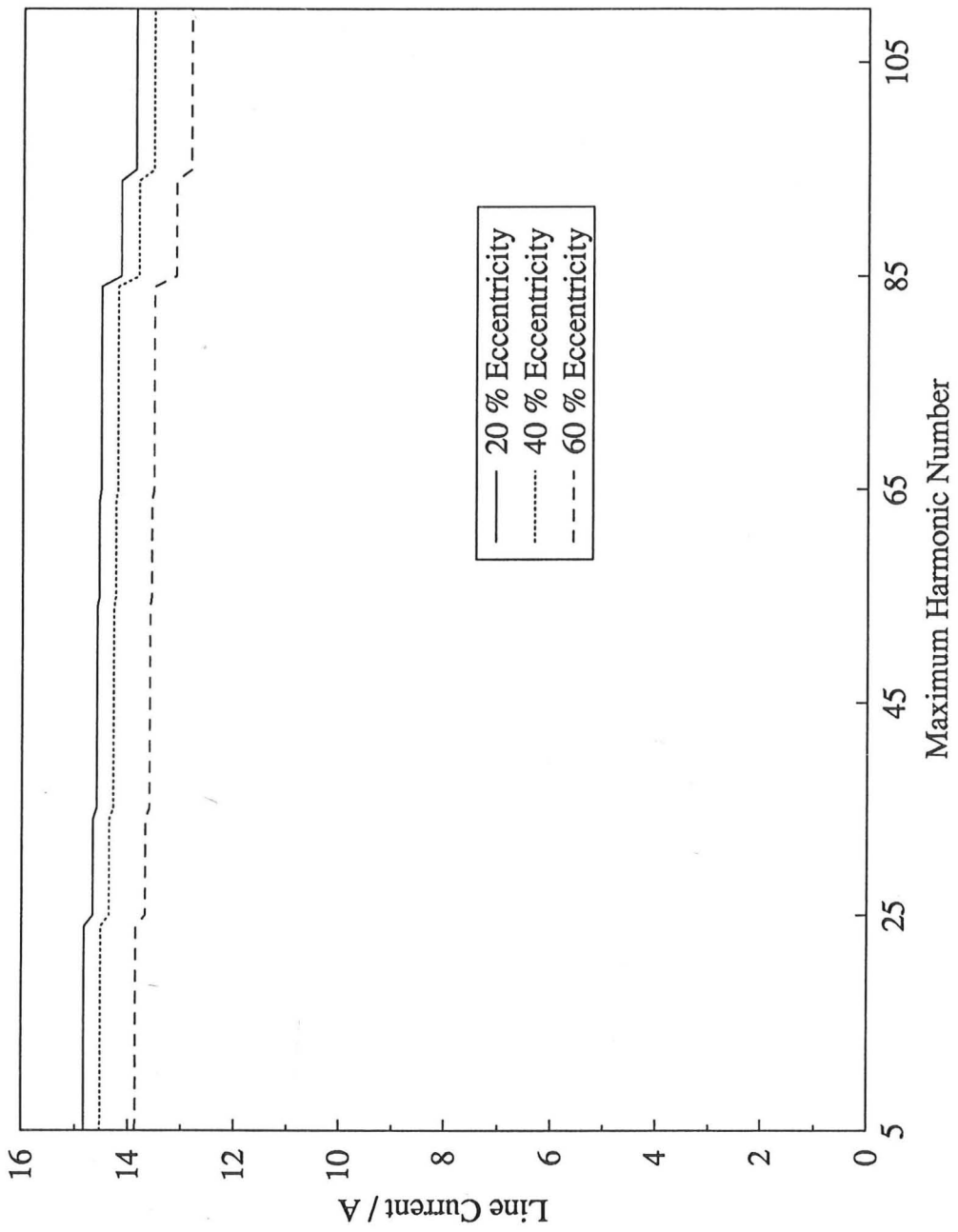


Figure 7.8: Predicted Variation of Line Current with Maximum Winding Harmonic Number at Several Eccentricities and slip values at a Line Voltage of 208 V for the Ten-Pole Series Connected Machine with Cage Rotor

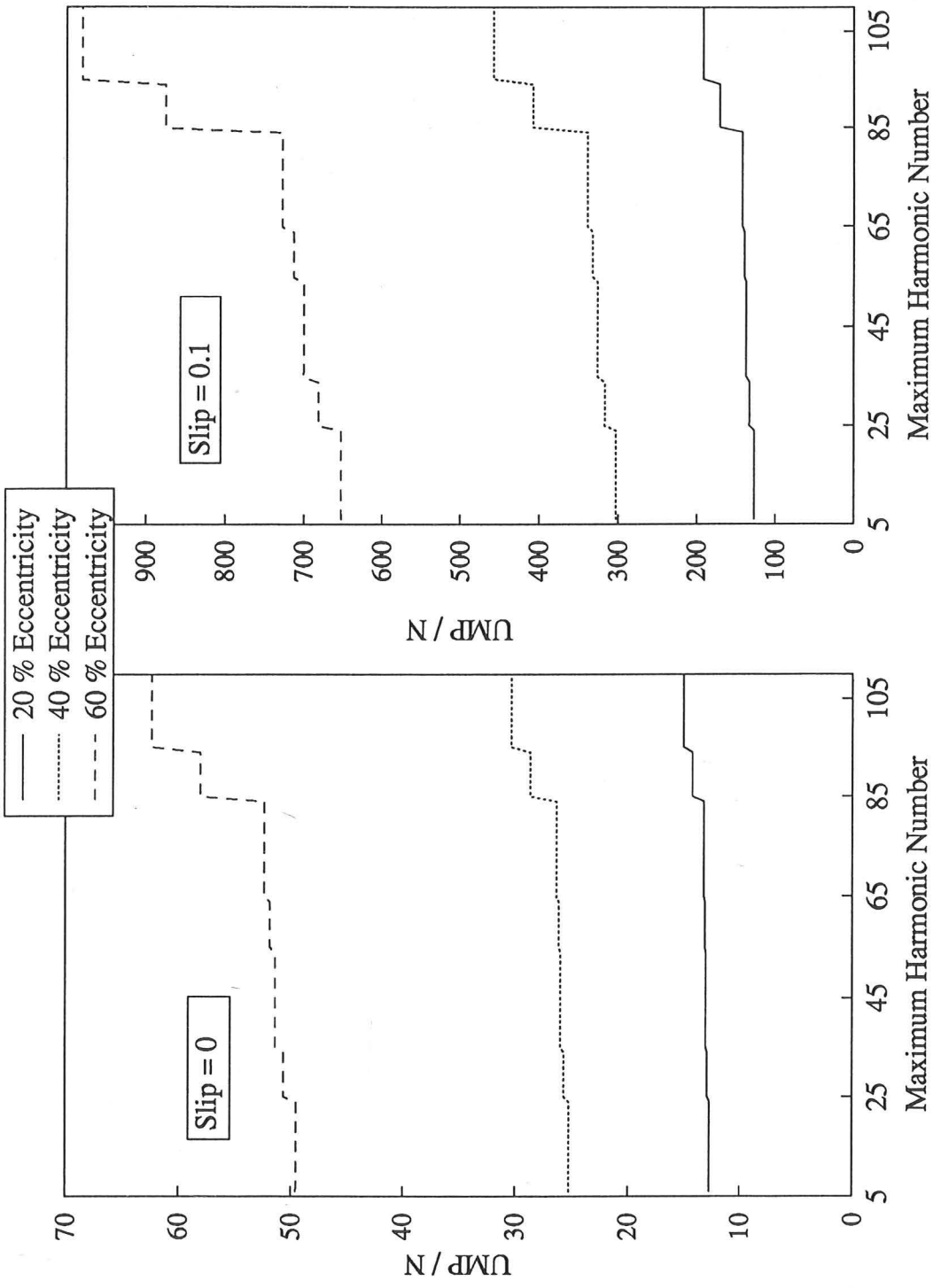


Figure 7.9: Predicted Variation of UMP with Maximum Winding Harmonic Number at Several Eccentricities, a Line Voltage of 208 V and Slips of 0 and 0.1 for the Ten-Pole Series Connected Machine with Cage Rotor

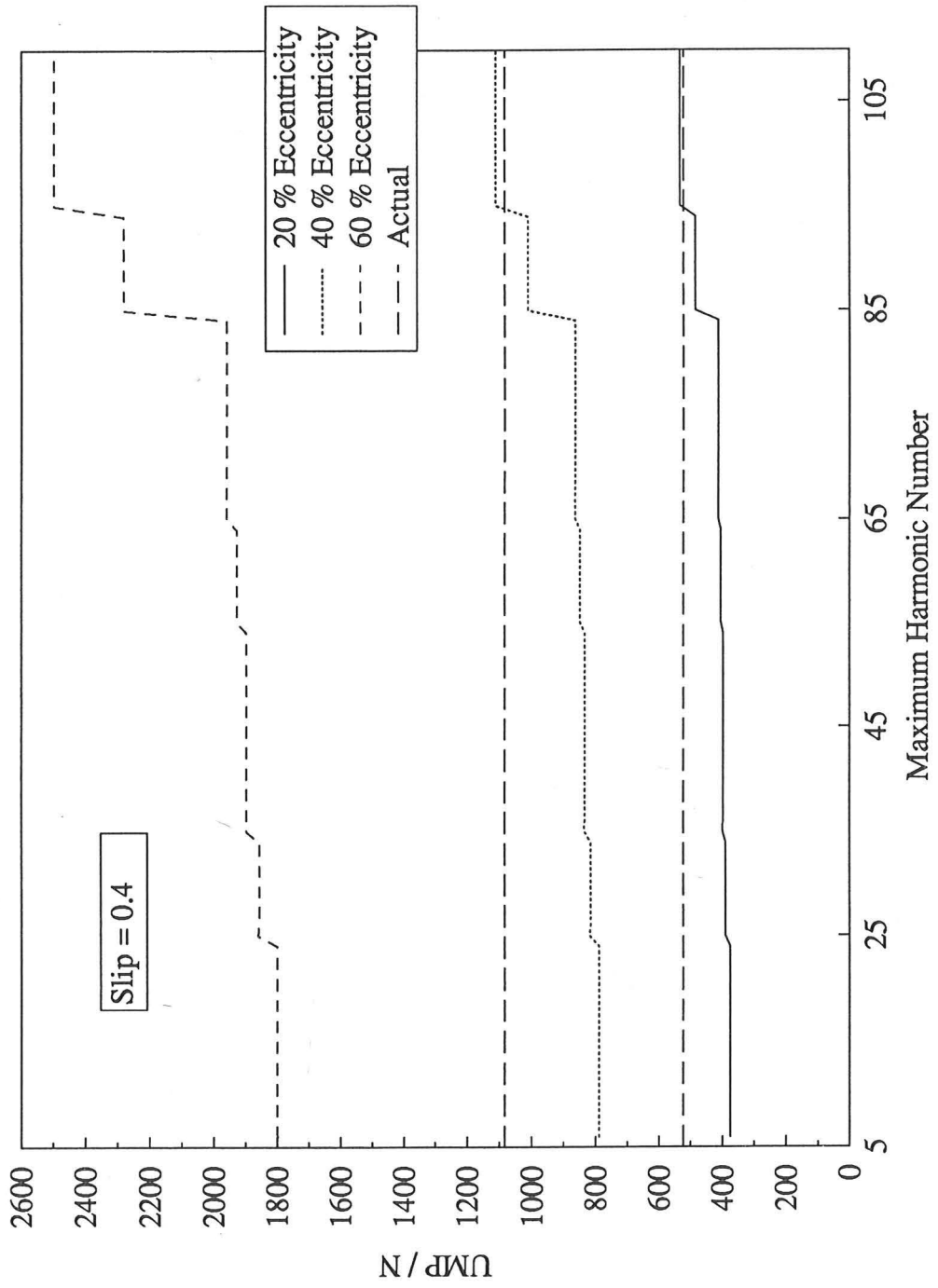


Figure 7.10: Predicted Variation of UMP with Maximum Winding Harmonic Number at Several Eccentricities, a Line Voltage of 208 V and a Slip of 0.4 for the Ten-Pole Series Connected Machine with Cage Rotor

### 7.2.3 Effect of Rotor Skew on UMP

Rotor skew has a great influence on the UMP. The primary reasons for skew are to remove slotting harmonics and prevent asynchronous cogging torques. However, it will also have the effect of reducing the magnitude of the rotor fields relative to the stator fields because the rotor currents will be attenuated to some degree. This is illustrated in figure 7.11 where the UMP is substantially increased by skewing the rotor (about 150 % at slips of 0.1 and 0.4). The variation of the line current is shown in figure 7.12, as expected the line current decreases with increasing skew since the e.m.f. induced in the rotor bars by the stator fields decreases.

The main effect of skewing will be on the fundamental since the higher harmonics are already undamped because their pole-pair numbers are close to the cage bar number. This is shown in figure 7.13 where the only stator winding harmonic considered is the fundamental. The increase in UMP with skew is only slightly greater than in figure 7.11. It is assumed therefore that the UMP caused by the higher field harmonics increases by only a small amount as the skew increases (as the difference between the graphs of figures 7.11 and 7.13 would indicate). The current variation is shown in figure 7.14, the decrease is similar to that in figure 7.12 (1 A between 0 and 0.8 slip) although the current magnitudes are slightly increased by 1 A across the slip range. This means that the increase in UMP in the graphs from figure 7.11 to 7.13 should be slightly higher even if the contribution to the UMP of the higher harmonic fields is constant across the slip range for both figures.

This effect has previously been neglected by authors and presents an interesting problem. Whilst skewing the rotor improves the running stability of the machine the predictions indicate it can significantly increase the UMP generated in the machine when the rotor is not centred. Whether these theoretical predictions would be born out in practice for a different machine which is running at full voltage is difficult to assess since the effect of axial saturation has not been taken into account.

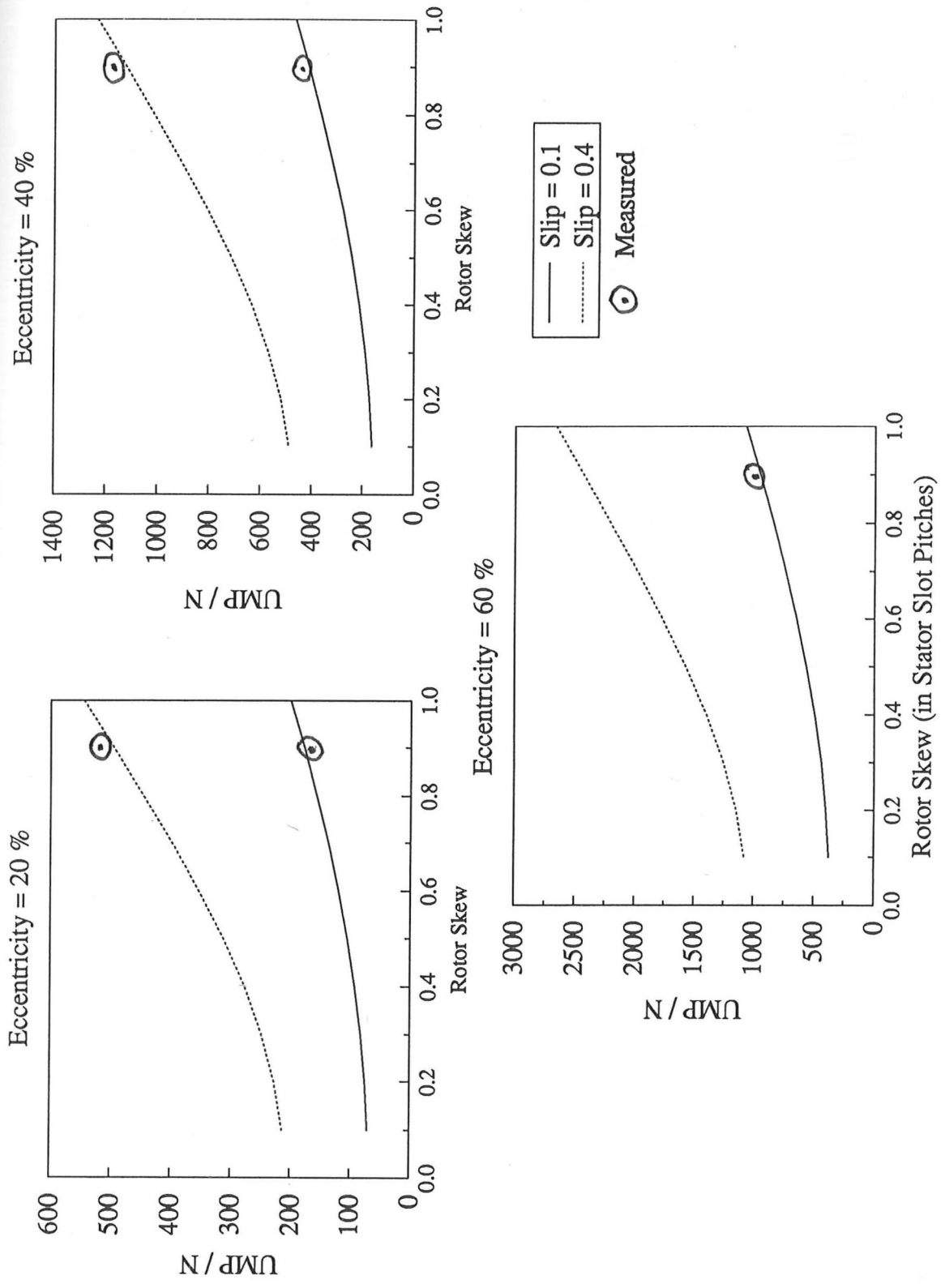


Figure 7.11: Predicted Variation of UMP with Rotor Skew at Several Eccentricities and slip values at a Line Voltage of 208 V for the Ten-Pole Series Connected Machine with Cage Rotor

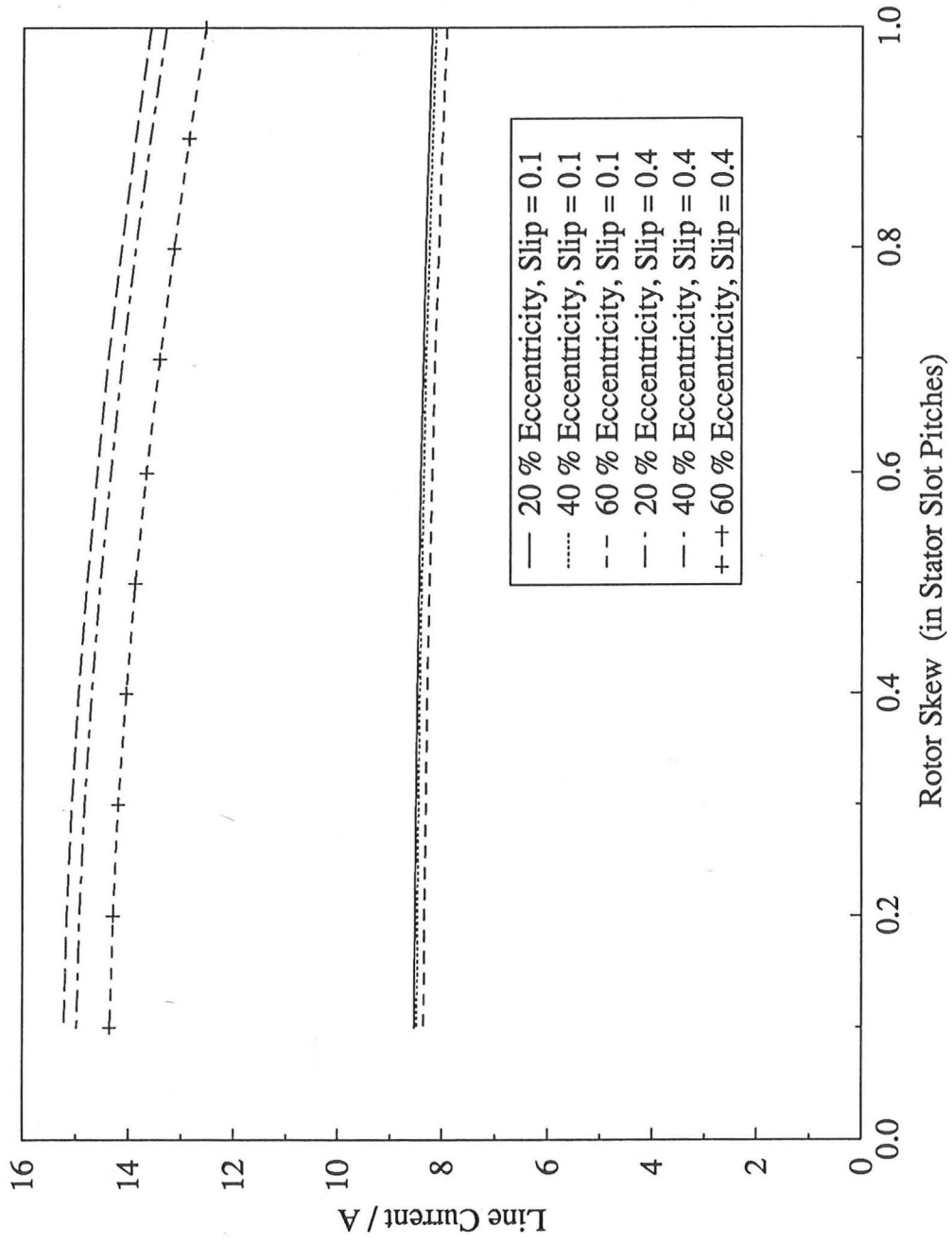


Figure 7.12: Predicted Variation of Line Current with Rotor Skew at Several Eccentricities and slip values at a Line Voltage of 208 V for the Ten-Pole Series Connected Machine with Cage Rotor

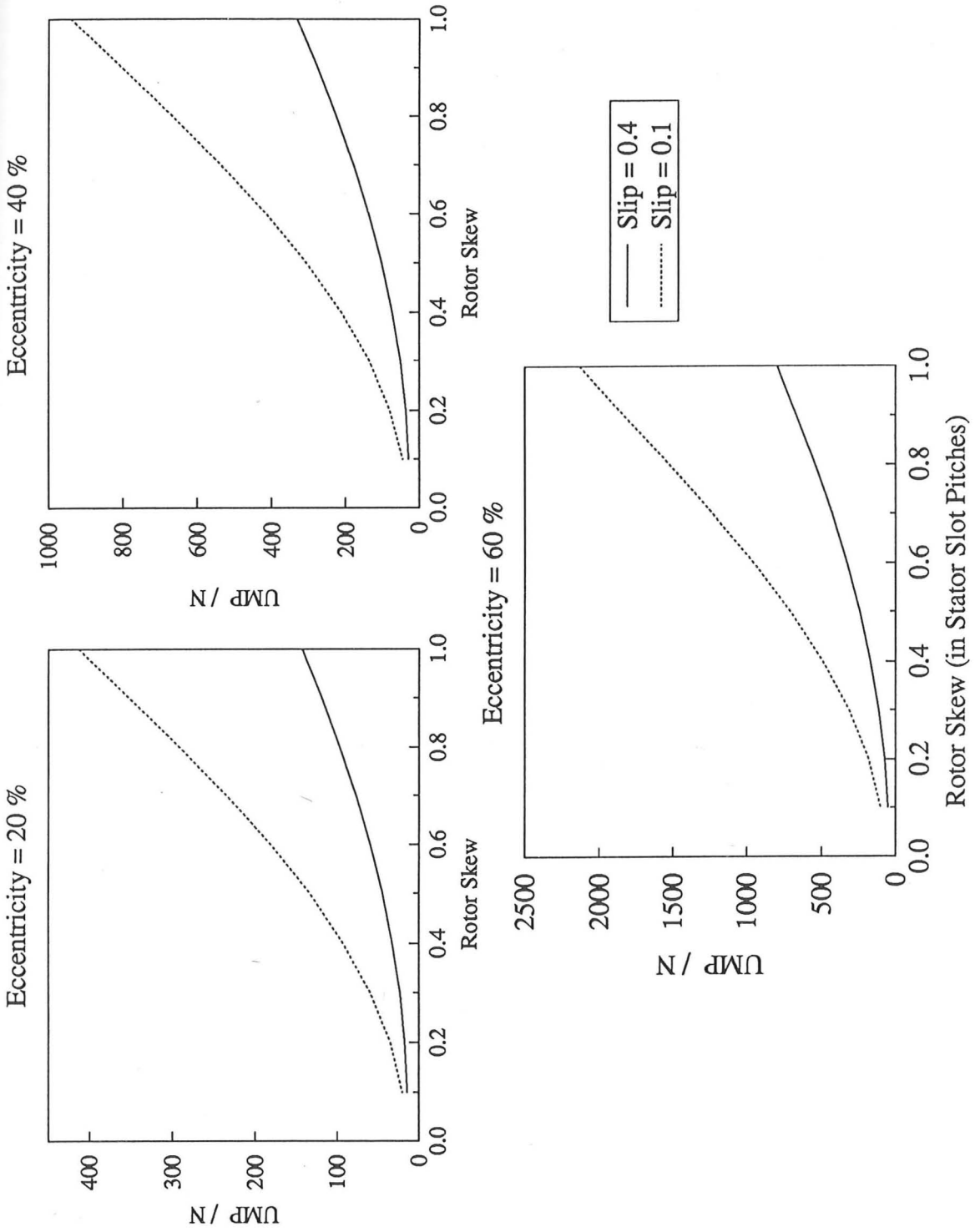


Figure 7.13: Predicted Variation of UMP with Rotor Skew at Several Eccentricities and slip values at a Line Voltage of 208 V for the Ten-Pole Series Connected Machine with Cage Rotor. Only the Fundamental Stator Winding Harmonic is Taken Into Account

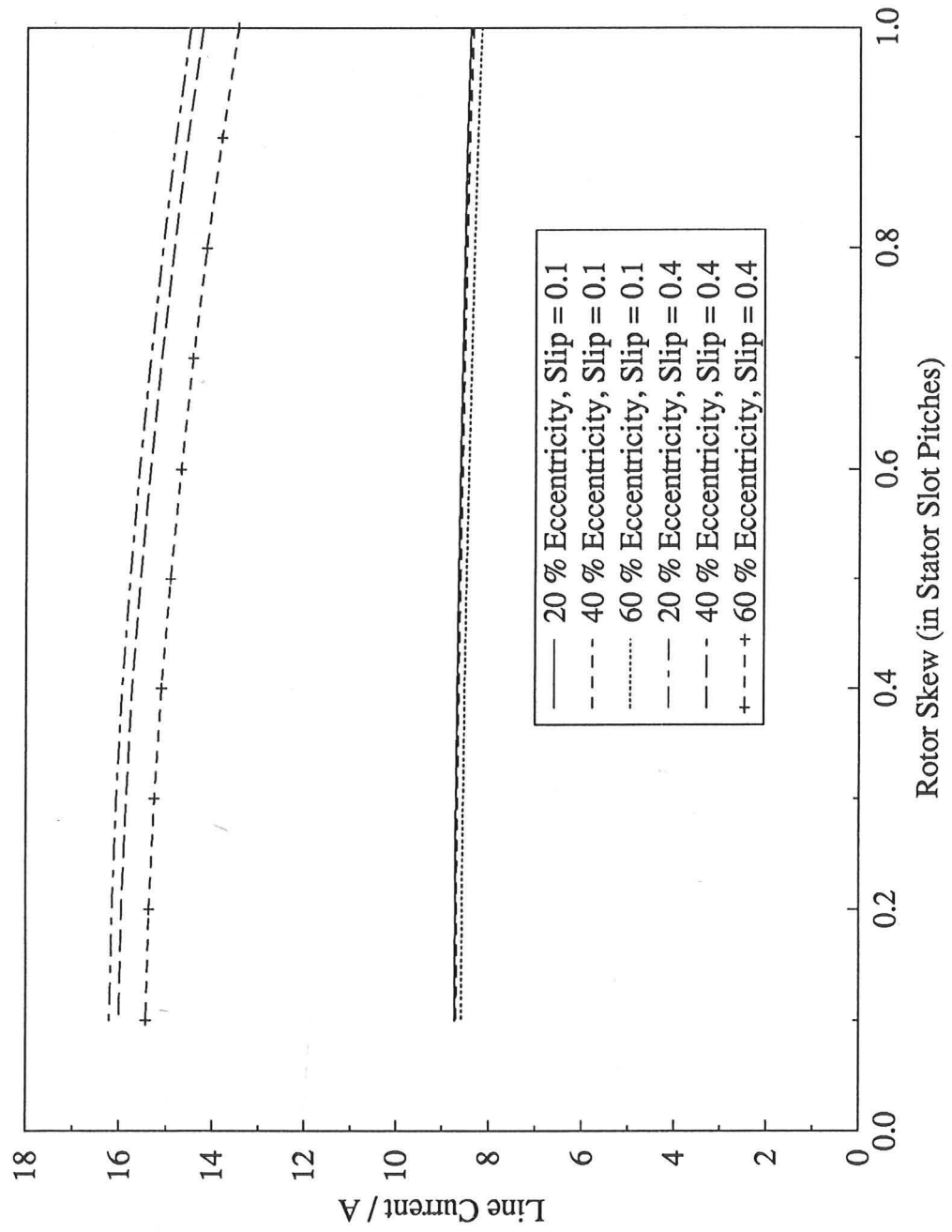


Figure 7.14: Predicted Variation of Line Current with Rotor Skew at Several Eccentricities and slip values at a Line Voltage of 208 V for the Ten-Pole Series Connected Machine with Cage Rotor. Only the Fundamental Stator Winding Harmonic is Taken Into Account

## 7.3 Parallel Connection

All ten phase bands were connected in parallel for the following results, the line voltage for these tests was 26 V which was the closest available voltage to 20.8 V (series voltage reduced by ten).

### 7.3.1 Variation of UMP with Slip for Several Eccentricities

Figures 7.15 and 7.16 show the variation of the steady UMP for several different eccentricities over the slip ranges 0 to 0.8 and 0 to 0.15. The predictions indicated very small 100 Hz pulsating forces which where not distinguishable from the 100 Hz mechanical vibration present even when the machine was running unexcited hence these are not shown. The steady force was directed only a few degrees away from the direction of narrowest airgap, the alignment of the machine made this a difficult point to define exactly so only the magnitude is given.

The results again appear to have poor correlation at high slip values (as in the series connected case). This can be explained with reference to figure 7.17 which shows the variation of all the phase band currents of one phase for slips of 0.08 and 0.4. It can be seen that the spread of the currents at a slip of 0.08 are very similar for the predicted and measured values (although the magnitudes are slightly different). When the slip is 0.4 the spread of the currents is different between the predicted and measured. The difference between the maximum and minimum for the measured values is much less than the predicted hence this would tend to make the measured values of UMP higher. This could be due to several reasons. No account is taken of the mutual reactance between stator coils in the same slot and the stator end-winding mutual reactances between phase bands. As has already been mentioned in section 7.2.1, $X_1$ is a substantial component of the terminal impedance at high slip since the terminal impedance is low, a large part of this is the end-winding leakage. The slot leakage and end-winding leakage are included in the model as simple lumped self inductances which assume that the mutually coupled coils have currents of equal magnitude and appropriate 120 degree phase shift if they are coils

of a different phase. Also, the rotor end-ring currents will link the end-winding, this was shown by reference [71]. Whilst it would be possible to include the mutual inductances for the slot leakage, the end-winding leakage is still difficult to calculate. If the mutual reactances were included then the current spread should be less. This is an important point for further investigation.

The predicted currents for all the phase bands of one phase at 40 % eccentricity over the slip range of 0 to 0.8 is shown in figure 7.18. This shows a considerable variation in current magnitudes with several currents crossing over. As has already been mentioned the spread of measured currents is not quite as pronounced.

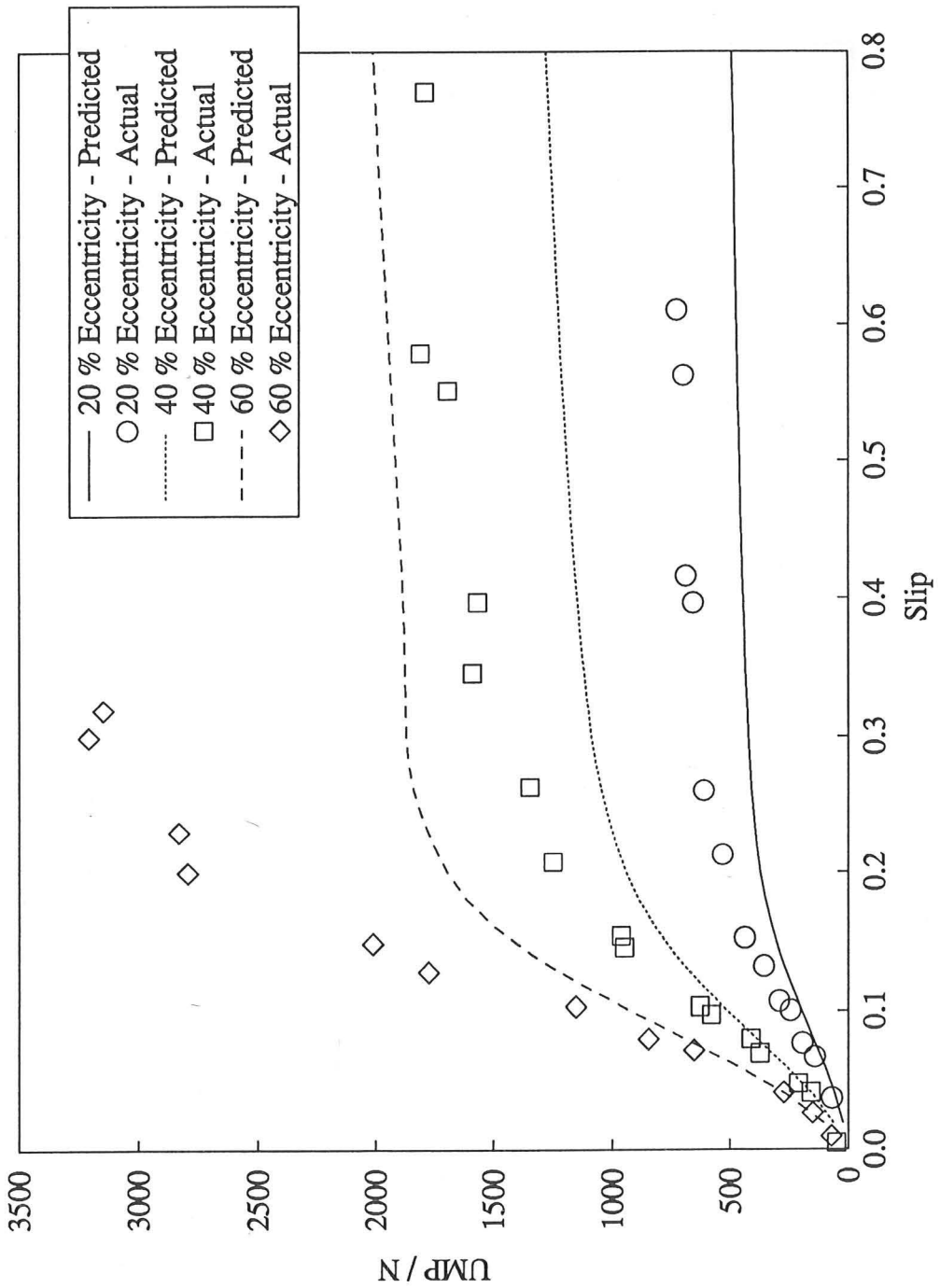


Figure 7.15: Variation of UMP Over the Slip Range 0 to 0.8 for several Eccentricities at a Line Voltage of 26 V for the Ten-Pole Parallel Connected Machine with Cage Rotor

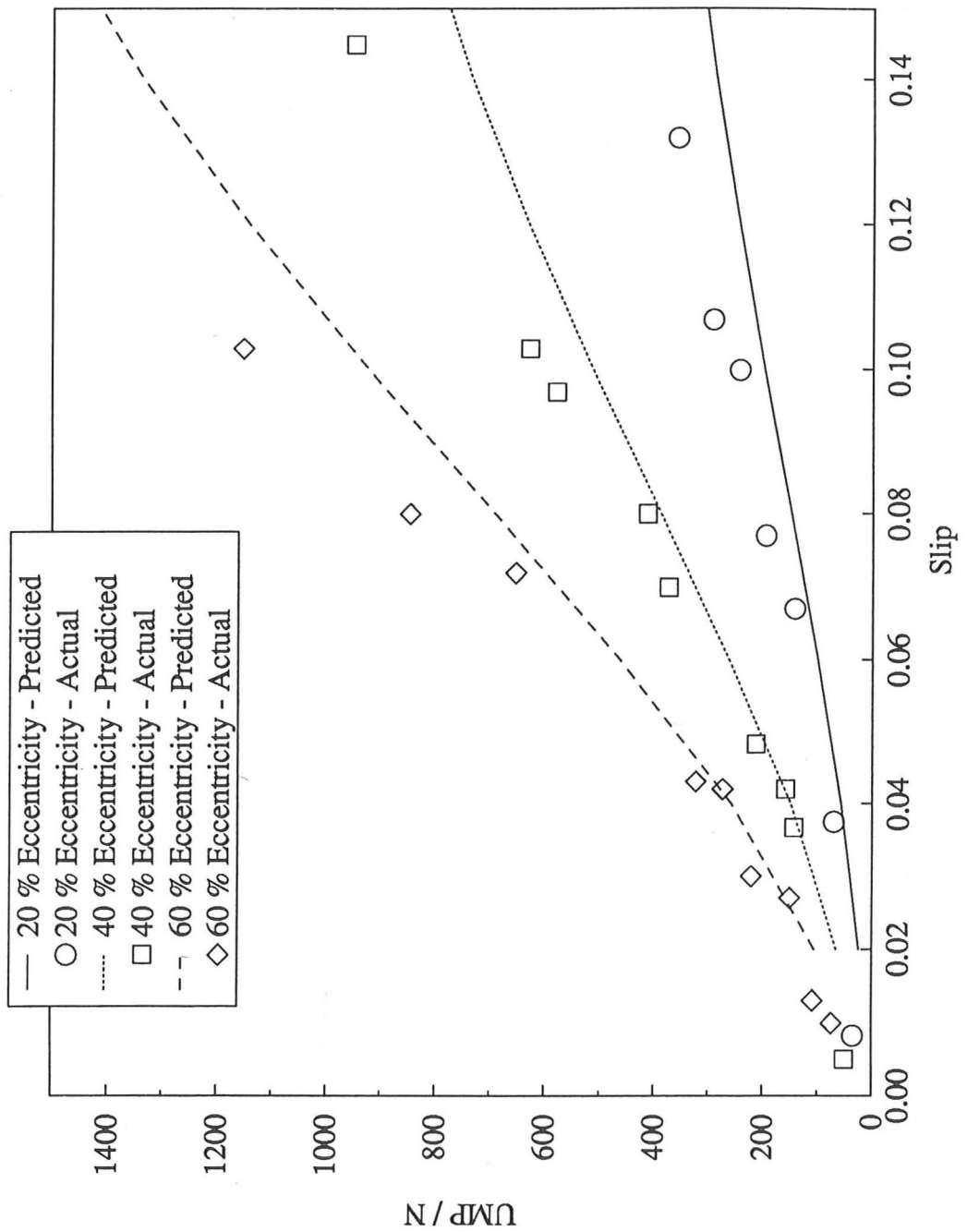


Figure 7.16: Variation of UMP Over the Slip Range 0 to 0.15 for Several Eccentricities at a Line Voltage of 26 V for the Ten-Pole Parallel Connected Machine with Cage Rotor

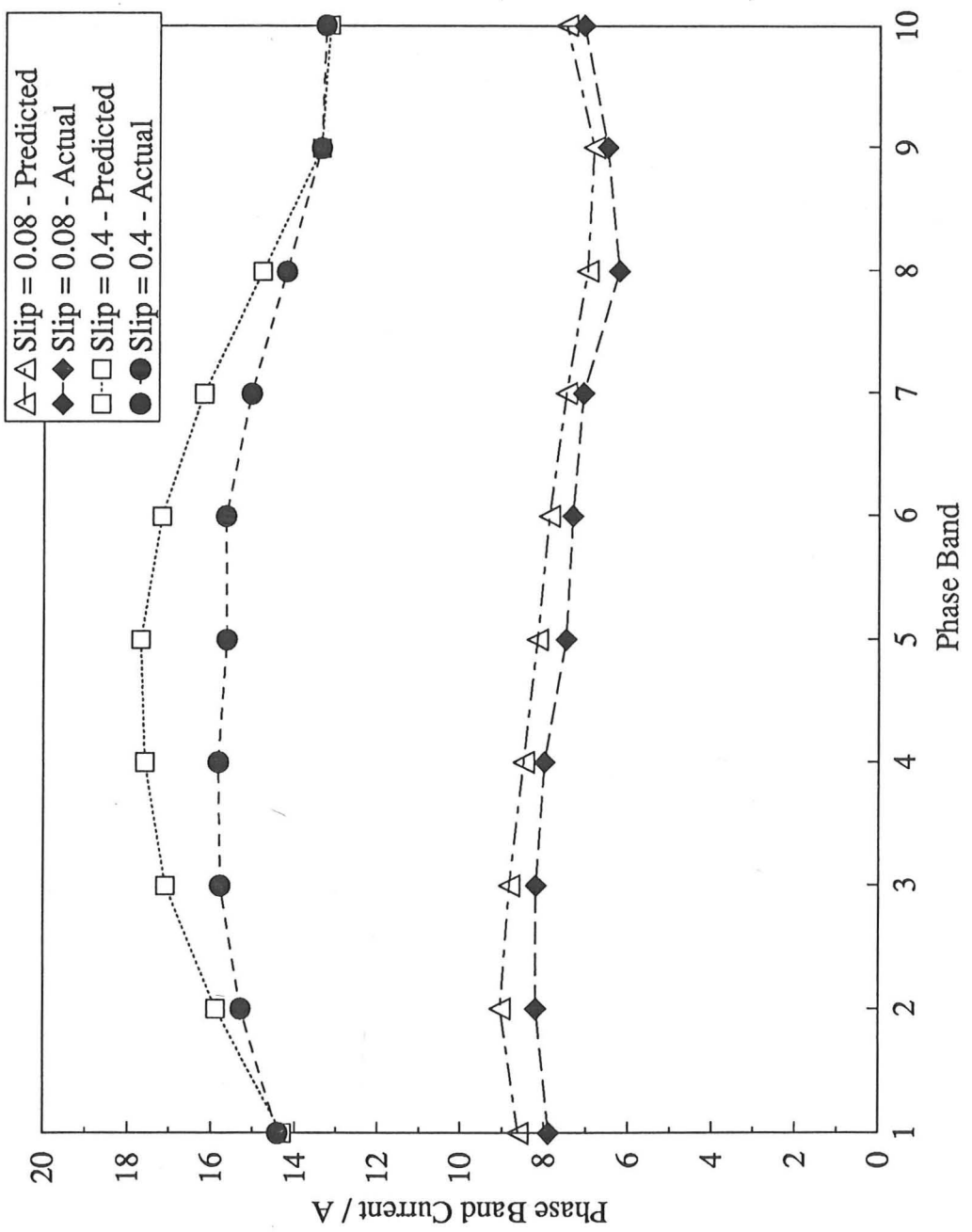


Figure 7.17: Variation of Phase Band Current for one Phase at Slips of 0.08 and 0.4 for 40 % Eccentricity at a Line Voltage of 26 V for the Ten-Pole Parallel Connected Machine with Cage Rotor

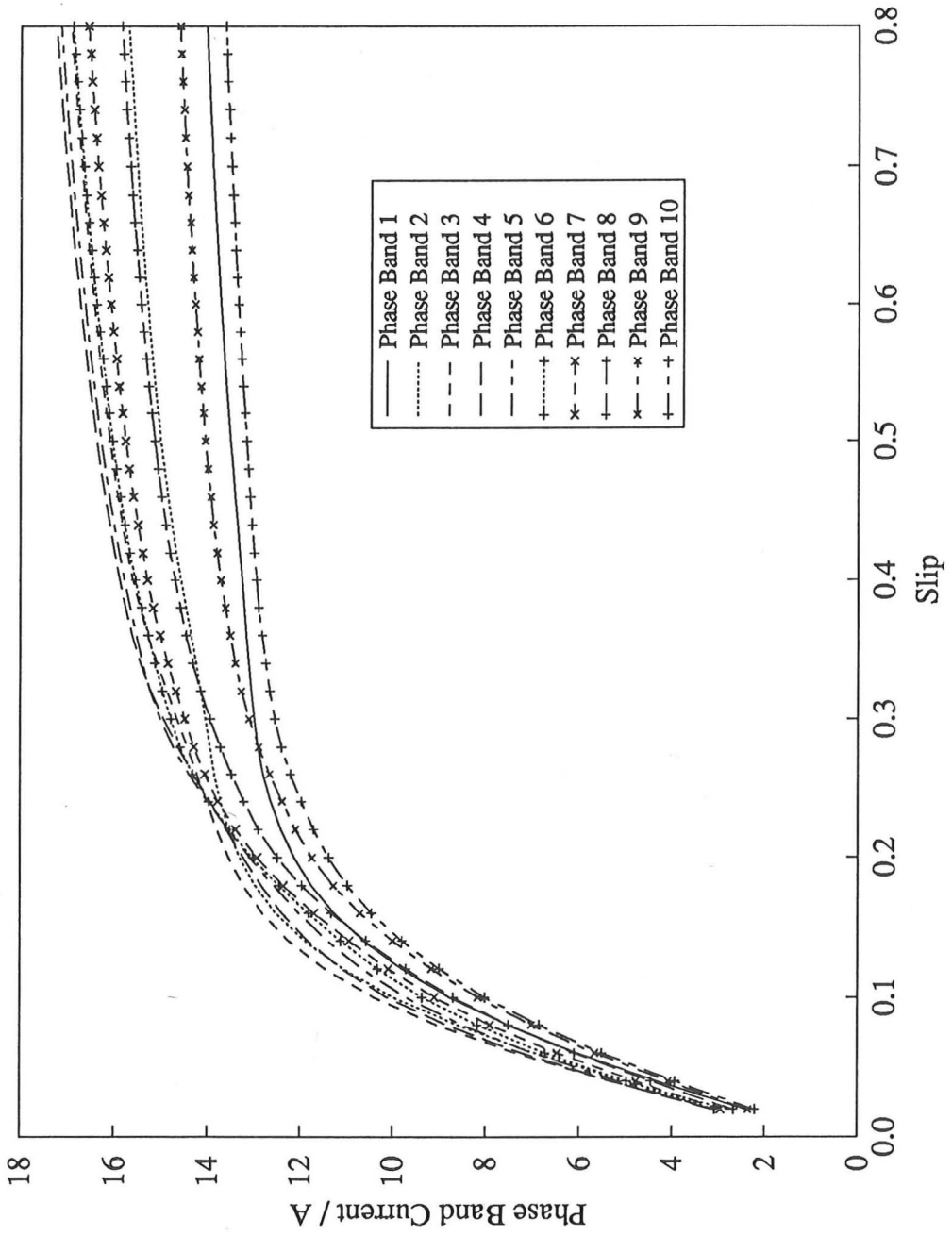


Figure 7.18: Predicted Variation of the Phase Band Currents of One Phase with Slip for an Eccentricity of 40 % and a Line Voltage of 26 V for the Ten-Pole Parallel Connected Machine with Cage Rotor

### 7.3.2 Effect of the Winding Harmonic Series on UMP

The effect of the maximum winding harmonic number is seen in figure 7.19 and is very similar to the series connected case (figures 7.9 and 7.10), the 85th and 95th winding harmonics again having a substantial influence on the pull. The initial high value of UMP when considering only the fundamental has been explained in section 6.3.3 where, when including the fundamental only, the currents have not reached their correct values so the UMP is high. In addition, the higher harmonic fields produced by the fundamental stator winding are not opposed by higher rotor harmonic fields (i.e. the highest rotor harmonic winding considered is five) or by fields due to higher stator winding harmonics (since the fourth, sixth, etc winding harmonics are non-zero for individual phase bands).

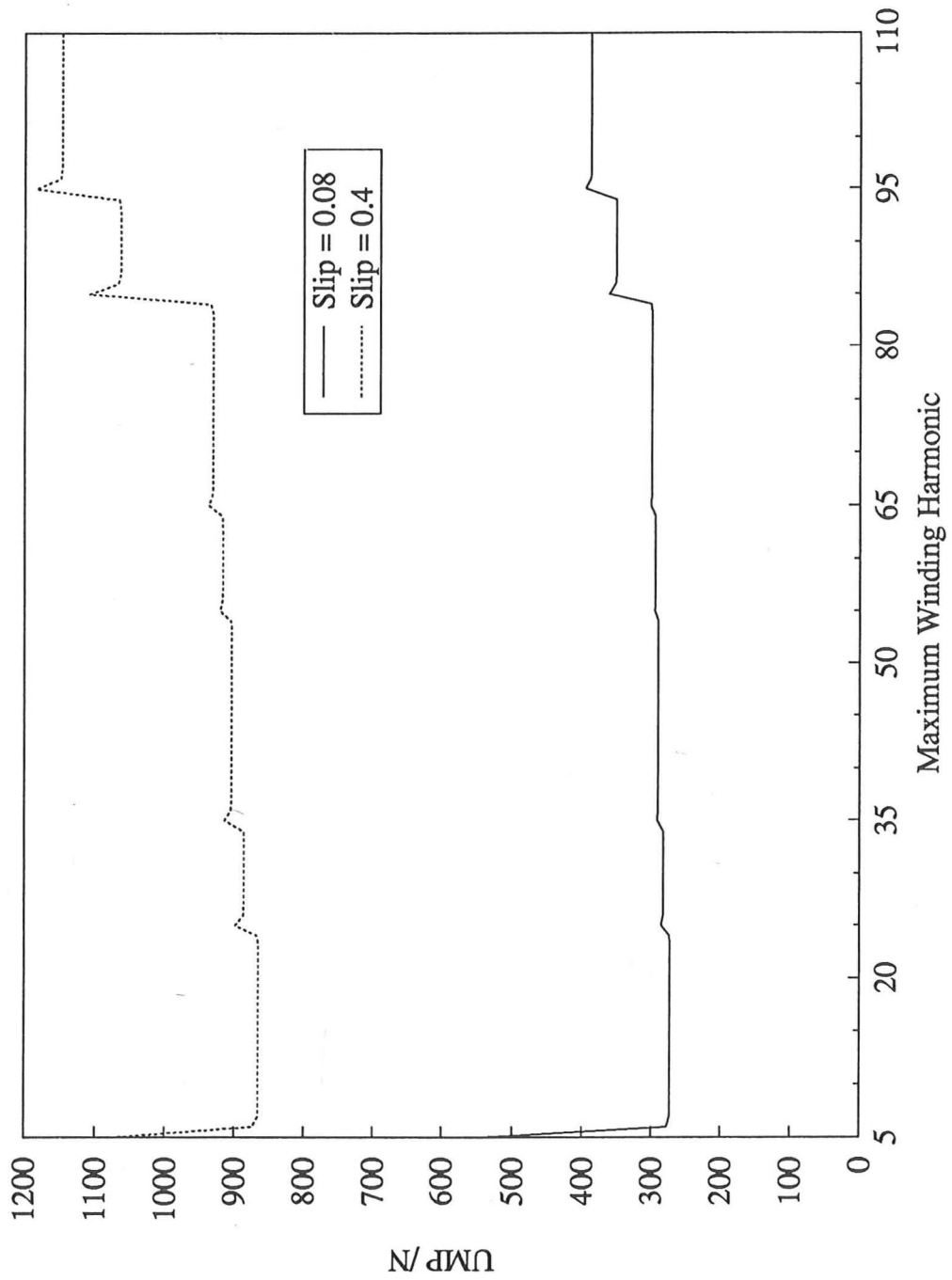


Figure 7.19: Predicted Variation of the UMP with Maximum Winding Harmonic for an Eccentricity of 40 % and a Line Voltage of 26 V for the Ten-Pole Parallel Connected Machine with Cage Rotor

## 7.4 Comparison Between Series and Parallel Connection

An interesting comparison is shown in figures 7.20 and 7.21 where the UMP against slip curves are displayed for the cases of series connection with a line voltage of 260 V and parallel connection with a line voltage of 26 V. It was shown in the previous section that the variation of the measured phase band currents when connected in parallel was not as pronounced as predicted when the machine was running at high slip. If there was no spread, i.e. if the magnitudes of the currents were equal, then this would be equivalent to connecting the machine in series. Therefore it would be expected that the measured values should lie between the curves for the series and parallel connections, this is shown to be the case.

At 40 % eccentricity and high slip the measured results are closer to the series predictions illustrating the fact that phase band current spread is very much less than predicted, as is shown in figure 7.17. At 0.08 slip the current spread is closer to the parallel connection predictions and hence the UMP is closer to the parallel connection curve. At 0.4 slip the measured spread is much less than predicted and hence the measured value is closer to the series connection curve. When the eccentricity is 20 % the results are less well defined with the results being closer to the series connected results right across the slip range. The variation of the currents at this eccentricity is predicted to be quite small and the measured current variation even less.

These results do show clearly the damping effects of parallel windings. Whilst they have a significant effect with the blank rotor (section 6.3.2), the cage rotor gives much less convincing results experimentally. This is mainly due to the current spread between phase-bands being much less than predicted. The UMP measurements for the particular machine used seem to suggest that parallel windings offer only limited improvement in UMP. However, this is the case for just one machine, the theoretical predictions suggested that the improvement in UMP should be much better and for other machines, this may happen.

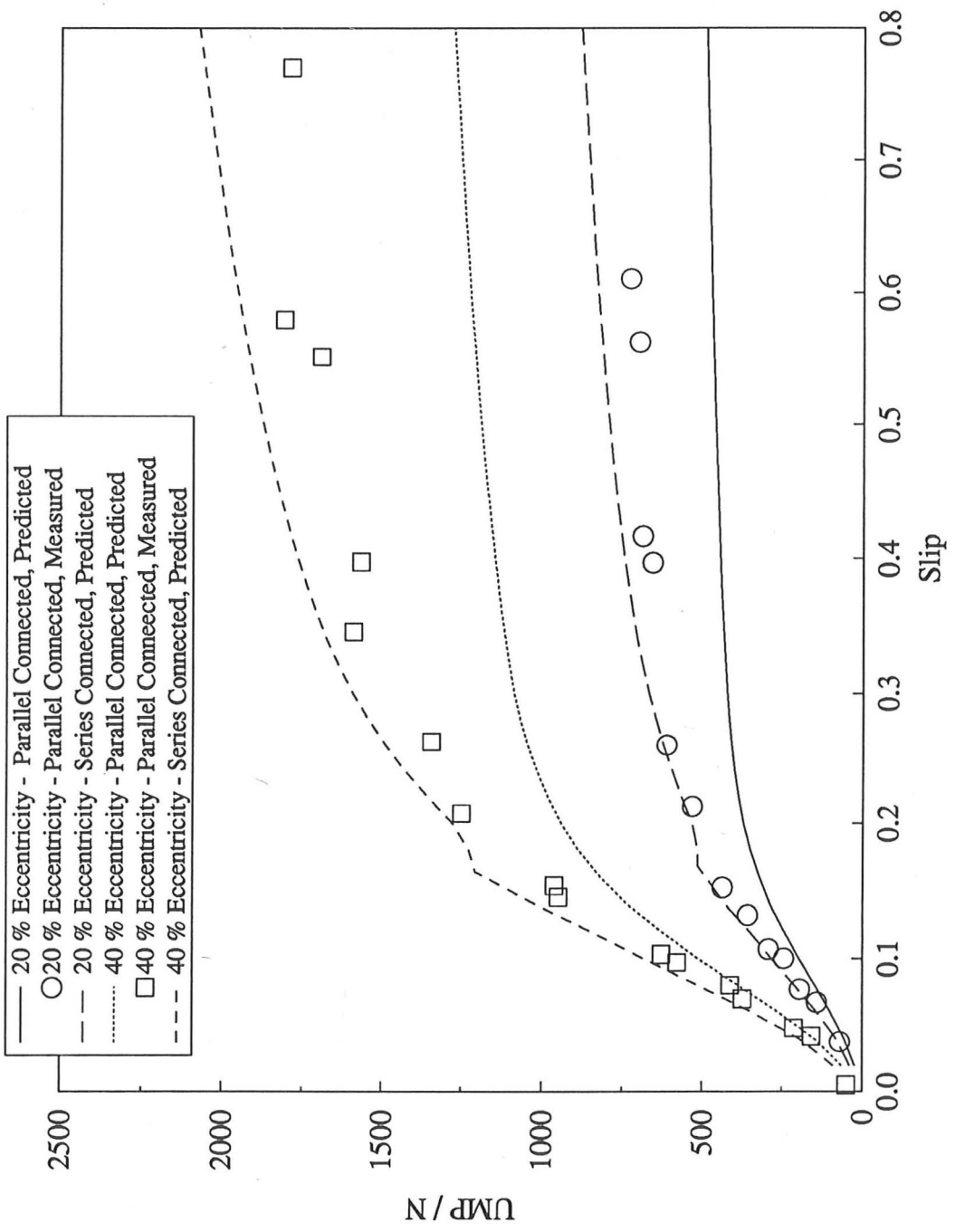


Figure 7.20: Variation of the UMP Against Slip When the Machine is Either Parallel or Series Connected for Eccentricities of 20 % and 40 %. The Line Voltage When Parallel Connected is 26 V, the Line Voltage When Series Connected is 260 V

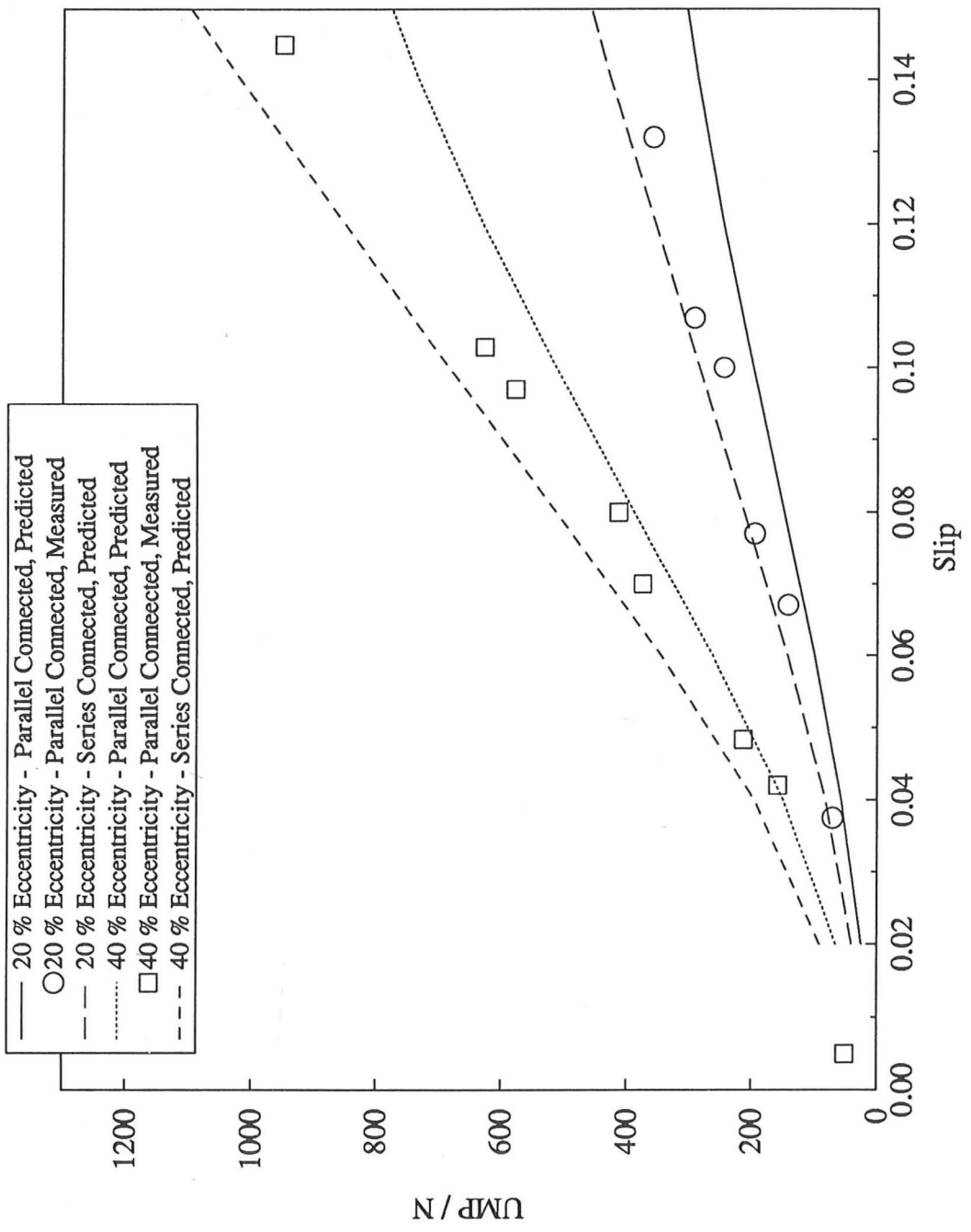


Figure 7.21: Variation of the UMP Against Slip When the Machine is Either Parallel or Series Connected for Eccentricities of 20 % and 40 %. The Line Voltage When Parallel Connected is 26 V, the Line Voltage When Series Connected is 260 V

# Chapter 8

# Two-Pole Machine

## 8.1 Introduction

The two-pole machine was used to verify the permeance model where the sub-fundamental fields can only exist as a homopolar flux. It was found that, as expected, these were negligible. However it still allowed verification of the theoretical model for the special case where no sub-fundamental fields exist.

It was found that the easiest method of assembly was to fit the bearings to the blank rotor as well as the cage rotor since the shafts were identical. This proved somewhat fortunate because the blank rotor (which still had the rotor slots) still experienced a residual torque which would run the machine up to about 2000 rpm unloaded. Therefore all the blank rotor tests were carried out at synchronous speed of 3000 rpm in order to obtain correct magnetising currents.

The experimental rig was satisfactory though not as robust as the ten-pole machine rig (probably due to cross member rotor supports having to be used). Excessive vibration was found and cage tests were conducted at a much reduced voltage.

Initially blank rotor tests were conducted to verify that the model incorporating the stator windings worked and that the homopolar flux was negligible. The cage rotor was then fitted and further speed/UMP tests conducted.

# Chapter 8

# Two-Pole Machine

## 8.1 Introduction

The two-pole machine was used to verify the permeance model where the sub-fundamental fields can only exist as a homopolar flux. It was found that, as expected, these were negligible. However it still allowed verification of the theoretical model for the special case where no sub-fundamental fields exist.

It was found that the easiest method of assembly was to fit the bearings to the blank rotor as well as the cage rotor since the shafts were identical. This proved somewhat fortunate because the blank rotor (which still had the rotor slots) still experienced a residual torque which would run the machine up to about 2000 rpm unloaded. Therefore all the blank rotor tests were carried out at synchronous speed of 3000 rpm in order to obtain correct magnetising currents.

The experimental rig was satisfactory though not as robust as the ten-pole machine rig (probably due to cross member rotor supports having to be used). Excessive vibration was found and cage tests were conducted at a much reduced voltage.

Initially blank rotor tests were conducted to verify that the model incorporating the stator windings worked and that the homopolar flux was negligible. The cage rotor was then fitted and further speed/UMP tests conducted.

The machine had the following specification

| | |
|---|---|
| Number of stator slots | 24 |
| Number of Poles | 2 |
| Winding | Concentric |
| Number of turns per coil | 40 |
| Resistance per Phase | 5.41 $\Omega$ |
| Leakage reactance per Phase | 0.92 $\Omega$ |
| Supply frequency | 50 Hz |
| Connection | Delta |
| Effective machine length ($l$) | 0.11 m |
| Effective airgap radius ($r$) | 45 mm |
| Effective (blank rotor) airgap length ($g_{av}$) | 0.26 mm |
| Effective (cage rotor) airgap length ($g_{av}$) | 0.22 mm |
| Rated voltage ( line ) | 415 V |
| Stator slot opening | 2.54 mm |
| Rotor slot opening | closed slot |
| Rotor slot depth (cage) | 15.8 mm |
| Rotor bar D.C. resistance (hot) | 0.097 m$\Omega$ |
| Rotor end-ring D.C. resistance (hot) | 2.81 $\mu\Omega$ |
| Rotor bar D.C. leakage inductance | 0.497 $\mu$ H |
| Rotor Skew | 1 Stator Slot |

## 8.2 Blank Rotor Verification

The blank rotor was fitted to verify the stator model. Figures 8.1 and 8.2 show the variation of UMP and current with line voltage when the machine was delta connected with 20 % and 38 % eccentricity. There was good agreement between the predicted and measured results with some saturation occurring at high voltage. The currents were found to be a balanced three phase set. No significant 100 Hz components were predicted though in practice there was much mechanical vibration which made any electromagnetic vibration difficult to measure. It should be noted

that the machine was rotating at synchronous speed during these tests. The limited range of the 38 % eccentricity results is because the UMP being generated was amplifying the noise and mechanical vibration and it was considered prudent not to increase the voltage beyond this point.

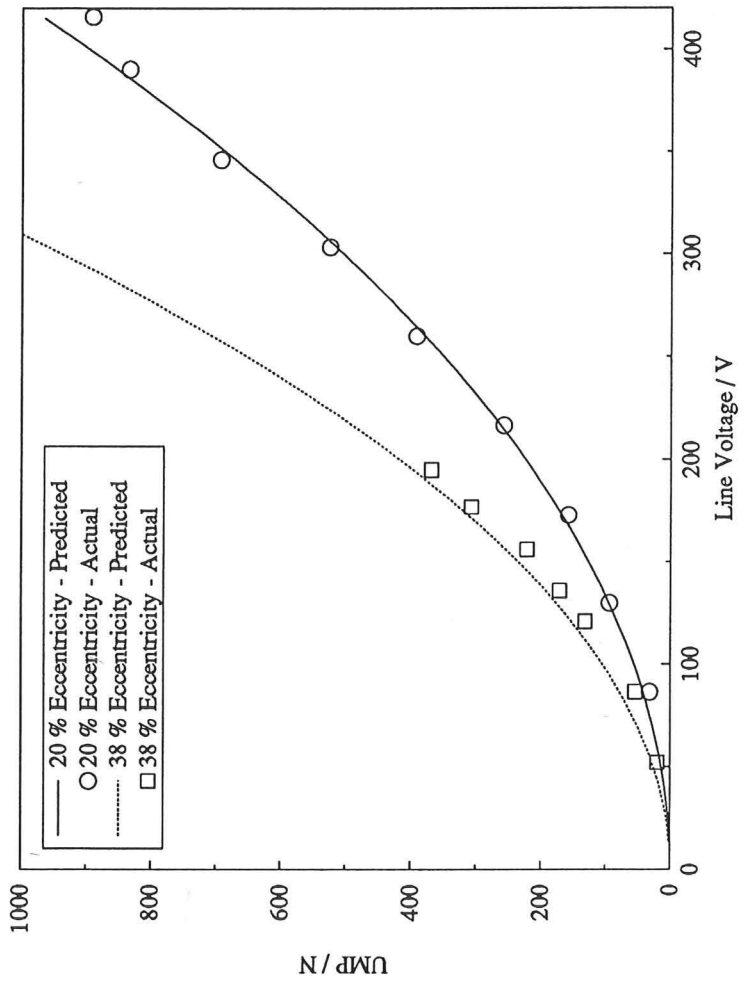


Figure 8.1: Variation of the UMP with Line Voltage at 20 % and 38 % Eccentricity for the Two-Pole Machine with Blank Rotor

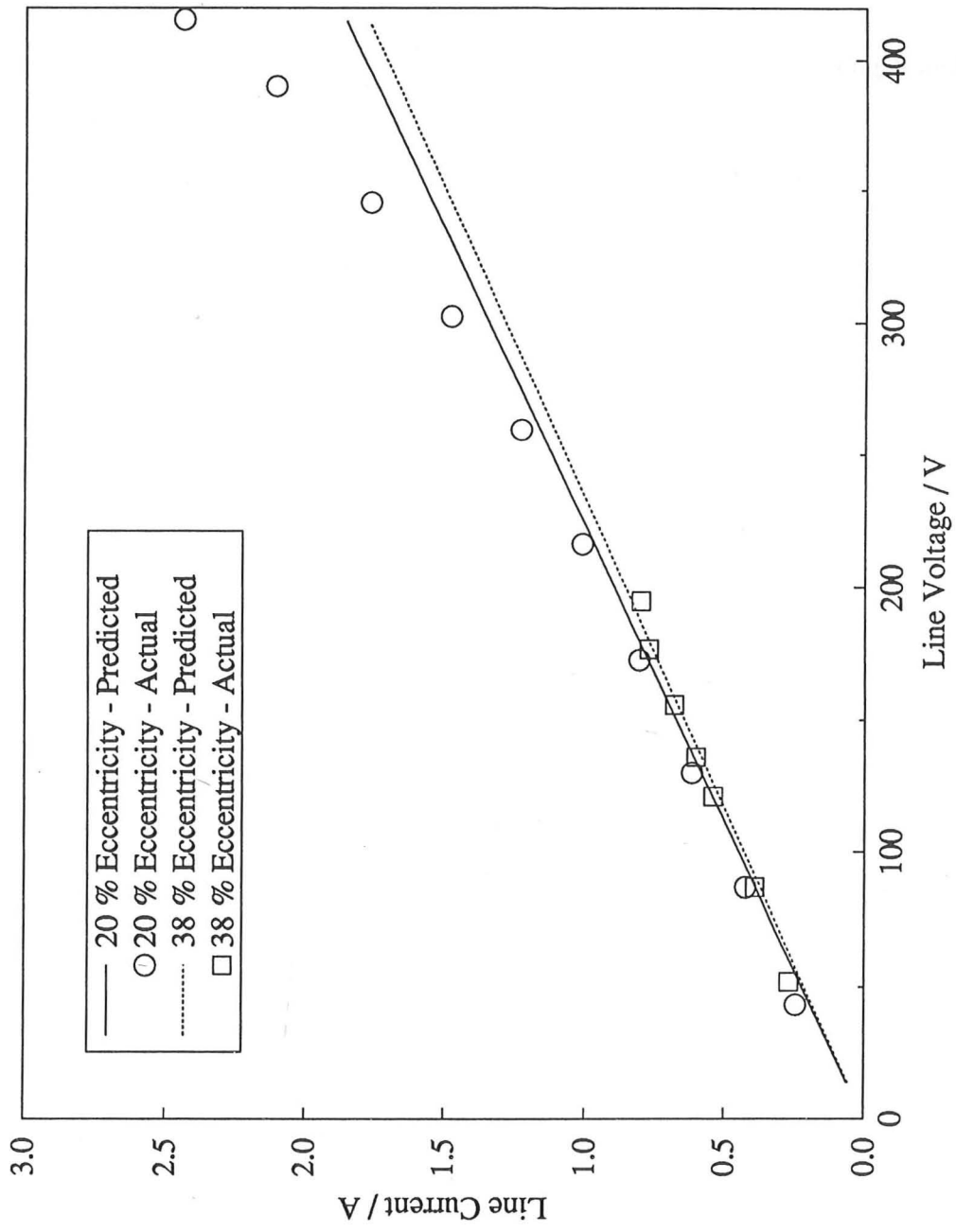


Figure 8.2: Variation of the Line Current with Line Voltage at 20 % and 38 % Eccentricity for the Two-Pole Machine with Blank Rotor

## 8.3 Cage Rotor Verification

### 8.3.1 Variation of UMP with Slip

Alignment of the rotor was very difficult due to the very small airgap length and the confined space at the ends of the machine. The end-rings of the cage made this even more difficult but eventually the rotor was set and the eccentricity was estimated to be about 45 %. Figures 8.3 and 8.4 show the variation of UMP and line currents for a line voltage of 120 V between 0 and 0.8 slip. It can be seen that the predicted and measured UMP results match well. However, the measured line currents appeared to be nearly a balanced three phase set whereas the predicted currents show an unbalanced set. This is consistent with findings of section 7.3.1 where the currents in the parallel windings of the ten-pole machine did not show the degree of current spread as predicted. It was suggested that this was due to neglecting the mutual slot leakage inductance and mutual end-winding inductances. In this case the winding is single layer so there is no mutual slot leakage inductance and only the mutual end-winding inductances have been neglected. As previously mentioned these are very difficult to calculate so $X_1$ was still included as a lumped self-inductance. Whilst the value of $X_1$ may seem too low, such that its influence on the current even at high slip is small, its value was derived from locked rotor tests using calculated values for the other components in the equivalent circuit. Saturation effects (as described in section 7.2.1) may lead to $X_1$ being underestimated. The effects of the end-regions in this particular case need further study to give more definite reasons the divergence of the predicted and measured currents.

The peaks at 0.5 and 0.67 slips are due to the machine rotating at the four-pole and six-pole synchronous speeds and hence these fields are not damped by the rotor. This gives small peaks in the UMP characteristics.

The UMP for the machine if the rotor is blank and the line voltage is 120 V at 45 % eccentricity is 182 N with a balanced three phase current set of 0.48 A. It can be seen that, while the cage damps the UMP at low slip (less than 0.075) the UMP soon increases beyond this point. It should be noted however that the currents are very high, therefore the cage still provides significant damping of the UMP.

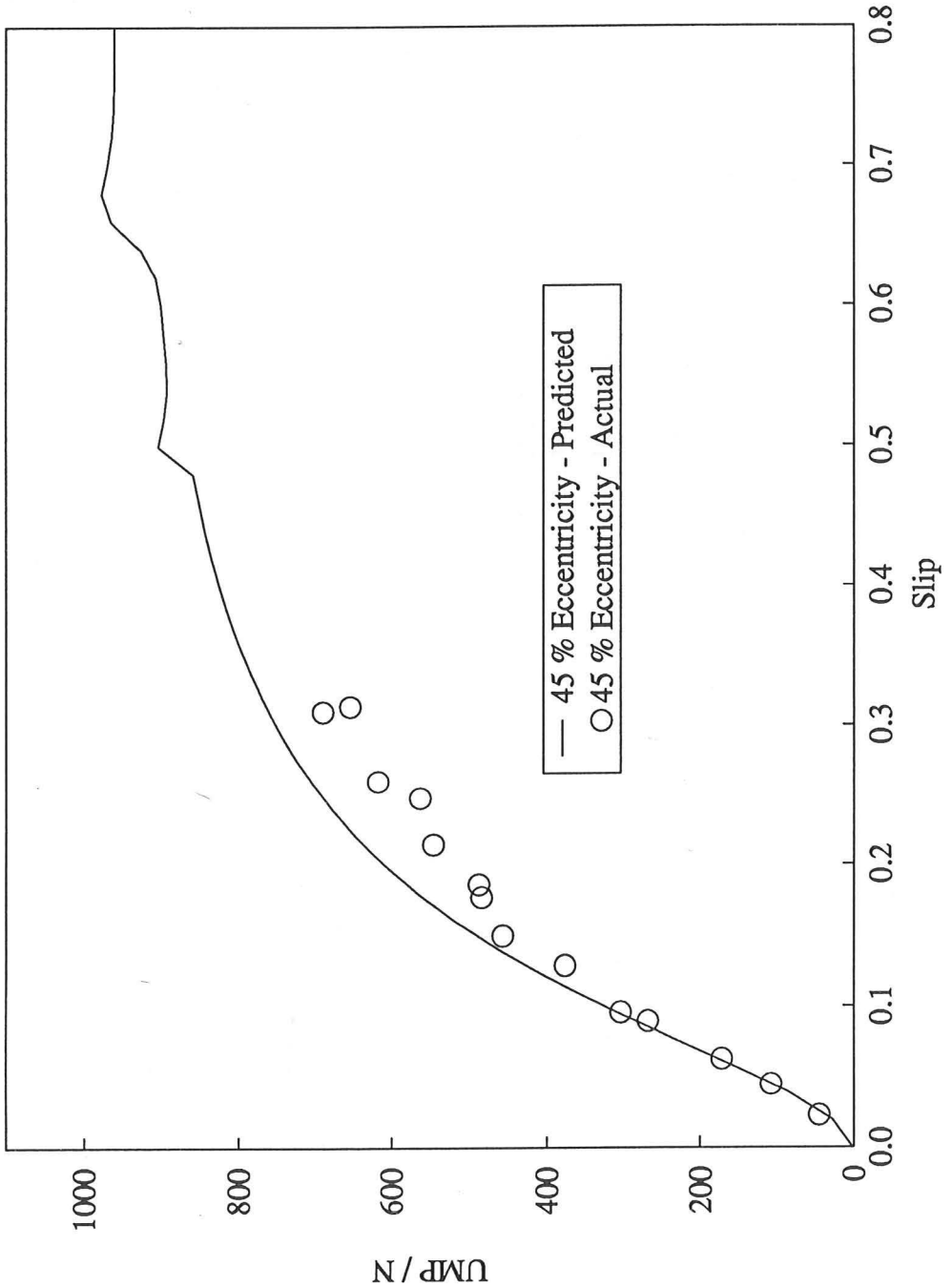


Figure 8.3: Variation of the UMP with Slip at 45 % Eccentricity and 120 V Line Voltage for the Two-Pole Machine with Cage Rotor

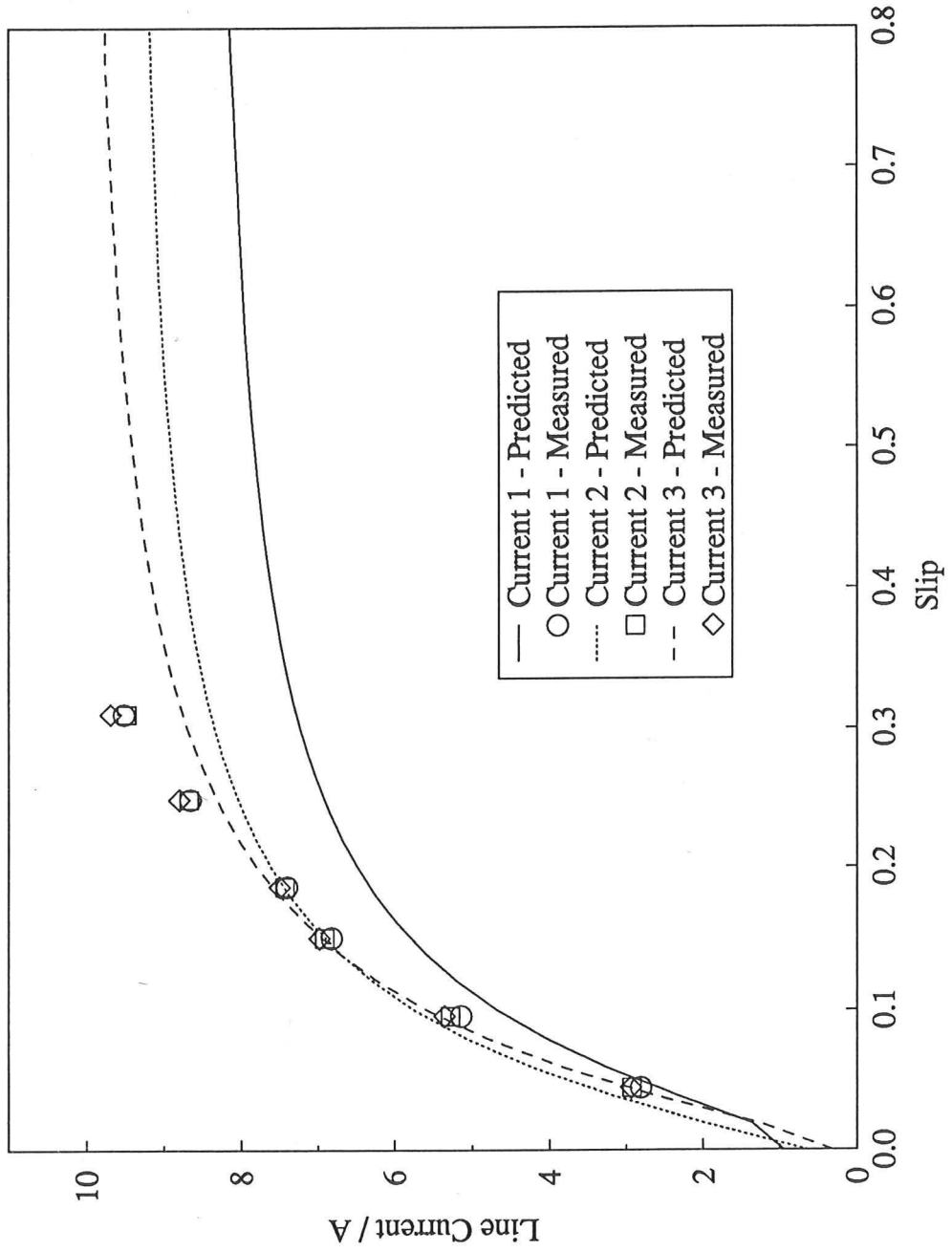


Figure 8.4: Variation of the Line Current with Slip at 45 % Eccentricity and 120 V Line Voltage for the Two-Pole Machine with Cage Rotor

### 8.3.2 Effect of Maximum Winding Harmonic Number on UMP

The effect of the higher fields on the UMP is shown in figure 8.5 for 45 % eccentricity and a line voltage of 120 V. There are significant contributions by the 23rd and 25th field harmonics. As with the ten-pole machine, these harmonics lie close to the number of bars in the rotor and hence are not damped by the rotor field to any large extent. Figure 8.6 shows the variation of the line current with winding harmonic number, the 23rd and 25th harmonics have a small effect on the currents but not as much as they have on the UMP. At a slip of 0.4 these harmonics contribute 50 % of the UMP.

The initial high values of UMP are due to the fact that the only rotor current density harmonic being considered is the two-pole harmonic. The higher stator field harmonics therefore are not being damped by the higher rotor winding harmonics.

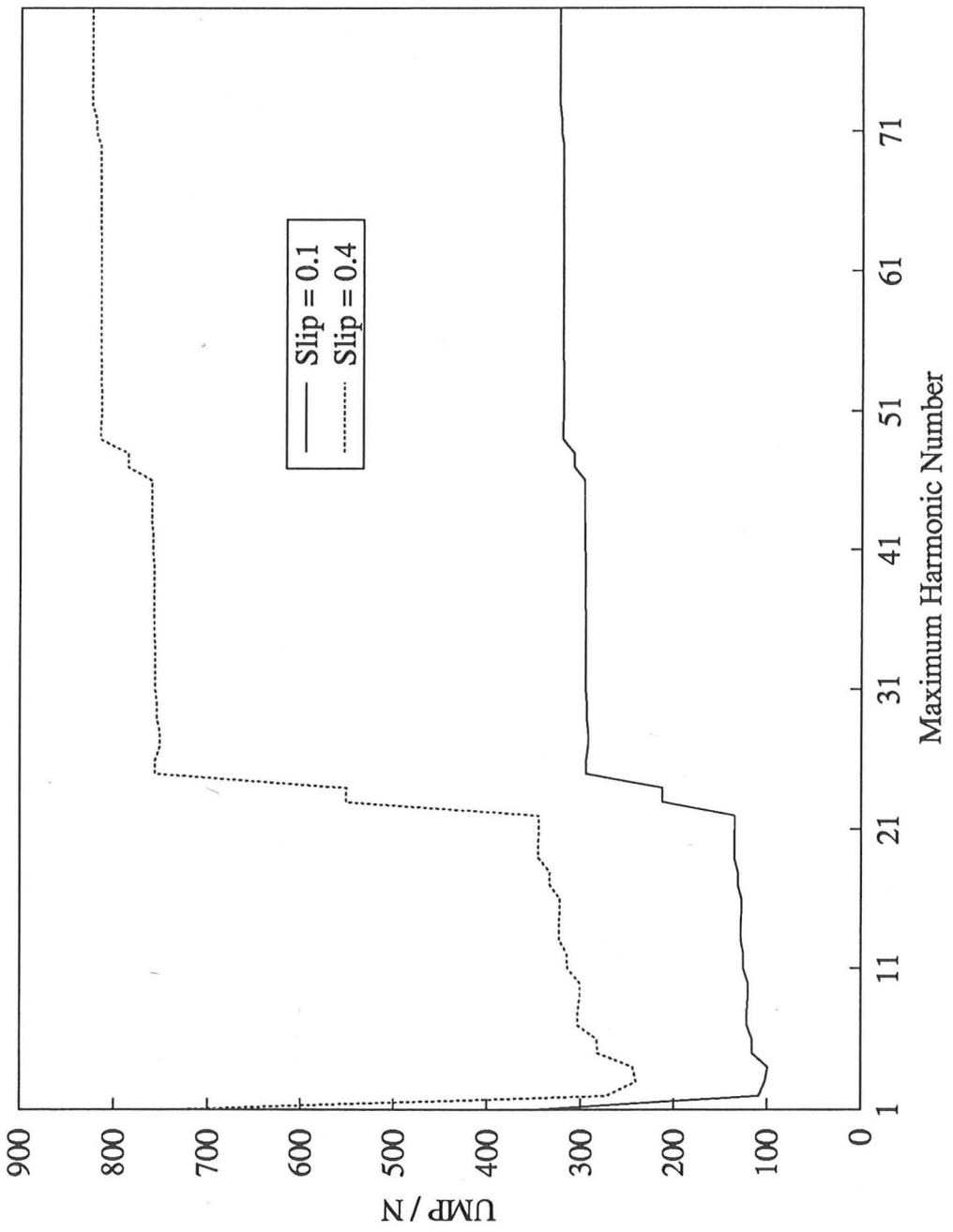


Figure 8.5: Predicted Variation of the UMP with Maximum Winding Harmonic for an Eccentricity of 45 % and a Line Voltage of 120 V for the Two-Pole Machine with Cage Rotor

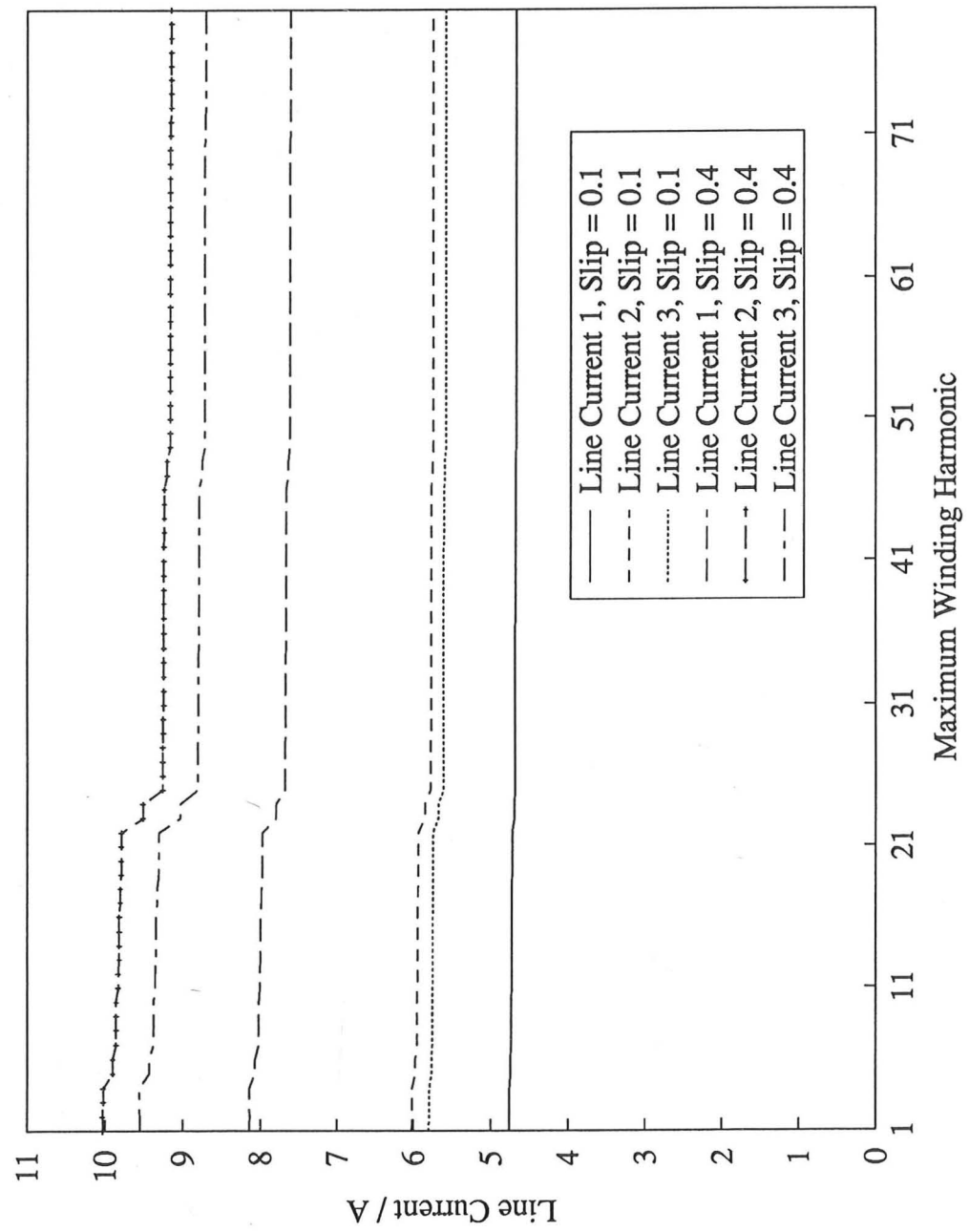


Figure 8.6: Predicted Variation of the Line Current with Maximum Winding Harmonic for an Eccentricity of 45 % and a Line Voltage of 120 V for the Two-Pole Machine with Cage Rotor

# Chapter 9

# Conclusions and Suggestions for Further Work

The review of the literature on unbalanced magnetic pull due to rotor eccentricity in cage induction machines produced suprisingly few models able to calculate this force. In addition, none of these models were verified experimentally. This thesis has attempted to rectify this situation using a harmonic conductor density technique and initially implementing it in two separate ways, one of which was fully developed to include a rotor model. These models proved very successful and led to several new aspects of rotor eccentricity being highlighted.

The first part of the project developed two machine models which could take into account an eccentric rotor and any stator winding configuration with the rotor considered as a laminated blank. These used the harmonic conductor density method, first in conjunction with a conformal transformation (which transforms the machine from having an eccentric rotor with symmetrical windings to having a concentric rotor but asymmetrical windings) then with an airgap permeance harmonic series (which modulates the flux density field).

The lack of experimental investigation of UMP is more understandable since high quality transducers for measuring UMP were scarce until relatively recently. The second part of the project was to investigate the UMP caused by an eccentric rotor in a cage induction motor and verify the computer models developed. Two machines were successfully tested, the first was a ten-pole 35 kW motor which allowed phase

bands to be connected in a variety of different ways. The second was a two-pole 4 kW motor. The experimental investigation was very extensive and proved the computer models to be accurate within certain limitations.

Comparison between the results with the blank rotor for the two methods showed little difference. However, both had advantages and disadvantages. The conformal transformation technique used a more straightforward algorithm to calculate the impedance matrix but required a mapping technique to obtain the flux density distribution. To calculate the UMP therefore a numerical solution was required. The permeance harmonic method used a more cumbersome algorithm to calculate the impedance matrix but gave analytical expressions for the UMP generated. It was anticipated that to incorporate a skewed cage rotor into the conformal transformation model would be difficult. The permeance harmonic technique would use the theory already developed with only relatively minor changes. Coupled with the analytical expressions which are derived from the permeance harmonic method, this algorithm was developed to include a cage rotor. The method used standard rotating airgap harmonic field theory and was able to point out the important influence of the stator winding harmonics, cage bar number and rotor skew on the UMP. This presents very useful information to the machine designer which has never been adequately presented before.

Previous models assumed that the UMP was produced by modulation of the fundamental field into fields with pole-pair numbers both above and below the fundamental. The fields caused by higher winding harmonics being considered negligible. Whilst this is a reasonable assumption for the case where the rotor is blank, the findings from this project show that it is a bad approximation when a cage rotor is used. There turns out to be a substantial component of UMP generated by fields with a pole-pair number close to the number of bars in the cage. This was shown to be the case with both test motors.

The use of parallel paths in the stator windings proved very effective when the blank rotor was fitted but proved less effective with a cage rotor. This seemed to be due to the effects of the mutual inductances between the stator end-windings and leakage inductance in slots (when double layered) though this is need of further

detailed investigation. This prevented the phase band current magnitudes varying to the degree predicted by the analytical model. There was still a substantial decrease in UMP with the cage rotor using parallel stator connections but not the ten-fold decrease found with the blank rotor. The cage rotor itself proved to be the most effective way of attenuating the UMP but only at low slip when the current magnitudes are less. This does however correspond to the operating range of the motor.

Rotor skew also seemed to play an important part in the calculation of UMP. The ten-pole machine showed a 150 % increase in UMP when the skew varied between 0 and 1 stator slot pitch. Again, this is a phenomenon which has not been reported before. It should be noted however that these were theoretical predictions at reduced voltage. The practical verification would be difficult with several rotors required with varying degrees of skew. However the results were good for the skew of the rotor used. It would be interesting to examine the influence axial saturation on the UMP when the machine is excited at rated voltage. Mechanical instability of the rig used prevented this.

The work presented in this dissertation represents a detailed theoretical and experimental study of UMP produced in a cage induction motor when the rotor is eccentric due to mechanical misalignment. Several points have been made which may help future understanding of this problem. The assumption made throughout is that the rotor misalignment is constant down the length of the machine. An interesting extension of the project would be the study of the UMP when only one end of the machine is misaligned (e.g. incorrect fitting of one bearing or end-cap).

A further development is to include dynamic UMP (i.e. rotor not turning on its own axis) in the algorithm. This is likely to occur when a flexible shaft machine is passing through a critical speed and would necessitate transient analysis of UMP. The experimental work carried out in this study was steady-state, transient analysis represents a further step forward in the investigation of UMP.

# Bibliography


[1] A. Gray and J. G. Pertsh. *Critical Review of the Bibliography on Unbalanced Magnetic Pull in Dynamo-Electric Machines.*

1918 Trans. Am. Inst. Elec. Eng.

[2] E. Rosenberg. *Magnetic Pull in Electric Machines.*

1918 Trans. Am. Inst. Elec. Eng., Part 2.

[3] R. C. Robinson. *The Calculation of Unbalanced Magnetic Pull in Synchronous and Induction Motors.*

1943 Electrical Engineering, October, -Discussion December.

[4] Liwschitz-Garik and Whipple. *Electric Machinery, Third Printing, Vol. 1, pp. 69 and Vol. 2, pp. 120.*

1947 Van Nostrand Company

[5] W.G. Crawford. *Unbalanced Magnetic Pull and the Mechanical Stability of Rotating Electrical Machines*

1951 Engineering, April 27.

[6] A. Covo *Unbalanced Magnetic Pull in Induction Motors with Eccentric Rotors.*

1954 Trans. Am. Inst. Elect. Eng.

[7] E.W. Summers *Vibration in 2-Pole Induction Motors Related to Slip Frequency.*

1955 Trans. Am. Inst. Elec. Eng.

[8] M.M. Liwschitz-Garik. *Computation of Skin Effect in Bars of Squirrel-Cage Rotors.*

1955 Trans A.I.E.E., Vol. 74, pp. 768-771.

[9] M. Krondl. *Self Excited Radial vibrations of the Rotor of Induction Machines with Parallel Paths in the Winding.*

1956 Bull. Assoc. Suisse, Elect. 47. Translation: E.R.A. Trans. IB2511.

[10] W. Freise and H. Jordan. *Unbalanced Magnetic Pull in 3-Phase A.C. Machines.*

1962 E. T. Z. -A 83 No. 9. Translation- C.E. Trans 7836

[11] P. von Kaehne. *Unbalanced Magnetic Pull in Rotating Electrical Machines. Survey of Published Work.*

1963 E.R.A. Report Ref. Z/T 142.

[12] R.C. Robinson. *Line Frequency Magnetic Vibration of A.C. Machines*

1963 A.I.E.E. Trans Power Apparatus and Systems Vol 81.

[13] S. A. Swann. *Effect of Rotor Eccentricity on the Magnetic Field in the Air-Gap of a Non-Salient- Pole Machine.*

1963 Proc. I.E.E. V110 N0. 5.

[14] D. Harlin. *Oscillation Behaviour in Asynchronous Motors as a Result of Unbalances*

1965 Dr. Ing. Thesis, Technical High School, Stuttgart. Translation: E.R.A. Trans IB2520.

[15] M. Bradford. *Misalignment of Rotating Machines, Determination of Unbalanced Magnetic Pull.*

1966 Elec. Review Vol. 178.

[16] H. Frohne. *The Practical Importance of Unbalanced Magnetic Pull, Possibilities of Calculating and Damping It.*

1967 Conti Elektro Berichte, Vol 13 1967. Translation: E.R.A. Trans IB2617.

[17] H. Jordan, G. Roder and M. Weis. *Under What Circumstances May Mechanical Vibrations of the Stator Core be Expected at Supply Frequency in Four-Pole Three-Phase Asynchronous Machines?*

1967 Elecktrie Vol. 21, No. 3. Translation: E.R.A. Trans IB2578.

[18] T. Bratoljic and P. Vrkljan. *Magnetic Forces Created by Rotor Eccentricity in Electrical Machines*

1967 The Brown Boveri Review Vol. 54 No. 9.

[19] H.Frohne. *Unbalanced Magnetic Pull in Rotating Field Machines.*

1968 Archiv Fur Electrotechnic Vol 51.

[20] H. Frohne. *Calculation of the Fields of Eccentricity and the Unbalanced Magnetic Pull in Rotating Field Machines Taking Saturation and Damping into Consideration.*

1968 Archiv Fur Electrotechnic Vol 52. Translation: Indian National Scientific Doc. Centre No. 12166 or E.R.A. Trans. 2757.

[21] M. Bradford. *Unbalanced Magnetic Pull in a 6-Pole 10 kW. Induction Motor With a Series-Connected Stator Winding.*

1968 E.R.A. Report No. 5216.

[22] M. Bradford. *Unbalanced Magnetic Pull in a 6-Pole Induction Motor.*

1968 Proc. I.E.E. Vol. 115, No. 11.

[23] L.S. Stringer. *Unbalanced Magnetic Pull and Shaft Voltage in Electromagnetic Rotating Machines.*

1968 The Engineer, April 19.

[24] E.M. Freeman and E.R. Laithewaite. *Unbalanced Magnetic Push - Correspondence Item.*

1968 Proc. I.E.E. V115 No.4 page 538.

[25] M. Bradford and A. Nimalasuriya. *Unbalanced Magnetic Push - Correspondence Item.*

1968 Proc. I.E.E. V115 No.10 page 1522.

[26] A.J. Ellison and C.J. Moore. *Acoustic Noise and Vibration of Rotating Electric Machines*

1968 Proc. I.E.E. Vol. 115, No. 11.

[27] J. Eckert and A. Gahleitner. *Experimental Method of Determining The Unbalanced Magnetic Pull in A.C. Induction Motors*

1969 Siemens Z. Vol. 43. Translation: E.R.A. Trans. 2792.

[28] W.G. Crawford. *Unbalanced Magnetic Pull as a Cause of Vibration in Two-Pole Induction Motors.*

1970 Electrical Machines in the Seventies, Dundee 1-3 July.

[29] N. Kucera. *Effect of Eccentric Rotor Position in the Stator of an Induction Motor.*

1970 Electrotech Obzor, 59, No. 6. Translation: E.R.A. Trans. 2891.

[30] J. Stepina. *Space Vector Representation of radial Force Waves in Asynchronous Machines*

1970 Elektrotech Z ( E.T.Z.) A, 91. Translation: E.R.A. Trans. 2883.

[31] A.J. Ellison and S.J. Yang *Effects of Rotor Eccentricity on Acoustic Noise From Induction Machines*

1971 Proc. I.E.E. V118 No.1

[32] V. W. Schuisky *Magnetic Pull in Electrical Machines Due to Eccentricity of the Rotor.*

1971 Elektrotech und Maschinemball Vol. 88. Translation: E.R.A. 2958.

[33] G.B. Rai and M. Bradford. *Vibratory forces Resulting from Rotating Air-Gap Eccentricity in a Six-Pole Induction Motor.*

1971 E.R.A. Report 71-83.

[34] M. Dye. *Unbalanced Magnetic Pull in Squirrel Cage Induction Motors.*

1971 Ph.D. Thesis, Southampton University.

[35] H. Haase, H. Jordan and K.P. Kovacs. *Vibratory Forces as a Result of Shaft Fluxes with Two-Pole Induction Machines.*

1972 Elecktrotech ( E.T.Z.) Vol 93. Translation: C.E.G.B. C.E. 7822.

[36] K. J. Binns and M. Dye. *Identification of Principal Factors Causing Unbalanced Magnetic Pull in Cage Induction Motors.*

1973 Proc. I.E.E. V120.

[37] J.F. Eastham and S. Williamson. *Generalised Theory of Induction Motors with Asymmetrical Airgaps and Primary Windings.*

1973 Proc. I.E.E. Vol. 120, No. 7.

[38] G.B. Rai and J.C.H. Bone. *Discussion on above reference.*

1974 Proc. I.E.E. V121.

[39] G.B. Rai. *Air-Gap Eccentricity in Induction Motors.*

1974 E.R.A. Report 74-1188.

[40] Y. Akiyama. *Non-Uniform Heating Due to the Increase of Eccentricity of Cage-Type Induction motors*

1976 Electrical Engineering in Japan. Vol 96. No.6.

[41] K. P. Kovacs. *Two-Pole Induction-Motor Vibrations Caused by Homopolar Alternating Fluxes.*

1977 Trans. I.E.E.E..

[42] B. Heller and V. Hamata. *Harmonic Effects in Induction Machines.*

1977 Elsevier Scientific Publishing Company.

[43] M. Ito, N. Fugimoto, H. Okuda, N. Takahashi and S. Watahiki *Effects of Broken Bars on Unbalanced Magnetic Pull and Torque of Induction Motors.*

1980 Elect. Eng. in Japan, Vol. 100.

[44] S. Williamson and A.C. Smith. *Field Analysis for Rotating Induction Machines and its Relationship to the Equivalent-Circuit Method.*

1980 I.E.E. Proc. Vol 127, Pt. B, No. 2.

[45] S. J. Yang. *Low Noise Electrical Motors.*

1981 Oxford University Press.

[46] N. C. Enslin. *Modulation as a Basis for calculating the Balanced and Unbalanced Magnetic Forces in Rotating Field electrical Machines.*

1982 Trans. S.A. I.E.E..

[47] J. Fruchtenicht, H. Jordan and H. O. Seinsch. *Running Instability of Cage Induction Motors Caused by Harmonic Fields Due to Eccentricity, Part 1 Electromagnetic Spring Constant and Electromagnetic Damping Coefficient, Part 2 Self-Excited Transverse Vibration of the Rotor.*

1982 Archiv fur Elektrotechnik 65.

[48] S. Williamson and A. C. Smith. *Steady-State Analysis of 3-Phase Cage Motors With Rotor-Bar and End-Ring Faults.*

1982 Proc I.E.E. Pt. B No. 3.

[49] R. Belmans, W. Geysen, H. Jordan and A. Vandenput. *Unbalanced Magnetic Pull and Homopolar Flux in Three-Phase Induction Motors With Eccentric Rotors.*

1982 I.C.E.M.

[50] R. Belmans, W. Geysen, H. Jordan and A. Vandenput. *Unbalanced Magnetic Pull in Three Phase Two Pole Motors With Eccentric rotor.*

1983 Int. Conf. on Elec. Mach.- Design and Application, London.

[51] M. T. Wright, D. S. M. Gould and J.J. Middlemass. *The Influence of Unbalanced Magnetic Pull on the Critical Speed of Flexible Shaft Induction Machines.*

1983 Int. Conf. on Elec. Mach.- Design and Application, London.

[52] R. Belmans, G. Zeebroek and W. Geysen. *Influence of the Electromechanical Phenomena on the Vibrations of a Two-Pole Induction Motor With a Squirrel-Cage Rotor.*

1984 I.C.E.M. Lausanne, Switzerland.

[53] D.A. Thompson. *Transient Unbalanced Magnetic Pull in Induction Motors*

1984 I.C.E.M.

[54] F.M. Abdel-Kader *The Characteristic Performance of Induction Motors With Eccentricity.*

1984 Electric Machine and Power Systems (USA) Vol. 9 No. 1.

[55] R. Belmans, A. Vandenput, G. Zeebroek and W. Geysen. *Radial Vibrations of Induction Motors with Squirrel Cage.*

1984 Electrical Machines and Converters - Modelling and Simulation.

[56] R. Belmans, W. Heylen, A. Vandenput and W. Geysen. *Influence of Rotor-Bar Stiffness on the Critical Speed of an Induction Motor with an Aluminium Squirrel Cage.*

1984 I.E.E. Proc. Vol. 131, Pt. B, No. 5. H. Buyse and J. Roberts ( eds.), Elsevier Science Publishers,

[57] S. Williamson and M.A.S. Abdel-Magied. *Unbalanced Magnetic Pull in Induction Motors with Asymmetrical Rotor Cages.*

1985 2nd Int. Conf. on Elec. Mach.- Design and Application.

[58] R. Belmans, A. Vandenput and W. Geysen. *Influence of Torsional Vibrations on Lateral Oscillations of Induction Motor Rotors.*

1985 I.E.E.E. Trans. on P.A.S. Vol PAS-104 No.7.

[59] S. Williamson and K. Mirzoian. *Analysis of Cage Induction Motors With Stator Winding Faults.*

1985 I.E.E.E. Trans on P.A.S. Vol PAS-104.

[60] J.R. Cameron, W.T. Thomson and A.B. Dow *Vibration and Current Monitoring for Detecting Airgap Eccentricity in Large Induction Motors*

1986 Proc. I.E.E. V133 Pt.B No.3.

[61] R. Belmans, A. Vandenput and W. Geysen. *Influence of Unbalanced Magnetic Pull on the Radial Stability of Flexible-Shaft Induction Machines.*

1987 Proc. I.E.E. V134 Pt. B No. 2.

[62] R. Belmans, A. Vandenput and W. Geysen. *Calculation of the Flux Density and the Unbalanced Pull in Two-Pole Induction Machines.*

1987 Archiv fur EleKtrotechnik 70.

[63] R. Belmans, A. Dexters, R. Reekmans, A. Vandenput and W.Geysen. *Homopolar Fluxes Due To A Non-Constant Airgap In Three Phase Induction Motors.*

1987 Conf. on Induction Motors - Design and Application.

[64] J. R. Cameron, W. T. Thomson and A. B. Dow. *On-Line Current Monitoring of Induction Motors - A Method For Calculating The Level of Airgap Eccentricity.*

1987 Conf. on Induction Motors - Design and Application.

[65] J.R. Cameron. *Vibration and Current Monitoring for On-Line Detection of Air-Gap Eccentricity in Induction Motors.*

1987 Ph.D. Thesis ( C.N.A.A.), Robert Gordon's Institute of Technology.

[66] S. Williamson and M.A.S. Abdel-Magied. *Steady-State Analysis of Double-Cage Induction Motors with Rotor-Cage Faults.*

1987 Proc. I.E.E. 134 Pt. B.

[67] S. Williamson, M.A.S. Abdel-Magied and A.C. Smith *Effects of Rotor Cage Asymmetry on the Performance of Three-Phase Induction Motors.*

1988 R. Belmans et al ( eds ), Vibrations and Audible Noise in Alternating Current Machines, Kluwer Academic Publishers.

[68] R. Belmans, A. Vandenput and W. Geysen. *Electromagnetic Influence on the Radial Vibrations of Two-Pole Induction Motors.*

1988 R. Belmans et al ( eds ), Vibrations and Audible Noise in Alternating Current Machines, Kluwer Academic Publishers.

[69] W.T. Thomson, J.R. Cameron and A.B . Dow. *On-Line Diagnostics of Large Induction Motors.*

1988 R. Belmans et al ( eds ), Vibrations and Audible Noise in Alternating Current Machines, Kluwer Academic Publishers.

[70] S. Williamson, M.A. Mueller, J. F. Eastham and L. H. Lim. *Transient Unbalanced Magnetic Pull in Change-Pole Induction Motors.*

1989 4th Electrical Machines and Drives Conference I.E.E..

[71] M.A. Mueller. *Improved Calculation Methods for Particular Aspects of Induction Motor Performance.*

1991 Ph.D. Dissertation, University of Cambridge.

[72] S. Salon, M. DeBortola, D. Burrow and C. Slavik. *Calculation of Circulating Current Between Parallel Windings in Induction Motors with Eccentric Rotors by the Finite Element Method.*

1992 I.C.E.M.

[73] M.J. DeBortola, S.J. Salon, D.W. Burrow and C.J. Slavik. *Effect of Rotor Eccentricity and Parallel Windings on Induction Machine Behavior: A Study Using Finite Element Analysis.*

1993 I.E.E.E. Transactions on Magnetics Vol. 29, No. 2, March.

# Appendix A

# Complex Fourier Analysis of a Machine Winding

Consider a coil (number of turns, $C$) on the stator surface of a linearised machine (fig. A.1), where $x$ is the variation in the axial direction, $y$ is the variation in the tangential direction and $z$ is the variation in the radial direction. If this is represented as having finite conductor width $b_s$ (the slot opening), the conductor density over the slot opening is the number of coil turns divided by the slot opening. Its distribution can be then represented as a complex Fourier series as follows

$$n(y) = \sum_{n=-\infty}^{\infty} \left( \overline{C}^{\wedge} e^{-jnky} \right) \tag{A.1}$$

with

$$\overline{C}^{\wedge} = \int_{y_1-b_s}^{y_1+b_s} \frac{C}{b_s} e^{jnky}.\mathrm{d}y - \int_{y_2-b_s}^{y_2+b_s} \frac{C}{b_s} e^{jnky}.\mathrm{d}y \tag{A.2}$$

which becomes

$$\overline{C}^{\wedge} = \frac{k_s^n C}{2\pi r} \left( e^{jnky_1} - e^{jnky_2} \right) \tag{A.3}$$

where the slot opening factor is defined as

$$k_s^n = \frac{sin\left(nk\frac{b_s}{2}\right)}{nk\frac{b_s}{2}} \tag{A.4}$$

$k = \frac{1}{r}$ and $r$ is the average airgap radius.

An expression for a number of series connected coils (or winding) can then be obtained in a similar manner by summing

$$n_x(y) = \sum_{n=-\infty}^{\infty} \overline{N}_x^n e^{-jnky} \tag{A.5}$$

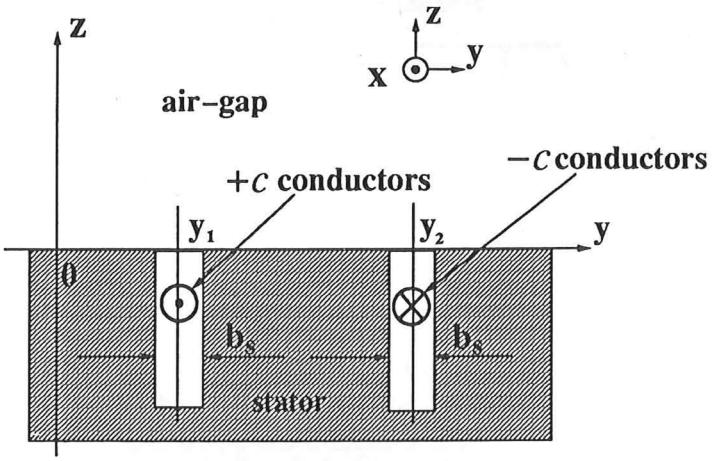


Figure A.1: Single Coil Positioned on Stator

where $n = -\infty,...,-1,1,...,\infty$. The winding coefficient is then defined by the spatial distribution of all the coils

$$\overline{N}_x^n = \frac{1}{2\pi r} \sum_{w=1}^{N} k_s^n C_w e^{jnky_w} \tag{A.6}$$

where $C_w$ is the number of conductors of the winding in $w$th slot (the sign will indicate whether the path is outgoing or returning) and $N$ is the total number of slots in which the $x$th winding lies. If the $x$th winding has a current

$$i_x(t) = \mathrm{Re}\left[\overline{I}_x e^{j\omega t}\right], \tag{A.7}$$

the current density distribution of the $x$th winding on the surface is then

$$j_x(y,t) = \mathrm{Re}\left[\sum_{n=-\infty}^{\infty} \overline{N}_x^n \overline{I}_x e^{j(\omega t - nky)}\right], \tag{A.8}$$

from which an expression for the air-gap flux density can then be derived. A similar expression can also be found for the bar current distribution of a squirrel cage rotor.

The rotor conductor distribution is obtained in a similar manner to the stator phase windings. Considering figure A.2, the cage can be represented as small loops consisting of two parallel bars and the connecting end-ring segments. The number of loops will then correspond to the number of bars in the rotor. It is assumed that there are no inter-bar currents. The conductor distribution of the $l^{th}$ rotor loop will

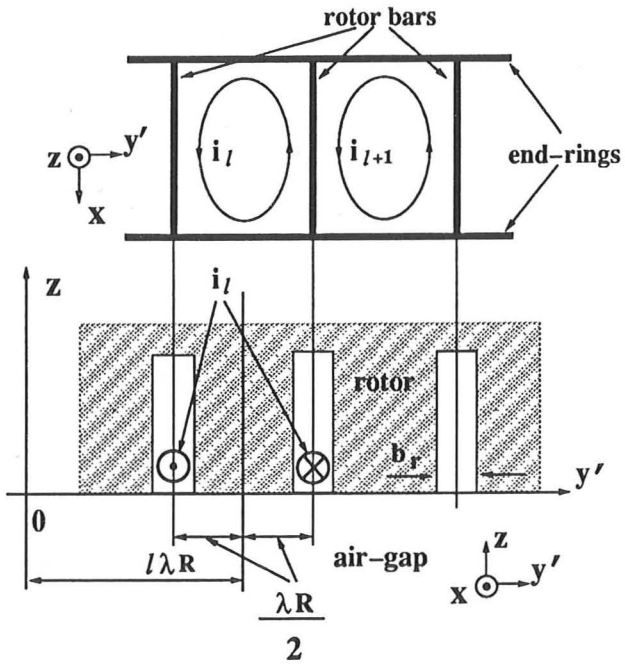


Figure A.2: Rotor Loop Representation

therefore be

$$n_{rl}(y') = \sum_{n=-\infty}^{\infty} \left( \overline{N}_{rl}^{n} e^{-jkny'} \right) \tag{A.9}$$

where

$$\overline{N}_{rl}^{n} = \frac{k_r^n e^{jnl\lambda}}{2\pi R} \left( e^{-j\frac{n\lambda}{2}} - e^{j\frac{n\lambda}{2}} \right) \tag{A.10}$$

with the rotor slot opening factor defined as follows

$$k_r^n = \frac{sin\left(nk\frac{b_r}{2}\right)}{nk\frac{b_r}{2}}. \tag{A.11}$$

where $b_r$ is the rotor slot opening and $k$ is the average airgap radius.

This expression does not include any rotor skewing, this can be included using the method explained in appendix D.

# Appendix B

# Rotor Loop Current Summation

The total $\nu^{th}$ harmonic current density of all the rotor loops can be obtained from

$$j_r^{\nu}(x,y',t) = \sum_{l=0}^{N_b-1} j_{rl}^{\nu}(x,y',t) \tag{B.1}$$

where $N_b$ is the number of bars and $j_{rl}^{\nu}(y',t)$ defines the $\nu^{th}$ harmonic current in the $l^{th}$ loop.

This can be simplified using the summation

$$\begin{aligned}\sum_{l=0}^{N_b-1} e^{jl(n-\nu)\lambda} &= \frac{sin\left(N_b\left(n-\nu\right)\frac{\lambda}{2}\right)}{sin\left(\left(n-\nu\right)\frac{\lambda}{2}\right)} e^{j(N_b-1)(n-\nu)\frac{\lambda}{2}} \\ &= 0|_{n-\nu\neq\mu N_b} \\ &= \sum_{\mu=-\infty}^{\infty} N_b e^{j\mu N_b l\lambda}\Big|_{n-\nu=\mu N_b}\end{aligned} \tag{B.2}$$

where $\mu = 0 \pm 1, \pm 2, ....$

Since $N_b\ \lambda = 2\pi$ then making $n = \mu N_b + \nu$ produces

$$j_r^{\nu}(x,y',t) = \mathrm{Re} \sum_{\mu=-\infty}^{\infty} \overline{J}_r^{\nu,\mu} e^{j(\omega_\nu t-(\mu N_b+\nu)ky'-(\mu N_b+\nu)kx\tan\delta)} \tag{B.3}$$

where

$$\begin{aligned}\overline{J}_r^{\nu,\mu} &= \frac{-jsin\left(\left(\mu N_b+\nu\right)\frac{\lambda}{2}\right)}{\pi r} N_b k_r^{(\mu N_b+\nu)} \overline{I}_r^{\nu} \\ &= N_b \overline{N}_r^{\nu,\mu} \overline{I}_r^{\nu}.\end{aligned} \tag{B.4}$$

Hence any complete harmonic distribution is defined by the current harmonic flowing in just one loop.

# Appendix C

# Calculation of the Airgap of an Eccentric Rotor

Consider figure C.1, if the stator is expressed as a circle with the equation

$$(\Delta + x)^2 + y^2 = R^2. \tag{C.1}$$

Expanding

$$\begin{aligned} z^2 &= R_1^2 - 2\Delta x - \Delta^2 \\ &= R_1^2 - 2\Delta z \cos\theta - \Delta^2 \end{aligned} \tag{C.2}$$

where

$$z^2 = x^2 + y^2. \tag{C.3}$$

Rearranging

$$z^2 + 2\Delta z_1 \cos\theta + \Delta^2 \cos^2\theta = R_1^2 - \Delta^2\left(1 - \cos^2\theta\right) \tag{C.4}$$

giving

$$\begin{aligned} z + \Delta\cos\theta &= R_1\sqrt{1 - \frac{\Delta^2}{R_1^2}(1 - \cos^2\theta)} \\ &= R_1\sqrt{1 + \frac{\Delta^2}{2R_1^2}(\cos 2\theta - 1)}. \end{aligned} \tag{C.5}$$

The nature of the induction machine is such that $\Delta \ll R_1$, therefore

$$\sqrt{1 + \frac{\Delta^2}{2R_1^2}(\cos 2\theta - 1)} \simeq 1 \tag{C.6}$$

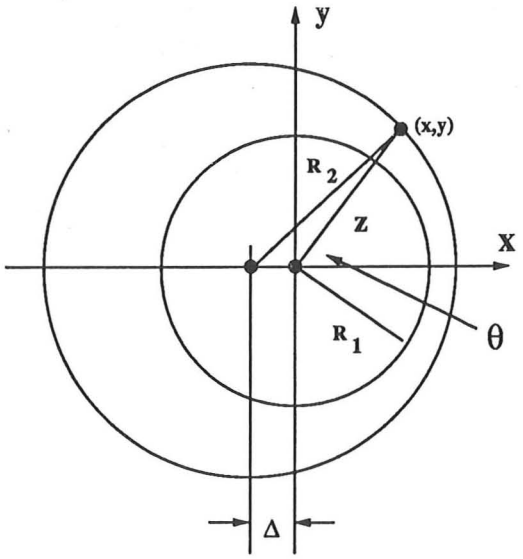


Figure C.1: Rotor and Stator Positioning

hence

$$z \simeq R_1 - \Delta \cos\theta. \tag{C.7}$$

If the radial distance between the rotor and stator ( $g$ ) is approximated to

$$g \simeq z - R_2 \tag{C.8}$$

then

$$\begin{aligned} g &\simeq R_2 - R_1 - \Delta \cos\theta \\ &\simeq g_{av}\,(1 - \Lambda \cos\theta) \end{aligned} \tag{C.9}$$

where $\Delta = \Lambda g_{av}$.

# Appendix D

# Rotor Skew

Many cage induction motors have rotor or stator slots which are skewed with respect to one another. It is important therefore to include this in the analysis. Consider figure D.1, the axial centre is described by $x = 0$, at this point the $l^{th}$ bar lies at point $y = y_l$ whilst the ends of the bars lie at $y_l \pm \frac{l}{2}$. This leads to a rotor conductor density (from equation A.9)

$$n_{rl}(x, y') = \sum_{n=-\infty}^{\infty} \left( \overline{N}_{rl}^{n} e^{-jkny'} \right) e^{-jnx \tan \delta}. \tag{D.1}$$

The standard expression for rotor bar skew can be obtained by integrating with respect to $x$ between $-\frac{l}{2}$ and $\frac{l}{2}$

$$\begin{aligned} k_{sk}^{n} &= \frac{1}{l} \int_{-\frac{l}{2}}^{\frac{l}{2}} e^{jknx \tan \delta} . \mathrm{d}x \\ &= \frac{\sin\left(\frac{2\nu l \tan \delta}{R}\right)}{\frac{2\nu l \tan \delta}{R}}. \end{aligned} \tag{D.2}$$

Hence rotor skew can easily be incorporated into the harmonic conductor density method easily.

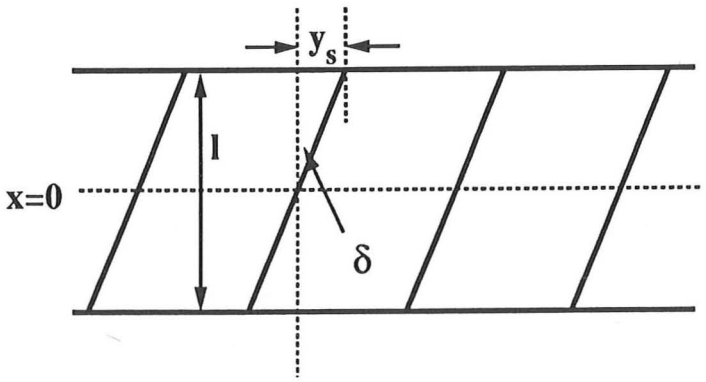


Figure D.1: Rotor Bar Skew

# Appendix E

# Vibration Components of The Ten-Pole Machine Connected in a Two-Pole Configuration

The two-pole connection gave rise to excessive 100 Hz vibration of the whole rig, which also seemed to cause 200 Hz and 50 Hz components. This can be explained by consideration of either stator roll on its mountings or the rotation of the rotor pillar supports round a point on the bed-plate. Whichever is the main cause, movement would tend to be lateral. This is shown in figure E.1 where a two-pole field is represented as two equal forces on opposite sides of the rotor or stator. It can be seen that if there is slight deformation of the stator then an eccentric airgap would be set up and hence UMP caused. The rotor may also move laterally due to pillar rotation on the bed-plate. The net torque acting on the pillars is

$$T_{pillars} = F\,(l_2 - l_1)\cos\theta \tag{E.1}$$

Assuming that the movement is very small and that the stator is still circular then the airgap permeance can be expressed as

$$\lambda\,(y,t) = \Lambda + \delta\cos\,(2\omega t + ky) + \delta\cos\,(2\omega t - ky)\,. \tag{E.2}$$

If the current density of the two-pole winding is expressed as

$$j\,(y,t) = J\cos\,(wt + ky + \phi) \tag{E.3}$$

where $\phi$ represents a phase difference.

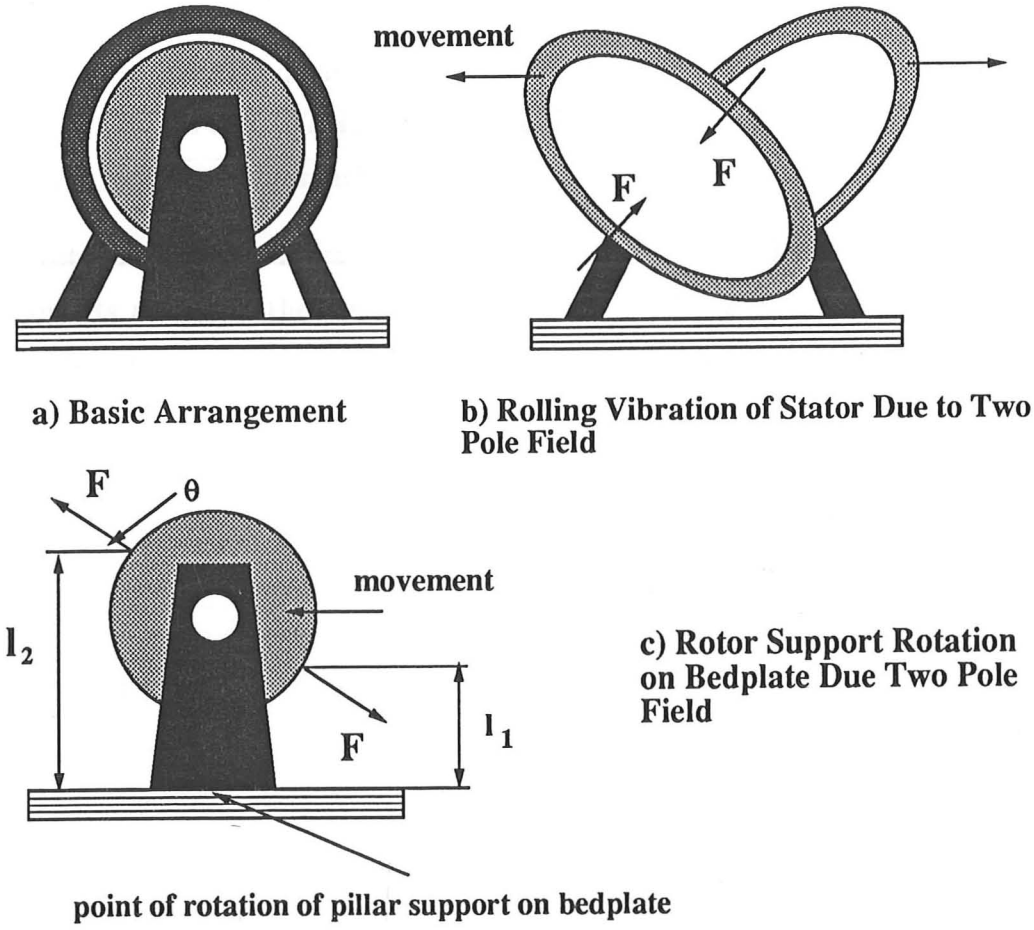


Figure E.1: Causes of Sideways 100 Hz Vibration on the Ten Pole Machine When Used With a Two-Pole Winding Connection

The flux density in the airgap then becomes

$$\begin{aligned} b(y,t) &= \mu_o J \left[ r\Lambda \sin(\omega t + 2ky + \phi) \right. \\ &\quad + \frac{\delta}{4} \left[ r \sin(3\omega t + 2ky + \phi) + 2y \sin(\omega t - \phi) \right. \\ &\quad \left. \left. + 2y \sin(3\omega t + \phi) + r \sin(\omega t - 2ky - \phi) \right] \right]. \end{aligned} \tag{E.4}$$

It can be seen that there are homopolar and four-pole fields with three-times mains frequency components, therefore, when UMP components are calculated, there will be four-times mains frequency as well as twice mains frequency vibrational components (i.e. 200 Hz and 100 Hz). Assuming that $\delta \ll \Lambda$ then the 300 Hz components also produced should be much smaller.

If the rotor is eccentric it was noticed that there were considerable mains frequency components acting in the direction of eccentricity. This phenomena was reported well by Robinson [12] who states that if there is any 50 Hz vibration then these are self sustaining. If mains frequency vibration is used in the above derivation then, indeed, this found to be the case.

# Appendix F

# Publications

The following paper has been accepted for presentation at the IEEE Power Engineering Society Summer Meeting, July 18-22, 1993 Vancouver. It has also been recommended for publication in the IEEE Power Engineering Society Transactions.

93 SM 356-6 EC

# CALCULATION OF U.M.P. IN INDUCTION MOTORS WITH SERIES OR PARALLEL WINDING CONNECTIONS

D. G. Dorrell A. C. Smith, Member IEEE
Dept. of Engineering, Cambridge University,
Cambridge, CB2 1PZ, U.K.

Keywords: Induction motors, stator windings, parallel-paths, performance, unbalanced magnetic pull.

## ABSTRACT

This paper presents a general analytical method for determining the UMP produced in three-phase induction motors with an eccentric rotor. The model uses the conformal transformation technique coupled to a winding impedance approach that is capable of accomodating any stator winding connection. The paper examines the influence of using parallel stator winding paths as a means of reducing the resultant UMP ( static and pulsating ). The results clearly demonstrate the significant reduction of static UMP of a typical stator winding with parallel paths together with the unbalanced winding currents that are produced.

## 1 INTRODUCTION

The radial forces acting upon the surface of the rotor are very large but cancel when the rotor is concentric with the stator. Similarly, the tangential forces are balanced such that only an axially rotating moment is produced. If the rotor becomes eccentric then unbalanced magnetic pull ( UMP ) occurs. The phenomenon can be described as an imbalance of the radial and tangential forces acting upon the rotor ( or stator ) surface such that a net radial force is developed. This can result in vibration and noise, particularly if exacerbated by a flexible shaft, culminating with the possibility of the stator and rotor touching. It can also lead to a reduction in the critical speed, which is an important criterion in high-speed machine design. The primary objective of this paper is to study UMP produced by rotor eccentricity and to show how the resultant radial force can be damped by the use of parallel stator connections.

Unbalanced magnetic pull due to eccentricity takes two forms; static and dynamic. Static UMP is caused by the rotor axis being positioned parallel to, rather than being on, the stator axis and is due manufacturing tolerences. Dynamic UMP is caused by the rotor not rotating about its axis, this could be produced by either manufacturing tolerences or rotor "whirl" near a critical speed. The two forms can exist together but only static UMP will be considered in this paper.

93 SM 356-6 EC A paper recommended and approved by the IEEE Electric Machinery Committee of the IEEE Power Engineering Society for presentation at the IEEE/PES 1993 Summer Meeting, Vancouver, B.C., Canada, July 18-22, 1993. Manuscript submitted January 20, 1993; made available for printing April 5, 1993.

PRINTED IN USA

The methods of calculation of UMP are many and varied, von Kaehne [1] in 1963 ( who provides a substantial review ) and Binns and Dye [2] in 1973 surveyed many of the empirically-based formulae already available. Since then several people have studied UMP due rotor eccentricity, most notably Belmans et al [3], Yang [4], Kovacs [5] and Fruchtenicht et al [6]. The objectives of these mainly being the effects of rotor eccentricity on machine noise [4], vibration [5] and on flexible shaft machines [3, 6]. Bradford, in 1968 [7, 8], published the results of an extensive investigation into UMP in which calculated and experimental results were compared. His experimental machine was a 6-pole series-connected type which could be used in conjunction with a blank, wound or cage rotor. He found that the blank and wound rotors gave very similar UMP characteristics whilst the cage rotor damped the UMP to a much higher degree. Calculation of this damping effect was omitted due to the complexity of modelling the parallel loops of a squirrel-cage rotor.

The usual approach for predicting UMP is to approximate the air-gap length by a constant plus a cosine term due to the rotor eccentricity. This is inverted to produce a permeance expression in terms of a Fourier series. The expression for the air-gap MMF is usually assumed to be a sinusoid of known amplitude. The permeance series will modulate the MMF to give the fundamental flux density field together with a series of harmonic components of order both greater and lower than the fundamental. The UMP can easily be calculated by consideration of the Maxwell stress around the rotor surface and can be shown to be caused by the interaction of two fields with pole numbers differing by two. An interesting result of this approach is the production of a field component that varies in time only, i.e. a component of flux which crosses the air-gap only once ( commonly called a homopolar flux ). The presence of this component relies on a good magnetic circuit through the rotor shaft and casing to enable the flux to return to the stator core. This phenomenon is most noticable in two-pole machines [3] when it is the first harmonic below the fundamental. Homopolar flux becomes negligible as the machine pole-number increases and often the magnetic path through the shaft and casing is poor ( e.g. aluminium casing ). The two-dimensional analysis put forward in the paper will assume that the homopolar flux does not exist.

It is common practice for manufacturers to use parallel stator windings to damp UMP in cage motors since it is well known that they will reduce motor noise, vibration and UMP [9, 10]. Krondl, in 1956 [9], attempted to model parallel stator paths but since this time few have considered them. The usual approach of assuming sinusoidal MMF is a poor approximation if there are parallel stator paths and a non-uniform air-gap. This paper will describe a method which will allow the self and mutual impedances between parallel winding groups to be calculated. The method is based upon the conformal

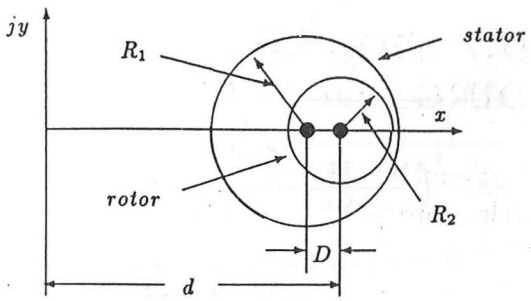


Figure 1: Z-Plane

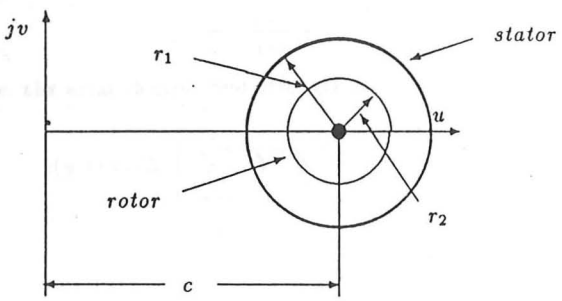


Figure 2: T-Plane

transformation technique, as described by Swann in 1963 [11]. This tranforms the machine from being magnetically asymmetric to one which is magnetically symmetric but electrically asymmetric, i.e. to a machine which has a uniform air-gap but non-uniform winding distribution. An impedence matrix formulation using the conductor density distribution technique ( which has become popular [12, 13, 14] ) is utilised in order to calculate the current components in individual winding groups, the flux density distribution and hence the UMP. The strength of this technique is its flexibility in accommodating any stator winding connection and its influence on the UMP ( static and pulsating ) and the individual winding currents for an induction motor with an eccentric rotor.

# 2 ANALYSIS

The analysis will be applied to various combinations of phase band winding connections of a double-layer induction motor. The method used for the calculation of the various winding currents is based on a generalised version of conductor harmonic analysis [12]. An impedance matrix is formulated which relates the applied voltages to all the current components flowing in each independent winding circuits. It follows that a winding can be defined as any series-connected set of coils, which, in this case, will be terms of complete phase bands. The following assumptions are made in the analysis.

1. The stator and rotor are considered as cylinders with smooth surfaces, i.e. the slotting effects are ignored ( except for a Carter factor correction ).
2. The iron cores of the stator and rotor have infinite permeability and are perfectly laminated.
3. The air-gap is much smaller than the rotor diameter and curvature effects are negligible.
4. The flux crosses the air-gap in a radial direction only.
5. The stator windings are replaced by point filaments of equal amp-turns, positioned on the surface of the stator, in the centre of the slot location.
6. The machine is supplied from a balanced three-phase voltage source with negligible impedance.

## 2.1 The Conformal Transform

The conformal transformation of two eccentric circles to two concentric circles utilises a simple inversion

$$\bar{z} = \frac{1}{\bar{t}}. \tag{1}$$

By finding a suitable values for $d$ in figure 1 and $c$ in figure 2 the eccentric rotor machine as represented by circles 1 and 2 in the Z-plane, can be mapped on the T-plane as two concentric circles ( 1 and 2 ). The transform results in an irregular slot pattern in the T-plane and hence any method based upon this technique must be capable of accomodating general asymmetrical windings.

The Z-plane circles can be written as

$$\bar{z}_1 = d - D + R_1 e^{j\theta_z} \tag{2}$$

and

$$\bar{z}_2 = d + R_2 e^{j\theta_z}. \tag{3}$$

Similarly, for the T-plane circles

$$\bar{t}_1 = c + r_1 e^{j\theta_t} \tag{4}$$

and

$$\bar{t}_2 = c + r_2 e^{j\theta_t}. \tag{5}$$

The radius of the rotor can be written as

$$R_2 = |\bar{z}_2 - d|. \tag{6}$$

Since

$$\bar{t} = u + jv, \tag{7}$$

we can use the inversion to give

$$R_2 = \left| \frac{1}{u + jv} - d \right|. \tag{8}$$

Rearranging

$$\left( u - \frac{d}{d^2 - R_2^2} \right)^2 + v^2 = \left( \frac{R_2}{d^2 - R_2^2} \right)^2. \tag{9}$$

This is the equation of circle 2 in the T-plane, where

$$r_2 = \frac{R_2}{d^2 - R_2^2} \tag{10}$$

and

$$c = \frac{d}{d^2 - R_2^2}. \tag{11}$$

The equation for circle 1 can be obtained in a similar fashion

$$\left( u - \frac{d - D}{(d - D)^2 - R_1^2} \right)^2 + v^2 = \left( \frac{R_1}{(d - D)^2 - R_1^2} \right)^2 \tag{12}$$

where

$$r_1 = \frac{R_1}{(d - D)^2 - R_1^2} \tag{13}$$

and

$$c = \frac{d - D}{(d - D)^2 - R_1^2}. \tag{14}$$

The two equations for $c$ can be combined, from which

$$d = \frac{D^2 + R_2^2 - R_1^2}{2D} \pm \sqrt{\left(\frac{D^2 + R_2^2 - R_1^2}{2D}\right)^2 - R_2^2}. \tag{15}$$

Of the two solutions for $d$, one will give $r_1 > r_2$. The stator windings are considered as point filaments on the outer circle and can be re-located in the T-plane using the simple inversion relationship. The T-plane circles can now be centred on the origin ( by subtracting $c$ ) and the air-gap $g$ for the concentric rotor machine is then defined as $r_1 - r_2$.

The flux density distribution round the stator surface is different in the Z- and T-planes but, due to the re-location of the windings by the transform, the flux linkage between windings is the same whether it is in the T- or Z-plane. The machine now represented in the T-plane can be used to find an impedance matrix linking the stator currents and terminal voltages.

## 2.2 Calculation of Coupling Impedances

In a machine with asymmetrical windings, fields will be produced which may have sub-fundamental machine pole-numbers. It is therefore important to work from a fundamental pole-number of two, even though the actual pole-number of the machine may be much higher. All fields produced will then be integral harmonics of the fundamental. Any angles $\theta$ quoted will then be mechanical degrees.

The distribution of each phase band winding in the T-plane is determined using complex Fourier analysis. For the $b^{th}$ phase band of the $a^{th}$ phase the winding distribution is

$$\overline{n}_{b,a}(y) = \sum_{n=-\infty}^{\infty} \overline{N}_{b,a}^{n} e^{-jnky} \tag{16}$$

where

$$\overline{N}_{b,a}^{n} = \frac{1}{2\pi r} \sum_{w=1}^{N_w} C_{b,a}(w) e^{jn\theta_w} \tag{17}$$

and $y$ is the linear distance of a point along the air-gap circumference. The average air-gap radius in the T-plane is $r$ and $k$ is the fundamental wave number ( $\frac{1}{r}$ ), $C_{b,a}(w)$ is the number of turns of the phase band in the $w$th slot ( the sign will indicate whether the path is outgoing or returning ), $N_w$ is the total number of slots in which the phase band lies and $\theta_w$ is the angular position of the $w$th slot. The winding distribution for the rest of the phase bands are found in a similar manner.

The current flowing in the $b^{th}$ band of phase $a$ can be defined as

$$i_{b,a}(t) = Re\left[\overline{I}_{b,a} e^{j\omega t}\right]. \tag{18}$$

The current density distribution on the stator surface is then

$$j_s(y,t) = Re\left[\sum_{n=-\infty}^{\infty} \sum_{b} \sum_{a} \overline{N}_{b,a}^{n} \overline{I}_{b,a} e^{j(\omega t - nky)}\right]. \tag{19}$$

Applying Ampere's law gives

$$b(y,t) = Re\left[\sum_{n=-\infty}^{\infty} \sum_{b} \sum_{a} \overline{B}_{b,a}^{n} e^{j(\omega t - nky)}\right] \tag{20}$$

where

$$\overline{B}_{b,a}^{n} = -\frac{j\mu_o}{nkg} \overline{N}_{b,a}^{n} \overline{I}_{b,a}. \tag{21}$$

Hence, the axial electric field strength in the air-gap is

$$e(y,t) = Re\left[\sum_{n=-\infty}^{\infty} \sum_{b} \sum_{a} \overline{E}_{b,a}^{n} e^{j(\omega t - nky)}\right] \tag{22}$$

where

$$\overline{E}_{b,a}^{n} = -\frac{\omega \overline{B}_{b,a}^{n}}{nk}. \tag{23}$$

The EMF induced in the $b^{th}$ band of phase $a$ is then

$$u(t) = Re \int_0^{2\pi r} e(y,t) \overline{n}_{b,a}(y) l.dy \tag{24}$$

where $l$ is the effective stack length. The self impedance of the $b^{th}$ phase band of phase $a$ is

$$u_{ba,ba}(t) = Re\left[jX_{ba,ba} \overline{I}_{b,a} e^{j\omega t}\right]. \tag{25}$$

By similar argument the mutual coupling between the $b^{th}$ phase band of phase $a$ by the $d^{th}$ phase band of the phase $c$ is

$$u_{ba,dc}(t) = Re\left[jX_{ba,dc} \overline{I}_{d,c} e^{j\omega t}\right]. \tag{26}$$

Hence defining the mutual reactance as

$$X_{ba,dc} = \sum_{n=-\infty}^{\infty} \frac{2\pi\omega\mu_o l r}{(nk)^2 g} \overline{N}_{d,c}^{n} \overline{N}_{b,a}^{*n}. \tag{27}$$

The self impedances have phase band resistance and leakage inductance terms added to them to form

$$\overline{Z}_{ba,ba} = R_b + jX_b + jX_{ba,ba} \tag{28}$$

Series connected phase bands can be summed, reducing the size of the impedance matrix. All the components of the impedance matrix can now been defined by either equations 27 or 28.

## 2.3 Matrix Equation

A matrix equation can now be formulated such that

$$\begin{bmatrix} \overline{v}_{1,1} \\ \cdots \\ \overline{v}_{b,a} \\ \cdots \\ \overline{v}_{B,A} \end{bmatrix} = \left[\overline{\mathbf{Z}}\right] \begin{bmatrix} \overline{i}_{1,1} \\ \cdots \\ \overline{i}_{b,a} \\ \cdots \\ \overline{i}_{B,A} \end{bmatrix} \tag{29}$$

where

$$\left[\overline{\mathbf{Z}}\right] = \begin{bmatrix} \overline{Z}_{11,11} & .. & jX_{11,ba} & .. & jX_{11,BA} \\ .. & .. & .. & .. & .. \\ jX_{ba,11} & .. & \overline{Z}_{ba,ba} & .. & jX_{ba,BA} \\ .. & .. & .. & .. & .. \\ jX_{BA,11} & .. & jX_{BA,ba} & .. & \overline{Z}_{BA,BA} \end{bmatrix} \tag{30}$$

The phase band currents can be related to the terminal line currents by a connection matrix and consideration of the mesh loop currents

$$\left[\overline{I}\right] = [C]\left[\overline{I}_L\right]. \tag{31}$$

Similarly, the phase band voltages

$$\left[\overline{V}_L\right] = [C]^T \left[\overline{V}\right]. \tag{32}$$

The only non-zero loop voltages will be the voltage sources of the balanced supply. This gives an effective impedance matrix

$$\left[\overline{Z}'\right] = [C]^T \left[\overline{Z}\right] [C] \tag{33}$$

such that

$$[\overline{V}_L] = \left[\overline{Z}'\right] [\overline{I}_L]\,. \tag{34}$$

The solution sequence is then

1, Calculate the impedance matrix $\left[\overline{Z}\right]$.

2, Formulate the connection matrix and hence calculate the effective impedance matrix $\left[\overline{Z}'\right]$.

3, Solve for the loop currents

$$[\overline{I}_L] = \left[\overline{Z}'\right]^{-1} [\overline{V}_L]\,. \tag{35}$$

4, Solve for the phase band currents

$$[\overline{I}] = [C]\,[\overline{I}_L]\,. \tag{36}$$

## 2.4 Calculation of UMP

With a knowledge of the phase band currents the field distribution in the Z-plane can be found and hence the UMP calculated.

Any segment of the rotor surface $\delta\theta_z$ will have a flux $\delta\Phi_z$ crossing it. If this segment is mapped into the T-plane then the segment $\delta\theta_t$ will have a flux $\delta\Phi_t$ crossing it. By the nature of the mapping technique used then

$$\delta\Phi_z = \delta\Phi_t. \tag{37}$$

We can then write

$$\frac{\delta\Phi_z}{\delta\theta_z} = \frac{\delta\Phi_t}{\delta\theta_t}\frac{d\theta_t}{d\theta_z} \tag{38}$$

i.e.

$$b_z(y') = b_t(y)\frac{r_2 d\theta_t}{R_2 d\theta_z}. \tag{39}$$

where $y'$ is the distance around the rotor surface in the Z-plane.

Since

$$c + r_2 e^{j\theta_t} = \frac{1}{d + R_2 e^{j\theta_z}} \tag{40}$$

then, by rearranging and differentiating

$$\frac{d\theta_t}{d\theta_z} = -\frac{R_2 e^{j\theta_z}}{r_2 e^{j\theta_t}}\frac{1}{(d + R_2 e^{j\theta_z})^2}. \tag{41}$$

By combining equations 20, 39, 40 and 41 then the flux density can be found at any point on the rotor surface in the Z-plane.

From the assumption that the flux crosses the airgap radially and that there are no rotor currents, the Maxwell stress at any point on the rotor surface simplifies to

$$\sigma = \frac{b_n^2}{2\mu_o}. \tag{42}$$

The net force along the x axis is then

$$F_x = \int_0^{2\pi R} \frac{b_z^2(y')}{2\mu_o} l cos\left(k'y'\right).dy'. \tag{43}$$

Similarly for the y axis

$$F_y = \int_0^{2\pi R} \frac{b_z^2(y')}{2\mu_o} l sin\left(k'y'\right).dy' \tag{44}$$

where $k'$ is the fundamental wave number in the Z-plane ( $\frac{1}{R}$ ).

Using Gaussian integration, the UMP can then be calculated.

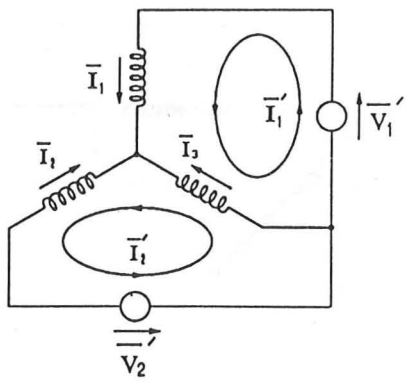


Figure 3: Series Connections

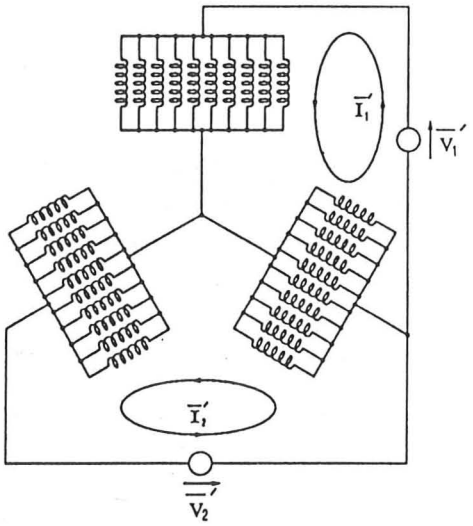


Figure 4: Parallel Phase Bands

# 3 APPLICATION

The analysis is best illustrated by example. A ten-pole double-layer machine has ten phase bands which can be connected in several different ways. The most common way is in series in which there will be two loop currents and two driving voltage sources ( fig.3 ). The connection matrix will then be

$$\begin{bmatrix} \overline{I}_1 \\ \overline{I}_2 \\ \overline{I}_3 \end{bmatrix} = \begin{bmatrix} 1 & 0 \\ 0 & -1 \\ -1 & 1 \end{bmatrix} \begin{bmatrix} \overline{I}_1' \\ \overline{I}_2' \end{bmatrix} \tag{45}$$

The phase bands can be connected in parallel ( fig.4 ). The impedance matrix is now $30 \times 30$ compared to $3 \times 3$ when series connected. Figure 4 shows the first two loop currents, the rest flow round loops formed by adjacent phase bands. An impedence matrix is formed in a similar way to above. Another possible winding pattern ( fig.5 ) has five parallel connected conbinations of two series phase bands. There are many variations of this pattern which include the use of equaliser connections ( as shown by the dotted line ) and connecting either adjacent or opposite phase bands in series. The size of the impedance and connection matrices will be governed by the use of the equaliser connections. There will be 14 loop cur-

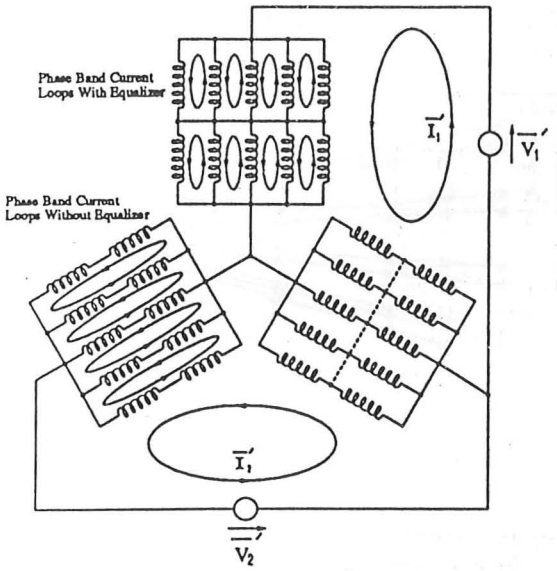


Figure 5: Series/parallel Connections Combined

rents without equalisers and 26 loop currents with equalisers. The final winding pattern possible has two parallel connected combinations of five series phase bands. Again the phase bands can be of various positioning within mesh and the option of equaliser connections is available. The arrangements studied in the section will be: phase bands connected in series; phase bands connected in parallel; two adjacent phase bands connected in series to form five parallel paths.

The analysis was applied to a machine with the following specification.

| | |
|---|---|
| Number of stator poles | 10 |
| Number of stator slots | 90 |
| Coil pitch ( slots ) | 9 |
| Number of turns per coil | 9 |
| Resistance per coil | 0.0532 Ω |
| Leakage reactance per coil | 0.06 Ω |
| Supply frequency | 50 Hz |
| Effective machine length | 0.2 m |
| Effective machine air-gap length | 1.5 mm |
| Mean air-gap diameter | 0.298 m |
| Rated voltage ( line ) | 415 V |

The line voltage used in the analysis was reduced as the number of parallel paths increased in an attempt to maintain a constant current level in the phase bands.

# 4 RESULTS

The motor described in the previous section was used to investigate the variation of UMP produced by three different stator winding connections. These are illustrated in figures 3-5: series connection; parallel connection ; and two series groups of five bands in parallel with no equaliser connections.

Figure 6 shows the variation in the static UMP produced by the series and parallel connections. As expected the use of parallel paths significantly reduces the magnitude of the UMP present in the motor. The direction of UMP acts along the axis of eccentricity for the series connection and approximately 17 degrees from the same axis for the parallel connection. The

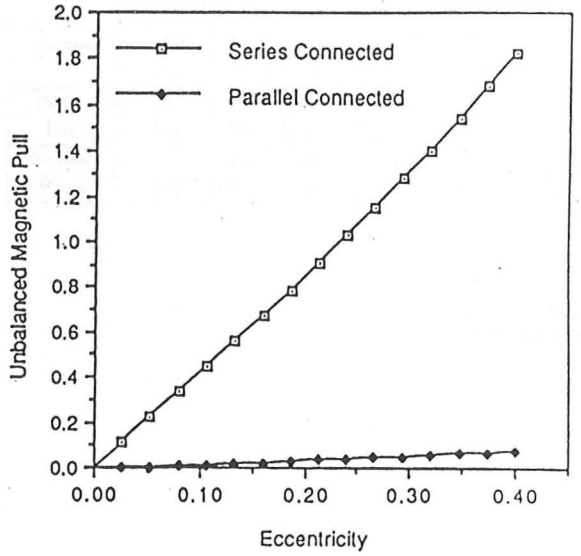


Figure 6: UMP for Series and Parallel Connections

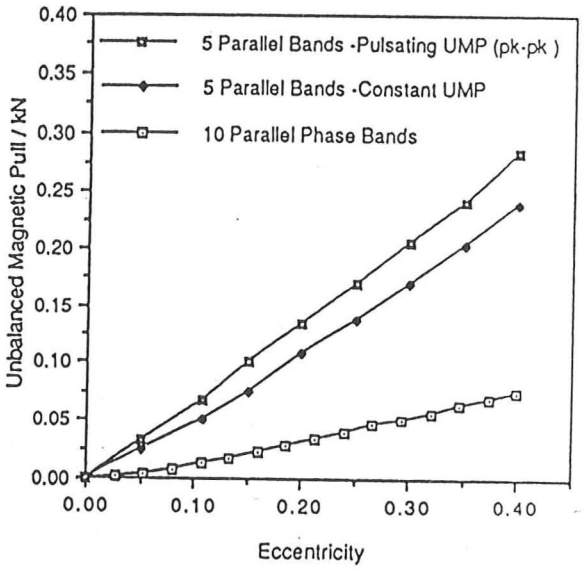


Figure 7: UMP for Parallel and Series/Parallel Connections

phase shift between the two connections can be explained in terms of the constant MMF that exists for the series connection and the constant flux linkage that is forced by the parallel connection. In the case of the parallel connection the winding resistance and leakage reactance produce a non-uniform phase shift in the phase band flux linkages and this results in the rotation of the UMP. This was verified by setting the coil resistances and leakage reactances to zero and the UMP was, as expected, found to act along the axis of eccentricity.

Figure 7 illustrates the static UMP produced in the parallel and series/parallel connections. Interaction between the air-gap permeance harmonics and the MMF harmonics can also result in a pulsating component of UMP at twice the line frequency. Figure 7 also demonstrates the presence of a relatively large component of oscillating UMP in the case of the series/parallel connection. This was found to be almost negligible in the series and parallel connections.

Figures 8 and 9 illustrate the variation in the phase band currents in both magnitude and phase for parallel connections.

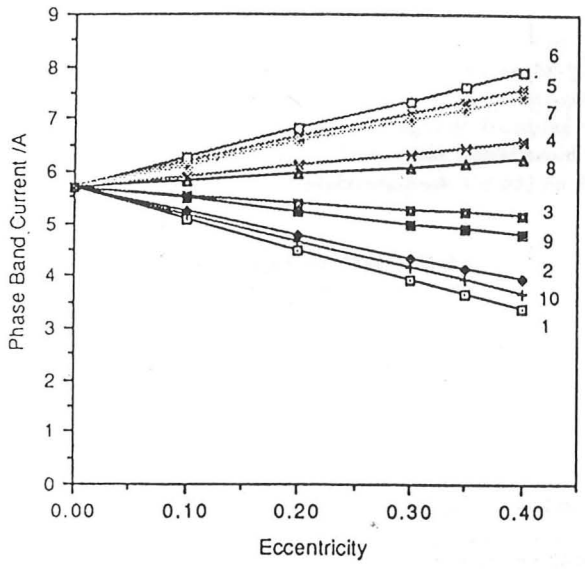


Figure 8: Current Magnitudes for Parallel Connections

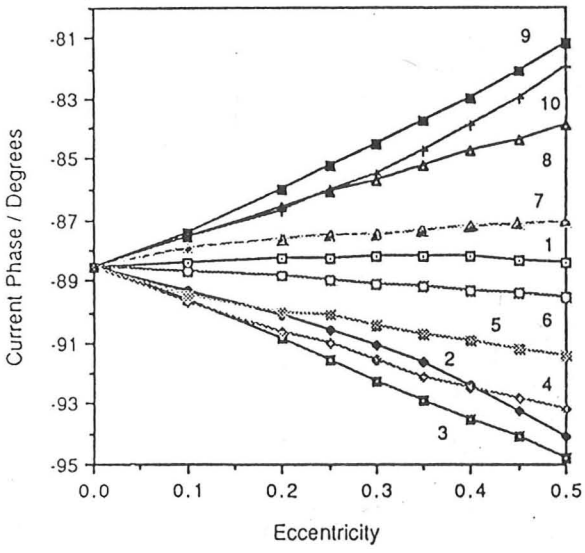


Figure 9: Current Phases for Parallel Connections

| Connection | Offset | Phase A | | Phase B | | Phase C | |
|---|---|---|---|---|---|---|---|
| | | A | Lag | A | Lag | A | Lag |
| Series | 0 | 5.66 | 88.6 | 5.66 | 88.6 | 5.66 | 88.6 |
| | 0.4 | 5.21 | 88.4 | 5.21 | 88.4 | 5.21 | 88.3 |
| Parallel | 0 | 56.6 | 88.6 | 56.6 | 88.6 | 56.6 | 88.6 |
| | 0.4 | 56.5 | 88.8 | 56.5 | 88.8 | 56.5 | 88.8 |
| Series -Para. | 0 | 28.3 | 88.6 | 28.3 | 88.6 | 28.3 | 88.6 |
| | 0.4 | 27.7 | 89.6 | 28.2 | 89.1 | 28.1 | 87.5 |

Clearly certain phase bands can carry much larger currents than normal and this is of particular relevance to motor designers. It is also evident that the phase band currents with the smallest change in magnitude display the largest variation in phase angle. It is worth noting that although certain phase band currents show leading power factor the overall input line currents are at a lagging power factor. This is demonstrated in the table in which the three line currents for all series, parallel and series/parallel connections are listed. These show clearly that the input line currents remain essentially as balanced three-phase sets.

# 5 CONCLUSIONS

The analysis presented in this paper has been shown to be capable of predicting the steady and pulsating UMP in an induction motor with an eccentric rotor. The method is based upon a conformal transformation coupled to an impedance approach that can accomodate any stator winding connection with ease. It has been used to examine the infuence of series and parallel paths in a typical ten-pole stator winding. The reduction in the static UMP by using parallel paths has been illustrated together with the unbalanced phase band currents that are produced. In all connections the line currents have been shown to remain essentially balanced three-phase sets. The flexibility of the general technique has been amply demonstrated from the variety of winding connections used in the results.

# 6 ACKNOWLEDGEMENTS

The authors would like to express their gratitude to GEC Alsthom Large Machines Ltd, Rugby, England for their assistance with this work.

# References

[1] P. von Kaehne. *Unbalanced Magnetic Pull in Rotating Electrical Machines. Survey of Published Work.* 1963 Electrical Research Association (U.K.) Report Ref. Z/T 142.

[2] K. J. Binns and M. Dye. "Identification of Principal Factors Causing Unbalanced Magnetic Pull in Cage Induction Motors." *1973 Proc. I.E.E., V120, No.3, pp.349-354.*

[3] R. Belmans, A. Vandenput and W. Geysen. " Influence of Unbalanced Magnetic Pull on the Radial Stability of Flexible-Shaft Induction Machines." *1987 Proc. I.E.E., V134 Pt.B, No.2, pp. 101-109.*

[4] S. J. Yang. *Low Noise Electrical Motors.* 1981 Oxford University Press.

[5] K. P. Kovacs. "Two-Pole Induction-Motor Vibrations Caused by Homopolar Alternating Fluxes." *1977 Trans. I.E.E.E., Vol.PAS-96, No.4, pp.1105-1108.*

[6] J. Fruchtenicht, H. Jordan and H. O. Seinsch. "Running Instability of Cage Induction Motors Caused by Harmonic Fields Due to Eccentricity, Part 1 Electromagnetic Spring Constant and Electomagnetic Damping Coefficient, Part 2 Self-Excited Transverse Vibration of the Rotor." *1982 Archiv fur Elektrotechnik Vol.65, pp.271-292.*

[7] M. Bradford. " Unbalanced Magnetic Pull in a 6-Pole Induction Motor." *1968 Proc. I.E.E. Vol.115, No.11, pp.1619-1627.*

[8] M. Bradford. *Unbalanced Magnetic Pull in a 6-Pole 10 kW. Induction Motor With a Series-Connected Stator Winding.* 1968 Electrical Research Association (U.K.) Report No.5216.

[9] M. Krondl. "Self Excited Radial vibrations of the Rotor of Induction Machines with Parallel Paths in the Winding." *1956 Bull. Assoc. Suisse, Elect., Vol.47, pp.581-588.*

[10] A.J. Ellison and S.J. Yang. "Effects of Rotor Eccentricity on Acoustic Noise from Induction Machines." *1971 Proc. I.E.E. Vol.118, pp.174-184.*

[11] S. A. Swann. "Effect of Rotor Eccentricity on the Magnetic Field in the Air-Gap of a Non-Salient- Pole Machine." *1963 Proc. I.E.E. Vol.110, No.5, pp.903-915.*

[12] S. Williamson and A. C. Smith. "Steady-State Analysis of 3-Phase Cage Motors With Rotor-Bar and End-Ring Faults." *1982 Proc I.E.E. Vol.129, Pt.B, No.3, pp.93-100.*

[13] S. Williamson and K. Mirzoian. "Analysis of Cage Induction Motors Stator Winding faults." *1985 I.E.E.E. Trans. Vol. PAS-104, No.7, pp.1838-1842.*

[14] S. Williamson and M.A.S. Abdel-Magied. "Steady-State Analysis of Double-Cage Induction Motors with Rotor-Cage Faults." *1987 Proc. I.E.E. Vol.134, Pt.B, pp.199-206.*

**David Dorrell** was born in St. Helens, England in 1965. He obtained a B.Eng. degree in Electrical and Electronic Engineering from the University of Leeds in 1988 and an M.Sc. degree in Power Electronics Engineering from Bradford University the following year. Since then he has been studying for a Ph.D. degree at the Engineering Department of Cambridge University, his main topic of research being the cause and calculation of unbalanced magnetic pull in squirrel cage induction motors.

**Alexander C. Smith** was born in Ballater, Scotland. He received the B.Sc. ( Eng.) and Ph.D. degrees from Aberdeen University in 1977 and 1980, respectively. He spent three years as a Research Fellow at Aberdeen University and six years as a Lecturer at Imperial College, London. He is currently employed as a Lecturer at Cambridge University. His reseach interests are directed towards the analysis of induction motors and devices under steady-state, transient and fault conditions.